

ROYAL INSTITUTE OF TECHNOLOGY

MASTER'S THESIS APPLIED MATHEMATICS

Validation of market commodity forward curves

Author:
Susanna KAAS

Supervisors:
Filip LINDSKOG KTH
Anna BAECKLUND
Handelsbanken

16 augusti 2015

Sammanfattning

I detta examensarbete var målet att föreslå en metod för att validera marknadskurvan för råvaruterminer och utvärdera den föreslagna metoden. Examensarbetet är begränsat till marknadskurvor för råvaruterminer med säsongsberoende och likafördelade förfallodagar upp till ett år. Valideringsmetoden som föreslås är att med en teoretisk modell skapa en referenskurva som kan jämföras med marknadskurvan. Metoden för att skapa referenskurvan är att simulera terminspriser med seasonal cost-of-carry model och sedan interpolera linjärt mellan de simulerade punkterna.

Valideringsmetoden appliceras på råvaruterminer med UK naturgas som underliggande tillgång och handlas på Intercontinental Exchange. Det historiska dataset som användes utgörs av observationsperioden 2011-01-01 till 2013-11-30. Referenskurvor skapades för varje handelsdag i december 2013 och verkade uppfylla det förväntade säsongsberoendet hos naturgas. Analyser visade dock att modellantagandena inte alltid var uppfyllda av de genererade processerna från historiskt data. Observationsperioden kortades ned men resultatet blev endast något bättre, dock uppfyllde fortfarande inte några av processerna de uppställda antagandena. Resultat visade också att vissa av processerna för båda observationsperioderna kunde reduceras till slumpvandringar.

Slutsatsen av arbetet är att den föreslagna metoden inte är lämplig för validering av marknadskurvan för den analyserade tidsperioden. Orsaken till detta var att modellantaganden inte var uppfyllda för alla tillståndsvariabler samt att några av processerna kunde reduceras till slumpvandringar. Dock är det möjligt att modellantaganden skulle kunna uppfyllas för en annan tidsperiod. Eftersom det är svårt att använda en metod för validering om historisk data inte alltid uppfyller modellantaganden och om processerna inte är stationära drogs slutsatsen att den föreslagna metoden inte är lämplig för den analyserade råvaran.

Abstract

In this thesis the aim was to propose a method that could be used to validate the market commodity forward curve and analyse if the method is possible to apply. The thesis is limited to forward curves with equally spaced maturities up to one year and seasonal price patterns. The method suggested is to construct a reference curve by simulating futures prices with the seasonal cost-of-carry model and perform linear interpolation between these simulated values.

The validation method was applied to UK natural gas futures traded on the Intercontinental Exchange for every trading day in December 2013. Estimates were based on settlement prices for the period 2011-01-01 to 2013-11-30. Resulting reference curves appeared to capture the seasonal behaviour of UK natural gas in a correct way and the shape of the curve seemed to follow the market curve. However the majority of observed time series representing the state variables did not fulfil model assumptions. Therefore the observation period was shortened to 2012-07-01-2013-11-30 but the result was only slightly improved. It was still the case that some of the state variable processes did not follow model assumptions. By performing likelihood ratio test it was found that for some state variables the speed of mean reversion could be set to zero.

The conclusion was that the proposed method is not appropriate to use for validating the market curve for the considered contracts. This is because model assumptions for state variables were not always fulfilled and some of the state variable process could be reduced to random walks. Perhaps model assumptions are fulfilled if the method is applied to another time period. However it is difficult to use a method for validation if historical data sometimes suggests that times series are not stationary and do not fulfil model assumptions. Finally the conclusion was drawn that for the chosen commodity the validation method is not applicable.

Acknowledgements

Firstly I would like to thank my supervisor Associate Professor Filip Lindskog at KTH for his support and valuable guidance throughout this thesis. I would also like to thank Anna Baecklund at Handelsbanken.

Susanna Kaas, Stockholm July 2015

Contents

1	Introduction	7
2	Background	8
2.1	Futures and forward contracts	8
2.2	Classification of commodities	10
2.3	Relation between forward and spot price	10
2.3.1	Investment assets	10
2.3.2	Consumption assets	11
2.4	Forward curve	12
2.4.1	Different shapes of forward curves	12
3	Objectives	14
4	Different models	15
4.1	Martingale based approach	15
4.2	The static arbitrage based approach	16
4.3	Properties of different models	21
5	Application of seasonal cost of carry model	23
5.1	Estimation of parameters	23
5.2	Simulating new samples	24
5.2.1	Simulation equations	24
5.2.2	Interference for diffusion processes	25
5.2.3	Building references curves	27
6	Results	28
6.1	UK natural gas futures	28
6.1.1	The average futures price	30
6.1.2	Seasonal premia	34
6.1.3	Convenience yield	34
6.1.4	Constructing the forward curve	43
7	Evaluation of results	45
7.1	Evaluation of created reference curve	45
7.2	Does the model fit historical data?	46
7.2.1	Original historical data set	46
7.2.2	Different set of historical observations	52
7.3	Reduce processes to random walks?	57
7.4	Analysis of maximum-likelihood estimation	61
7.4.1	OLS-estimation of parameters	61
7.4.2	MLE using rolling window of 200 days	64
7.4.3	Accuracy for ML-estimators	65

8	Summery and conclusion	72
	Appendices	77
	Appendix A Mathematical background	77
A.1	Probability theory	77
A.2	Time series analysis	78
A.2.1	IID noise	79
A.2.2	Random walk	80
A.2.3	Autoregressive process	80
A.3	Stochastic calculus	81
A.4	Maximum likelihood estimation	84
A.4.1	Independent normally distributed set of observations .	85
A.4.2	Interference for parameters in mean reverting process	86
	Appendix B Analytic solution	88
	Appendix C Model constraints	89
	Appendix D Futures price dynamics	90
	Appendix E Figures original set of observations	90
	Appendix F Figures different set of observations	98

1 Introduction

In the past, trading with commodities was mainly executed by exchanging the physical commodity for cash at different trading sites. Today commodity trading includes futures, forwards and many other instruments attracting investors wanting exposure to commodity price risk [11]. The investors investing in the commodity market often want to prognosticate trends of future spot prices analyse future demand and supply and compute calculations of different risk measures such as VaR (Value-at-Risk) and P&L (Profit and Loss). These analysis are often performed using a market forward curve [9]. Therefore it is of great importance that the forward curve reflects market prices in a correct way. In some cases market prices constructing the forward curve are erroneous due to technical errors. This affects the forward curve resulting in errors when calculating for example P&L. A method that could validate the market curve could contribute to find these erroneous prices making it possible to correct risk measurement calculations.

The objective of this project is to propose a method that could be used to validate the market commodity forward curve so that price errors due to technical errors are found more easily. In this thesis the validation method suggested is to create a reference curve using theoretical models and compare this curve to the market curve, in order to identify parts that deviate significantly indicating erroneous prices. The thesis will be limited to validation of forward curves with seasonal price patterns and with equally spaced maturities up to one year.

The report will be outlined as follows; starting with a section including relevant background information, then a more detailed description of the project objectives, following with a presentation of different theoretical models including a presentation of the chosen model. The suggested validation method is applied on a chosen commodity which is presented in the result section. After that the results are evaluated together with model assumptions and parameter estimations, followed by a summery and conclusion section.

2 Background

All commodities are traded on the *spot market*, where the exchange of commodity and cash take place with immediate exchange or with some small delay due to technical reasons. In the past, trading with commodities was only made at the spot market where buyer and seller met at certain trading sites to exchange cash for the physical commodity. During the 18th century farmers began to sell the crop long before harvest. This is known today as forward transactions and was the beginning for forward contracts. In the middle of the 19th century a demand grew for contracts with a pre-determined commodity quality, size and delivery location. This led to the opening of commodity exchanges such as Chicago Board Of Trade (CBOT) and New York Cotton Exchange (NYCE). Contracts trade on these commodity exchanges were so called futures contract. Today commodity trading is a big part of the world's economy exposing manufacturers, sellers, banks and other financial institutions to commodity price risks. Trading with commodities today still involve trading on the spot market but also in futures, forwards and options, making it possible to optimally hedge future demand and supply [11].

Forward curves are of great importance for commodity trading and strategic decisions about production and storage. The curves are also used to prognosticate trends for future spot price and in risk management for calculation of different risk measures such as VaR and P&L. In this report the market commodity forward curve is constructed by linear interpolation between a set of benchmark points. These benchmark points consist of a collection of futures prices with increasing time to maturity. The left end of the curve consists of the first-to-expire future and the right end of the contract with the most distant maturity. When the first-to-expire future matures, the entire curve is switched to the left and the next-to-expire future will then construct the left end of the curve [9].

In the following section the definition of forward and futures contract will be presented including differences among these two contracts, followed by a presentation about commodity classification. Finally the relation between spot and futures prices will be presented together with relevant facts about the forward curve.

2.1 Futures and forward contracts

Forward and futures contracts can be used to hedge future demand and supply of certain assets. Both these contracts are agreements between two parties to exchange cash for a certain asset at a future time point.

The underlying asset could be an *investment asset* or a *consumption asset*. Examples of consumption assets are aluminium, copper, crude oil which is purchased mainly for consumption. Assets that are categorized as investment are purchased for investment reasons giving an income from holding the asset. Examples of investment assets are gold, silver, stock and bonds. There are also assets that are categorized both as consumption asset and investment assets.

In this report futures contracts written on commodities are considered. Commodities are in most cases consumption assets with a few exceptions such as silver and gold. Forward and futures have the same purpose they both hedge for future delivery of a certain asset. However there are some differences between these two contracts. Below different properties among these contracts are going to be described.

Forward contracts

Forward contracts are traded over-the-counter (OTC) exposing buyer and seller for the risk that one part may not fulfil its contractual obligation. This risk is known as *credit risk*. Forward contracts are settled at maturity exposing the buyer and seller for loss or gain only at maturity [1].

Futures contracts

Futures contract written on commodities are traded on specialized exchange where each contract is standardized, meaning that every contract written on the same commodity at a certain exchange has the same size, quality of underlying commodity and delivery location. Since futures are traded on organized exchange the clearing house acts as counterpart for seller and buyer respectively, eliminating the credit risk. Futures contracts are on contrary to forward contracts settled every day exposing both seller and buyer to profit or loss every trading day [1]. The settlement procedure can be shown by considering a futures contract that has decreased in value between two trading days. Then the buyer of the contract must add cash to the position equal to the loss in order to adjust the position. This cash deposit is paid to the clearing house and is called *margin call*. On the other hand if the value of the contract increases the buyer of the contract will make an instantaneous gain. In order to trade on these specialized commodity exchanges there is also a fee that has to be paid in order to place an order. This fee is called *margin deposit*. Both the margin call and the margin deposit contributes to decreasing the credit risk to approximately zero [11].

In this report only futures contracts are going to be considered. However under some assumptions the same modelling approaches can be used for both futures and forwards contracts. When interest rates are constant the futures price and forward price are equal. For commodities there are other risk

factors affecting the price more than interest rate. Hence it will be assumed throughout the report that the interest rate is constant and therefore the term forward and futures price will be used conversely [9].

2.2 Classification of commodities

There are many differences among commodities when it comes to modelling framework. In this section classification groups for commodities are going to be presented and discussed.

There exists two major classification groups for commodities this is the division between *storable commodities* and *not storable commodities*. Most commodities belong to the group of storable commodities. Example of such is copper, natural gas and crude oil. These are all possible to store often for some cost. Examples of commodities that are not possible to store are weather, electricity and emission claims. However among commodities in these two groups there are significant differences.

The storable commodities can be divided into three smaller groups these are commodities that are produced and consumed continuously, produced continuously but consumed seasonally and lastly produced seasonally but consumed continuously. Examples of commodities that do not experience seasonality are industrial metals for example aluminium and copper. Commodities such as heating oil and natural are examples of commodities that are produced continuously however the demand heavily depends on season. Hence these commodities have a *seasonal price dependence*. For agricultural commodities such as grains, coffee and soya beans the production is seasonal but demand is continuous over the year. Therefore it is often the case that agricultural commodities also have a seasonal price dependence [9].

2.3 Relation between forward and spot price

In this section relation between spot and futures price for investment and consumption assets will be presented and discussed.

2.3.1 Investment assets

The relation between forward and spot price when storage costs are zero is given by the following relation

$$F(t, T) = S_t e^{r(T-t)}, \quad (1)$$

where S_t is the current spot price, r is the risk free interest rate, t is the current time and T is the maturity date.

In order to investigate arbitrage arguments it can be assumed that $t = 0$ and that $F(0, T) > S_0 e^{rT}$. If this is the case an investor could borrow the amount S_0 at $t = 0$ for a time period T . Buy the underlying asset for the price S_0 . At the same time the investor can sell a forward contract with delivery date T . The profit would then be

$$\text{Profit}_1 = F(0, T) - S_0 e^{rT}.$$

If the opposite case would occur an investor holding the asset could apply the same strategy but in opposite direction. For that case the investor could sell the asset at $t = 0$ for S_0 and place the money in a risk free bank account with interest rate r . At the same time the investor should buy a forward contract maturing at date T . The profit using this strategy would be

$$\text{Profit}_2 = S_0 e^{rT} - F(0, T).$$

For both these cases the forward price will adjust to the spot price making Profit_1 and Profit_2 equal to zero. Hence relation (1) will hold and no arbitrage opportunities exists. This argument will hold only for investment assets when the cost of storage is zero. This is because the forward price will adjust to the spot price. For investment assets that are storable for a certain cost denoted c , relation (1) must be modified to

$$F(t, T) = S_t e^{(r+c)(T-t)} \tag{2}$$

[1].

2.3.2 Consumption assets

For commodities such as gold and silver relation (2) will hold since these are also investment assets and the futures price will adjust to the spot price if the forward price is greater than the discounted spot price or if the opposite case arise. However most commodities are consumption assets having a consumption value meaning that they are held mainly for consumption now or in the future. Hence if the futures price is greater or less than the discounted spot price the forward price would probably not adjust to the spot price. The reason for this is because industries and companies holding the physical commodity are unwilling to sell it on the spot market and buy futures or forward contracts since these cannot be manufactured [1].

For commodities that are consumption assets the advantage of holding the physical commodity versus futures or forwards is called *convenience yield* and will be denoted δ' . For consumption assets the relation between spot and futures price can be modified to the following relation known as the classical *cost-of-carry* relation

$$F(t, T) = S_t e^{(r+c-\delta')(T-t)} \quad (3)$$

[12].

Letting $\delta = c - \delta'$ denote the convenience yield the above relation can be written as

$$F(t, T) = S_t e^{(r+\delta)(T-t)} \quad (4)$$

[9].

2.4 Forward curve

The forward curve can show many different shapes depending on the price properties for the considered commodity. In this section the dynamics of the forward curve is going to be presented starting with the concepts *contango* and *backwardation*.

2.4.1 Different shapes of forward curves

When prices of futures with shorter time to maturity are greater than prices for more distant the forward curve will have a downward slope. This is called that the forward curve is in *backwardation*. By observing the classical cost-of-carry relation given by (3) one can conclude that if the convenience yield is greater than the cost of storing and the risk free rate the market will be in backwardation. An example of a market in backwardation is shown in Figure 1 which illustrates the market curve for futures written on Brent Crude traded on the Intercontinental Exchange (ICE).

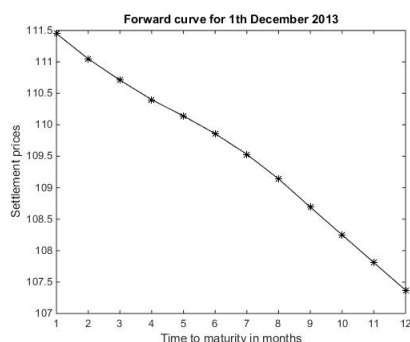


Figure 1: The market forward curve for ICE Brent Crude futures, where settlement prices are in cents per tonne. In the figure the contract maturing next month is January 2013 contract [8].

On the other hand if prices for futures with shorter maturities are less than prices for more distant the curve will be upward sloping, this is called that the curve is in *contango*. In order for the market to be in contango the convenience yield must be less than the cost of storage and the risk free interest rate, see equation (3).

For commodities where the demand or supply depends heavily on season, the forward curve will show a seasonal pattern. The seasonal pattern can be explained by limited storing and transportation possibilities that do not meet seasonal demands [9]. An example of a forward curve with seasonal behaviour is shown in Figure 2, where the price peaks for contracts maturing in the winter months and drops significantly for contracts maturing in the summer.

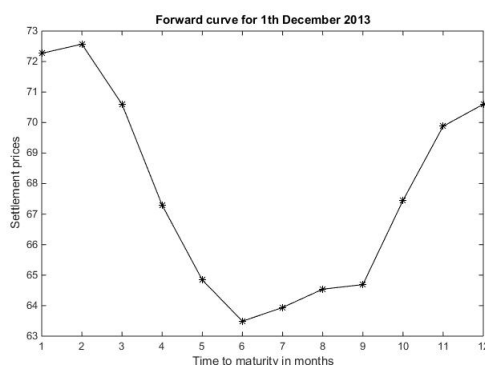


Figure 2: The market forward curve for UK natural gas traded on ICE where settlement prices are per therms in sterling and pence. In the figure the contract maturing next month is the January 2014 contract [5].

There are several reasons for why a market is in backwardation, some of these are low storage levels, strongly rising prices, dramatic price changes, and lack of the commodity. A market could be in contango due to high storage levels, small price changes and abundance of the commodity [3].

Forward contracts that mature in a near future are often more volatile than more distant maturities. Since the left end of the forward curve consist of futures with shorter maturities this end of the curve will be more volatile. This effect is known as Samuelson effect. Empirical observations also suggest that futures contract with different maturities are not perfectly correlated. In most cases the entire forward curve moves up and down together but can also change form in many other complex ways [12].

3 Objectives

The aim of this project is to find, a method that could be used to validate the market forward curve for commodities and investigate if the method is possible to apply. Validation of the market forward curve will here be referred to as a method for controlling if the curve correctly reflects market prices for a certain day. The curve is constructed by linear interpolation between benchmark points given by market futures prices. In some cases these prices are wrong due to different technical errors. Since the forward curve is often used for risk management purpose. These erroneous market prices can lead to incorrect calculation of different risk measures. Therefore validation of the market curve is of great importance because it can contribute to find erroneous prices more easily.

In this thesis a market curve is validated with the use of a reference curve. This method could control if one or several benchmark points in the market curve deviate significantly from the reference curve. The deviations could be indications that some of the market values might be incorrect. The scope of this thesis is limited to an analysis of futures experiencing seasonal price patterns and with equally spaced maturities up to one year.

In order to use the proposed method for validation the simulated reference curve must in a proper way reflect market observed prices. The method chosen to create the reference curve should also incorporate different price properties among different commodities such as seasonality and preferably be possible to apply to a range of different commodities. Hence in order to accomplish the project goal one can formulate the following objectives:

- Choose a theoretical model that could be used to create the reference curve.
- Choose commodity futures that have equally spaced maturities up to one year and seasonal price pattern and apply the validation method on an arbitrary time period.
- Analyse the result and check if model assumptions are fulfilled.
- Conclude if the suggested method is possible to apply for validation of the market curve for the considered commodity.

4 Different models

Examples of modelling approaches for commodity forward curves are; the martingale based approach and the static arbitrage based approach [10].

Futures price models using the martingale approach are based on the fact that forward prices are martingales under the risk neutral measure Q . Examples of models using the martingale approach are the one factor and multi factor model proposed by [12]. These models can be compared to Heath-Jarrow-Morton (HJM) models for yield curve modelling [9].

The methodology for the static arbitrage based approach is based on first determine a number of stochastic processes that drive the evolution of futures prices. The next step is to use the dynamics of the chosen factors together with no arbitrage arguments to derive relations for futures prices. An example of a model using static arbitrage based approach is the seasonal cost-of-carry model presented by [10], where dynamics that drive the forward price are given by two stochastic process and a deterministic term. Other examples are the one factor model that models the spot price as a mean reverting process, the two factor model presented by [18] that model the spot price and convenience yield as stochastic processes and the three factor model see [15] that also models the interest rate as a stochastic process [10].

In the following sections some methods using the martingale based approach are going to be presented and later some methods using the static no arbitrage approach. Lastly properties of the presented models are going to be discussed followed by a presentation of the model chosen to create the reference curve.

4.1 Martingale based approach

In this section example of models using the martingale based approach will be presented, starting with the one factor model and then the multi factor model.

One uncertainty factor

In the one factor model the dynamics that drive the evolution of the forward price is given by the following SDE

$$dF(t, T) = F(t, T)\sigma(t, T)dB_t, \quad (5)$$

where dB_t is a differential of a Brownian motion and $\sigma(t, T) = \sigma e^{-\alpha(T-t)}$ is the volatility at time t for a contract maturing at date T . The parameter σ reflects the entire forward curve volatility and the constant α gives the speed

of how fast the volatility decrease with time to maturity. In this model it is the Brownian motion that accounts for the uncertainty. One can notice that the SDE describing the dynamics has the solution of a GBM with no drift term. Since the dynamics do not include a drift term futures prices derived using this model are martingales.

From equation (5) it can be noticed that the volatility is exponentially decreasing with time to maturity. Hence the one factor model models short maturity contract as more volatile than more distant. This coincides with Samuelson Hypothesis. However empirical observation suggests that it is not really the case that contracts with far away maturities have volatilities approaching zero. Empirical observations also suggest that the forward curve seem to changes shape in more complex ways than one factor of uncertainty can capture. These lead us to the multi factor model that will be discussed in the following section where several uncertainty factors drive the evolution of the forward curve [12].

Multi factor model

The behaviour of the forward curve is more complicated than the one factor model can capture. If several uncertainty factors are taken into consideration one arrives with a more general model called a multi factor model. In this model the dynamics are given by the following SDE

$$dF(t, T) = F(t, T) \sum_{i=1}^n \sigma_i(t, T) dB_t^i, \quad (6)$$

where dB_t^i are differentials of Brownian motions and $\sigma_i(t, T)$ are volatilities. The n independent Brownian motions multiplied with the corresponding volatility function reflect how the curve in each point is affected by each uncertainty factor. In most cases three factors are enough to reflect the evolution of the curve. These factors symbolise "shift", "tilt" and "bending" the forward curve. The volatility functions and the number of uncertainty factors can be obtained by performing PCA (Principal Component Analysis) on historical price data.

For futures written on commodities experiencing seasonal price patterns the general multi factor model is not directly applicable but must firstly be modified, see [12].

4.2 The static arbitrage based approach

The static arbitrage based approach is based on finding dynamics that drive the evolution of the futures prices and then using this factor to derive relations for futures price while not introducing arbitrage opportunities. This

means that the futures price should be equal to the current price of the physical commodity and the price of storing it until maturity.

There exist several modelling methods under this approach. In this section two of them will be presented. The first model that is presented uses the spot price and convenience yield as stochastic factors that drive the evolution of futures prices. The second model modifies the classical of the cost-of-carry relation by substituting the spot price with the average futures price and introducing a constant representing seasonality [9].

Gibson and Schwartz two factor model

This model is an extension of the one factor models that only models the spot prices as a mean reverting process. In the two factor model the convenience yield is also assumed to be stochastic and represented by a mean reverting process. The stochastic factors in the two factor model have dynamics given by the following equations

$$\begin{aligned}dS_t &= (\mu - \gamma_t)S_t dt + \sigma_1 S_t dB'_t \\d\gamma_t &= \alpha'(\alpha - \gamma_t)dt + \sigma_2 \gamma_t dB''_t.\end{aligned}$$

In the above set of equations γ_t represents the convenience yield, S_t is the spot price, α' is the speed of mean reversion for the convenience yield, μ and α are constant mean, dB'_t and dB''_t are differentials of Brownian motion and σ_1 and σ_2 represent the volatility. In this model the Brownian motions B'_t and B''_t are positively correlated according to the following relation

$$dB''_t dB'_t = c dt,$$

where c is the correlation constant. The reason for choosing correlated Brownian motions is because when the spot price increases, commodity inventory levels drop. The increase in spot price and drop in inventory leads to an increasing convenience yield which result in limited amounts of commodity available. The limited availability will reflect in an increase of futures and spot prices. However the increase of futures price should be less than for the spot price. If the other case occurs, that is to say if inventories levels increase, then it should be the other way around. In this model the interest rate is assumed to be constant, however there exists an extension of the two factor model called the three factor model that also models the interest rate as a stochastic process [15].

These chosen stochastic factors can then be used to derive relation for futures prices while still preserving no-arbitrage arguments by using the cost-of-carry relation [10].

The seasonal cost-of-carry model

The model presented by [10] is based on the static arbitrage approach and includes a modification of the classical cost-of-carry relation, by replacing the spot price with the average futures price and introducing a new parameter that reflects seasonal features. According to the model the state variables that drive the evolution of futures prices are given by the stochastic convenience yield and the average futures price. The model is called *seasonal cost-of-carry model* and the forward price at time t for a contract with maturity date T is given by

$$F(t, T) = \bar{F}(t)e^{s(T) - \delta(t, T-t)(T-t)}, \quad (7)$$

where $\bar{F}(t)$ is the average futures price for day t defined by

$$\bar{F}(t) = \left(\prod_{T=1}^n F(t, T) \right)^{\frac{1}{n}}, \quad (8)$$

where n is the most faraway maturity. Taking the logarithm of the above relation gives the logarithm of the average futures price

$$\ln(\bar{F}(t)) = \frac{1}{n} \left(\sum_{T=1}^n \ln(F(t, T)) \right). \quad (9)$$

For commodities experiencing seasonality the number of contracts used to construct $\ln(\bar{F}(t))$ must be multiples of twelve. Because the average forward price is required not have any seasonal properties according to the model.

There are several reason for why [10] argue to use the average forward price as the first state variable instead of the spot price. The first reason is because the spot price often includes unobservable properties such as for example seasonality. The other reason is because the spot price in some commodity markets is not available. For those markets the futures price for the nearest maturity contract is used instead. However this approximation is questionable since often futures and spot market differ significantly from each other. Another positive aspect by using the average futures price instead of the spot price is because it is a more solid quantity.

Since the average futures price is constructed so that it does not include any seasonal properties this will also hold for the logarithm of the average futures price. Therefore $\ln \bar{F}(t)$ will behave like a process that oscillates around a constant mean and can be represented by an Ornstein-Uhlenbeck process. The SDE under the real world probability measure representing the dynamics of $\ln(\bar{F}(t))$ is given by

$$\begin{cases} \ln(\bar{F}(t)) = \alpha\mu dt - \alpha \ln(\bar{F}(t))dt + \sigma dB_t^1 \\ \ln(\bar{F}(s)) = \text{constant}. \end{cases} \quad (10)$$

If one for simplicity set $X_t = \ln(\bar{F}(t))$ the following equivalent SDE is obtained

$$\begin{cases} dX_t = \alpha\mu dt - \alpha X_t dt + \sigma dB_t^1 \\ X_s = \text{constant}, \end{cases} \quad (11)$$

where α is the speed of mean reversion, μ is the long term mean, σ is the volatility, dB_t^1 is the differential of a Brownian motion and X_s is the initial condition [10]. In the rest of the report the term state variable will be used interchangeably for the logarithm of average futures price and average futures price.

The analytical solution to (11) is determined see Appendix B for computations and is given by

$$X_t = X_s e^{-\alpha(t-s)} + \mu(1 - e^{-\alpha(t-s)}) + \int_s^t e^{-\alpha(t-u)} \sigma dB_u^1. \quad (12)$$

The third term in (12) is a stochastic integral with a deterministic integrand and is thereby normally distributed with mean 0 and variance $\int_s^t e^{-2\alpha(t-u)} \sigma^2 du$. Therefore the distribution for X_t is given by

$$X_t \sim N \left(X_s e^{-\alpha(t-s)} + \mu(1 - e^{-\alpha(t-s)}), \frac{\sigma^2}{2\alpha} (1 - e^{-2\alpha(t-s)}) \right). \quad (13)$$

[4].

The next parameter in equation (7) is called the *seasonal premia* and is denoted $s(T)$. This parameter depends on delivery date $T = 1, \dots, 12$ where 1 represents the month January and 12 represents December. The seasonal premia is defined as the average deviation from the price of a contract maturing in a certain calendar month from the average futures price. The parameter is deterministic given in percent and is estimated from historical price data. According to [10] it seems reasonable to demand that the sum of seasonal premia for all calendar months to be zero. This is because the parameter is an average deviation from the average futures price.

The role of the seasonal premia can be shown with the following example; the seasonal premia for a contract maturing the first February 2010, denoted $s(2)$ will be the same as for a contract maturing the first February 2011

with the same underlying commodity. Hence the effect of the parameter on the futures price is independent of current time. The seasonal premia can be positive, negative or zero. According to equation (7) the futures price should be either at premium or discount with respect to $\bar{F}(t)$. How much the futures price deviates from the average futures price is mainly determined by the seasonal premia. But not all deviation of $F(t, T)$ from the average futures price are due to the delivery month. That is why the stochastic parameter $\delta(t, T - t)$ is introduced in the model. The parameter is called *stochastic convenience yield* and can be compared to the convenience yield in the classical cost-of-carry relation. The stochastic convenience yield depends on both the maturity date T and the time to maturity $T - t$. For every maturity date T the stochastic convenience yield gives how the shape of the forward curve differ from seasonal patterns.

In order for relation (9) to hold the sum of the *aggregated convenience yield* denoted $(T - t)\delta(t, T - t)$ for $T = 1, \dots, 12$ must be equal to zero see Appendix C for derivation. According to the model all systematic deviations of the futures price from the average futures price are because of seasonal effects. Hence the stochastic convenience yield must fluctuate around zero and can therefore be modelled as an Ornstein-Uhlenbeck process with zero mean. If one for simplicity set that $\delta(t, T - t) = \delta_t^\kappa$ where $\kappa = T - t$ the SDE under the real world measure representing the dynamics for the stochastic convenience yield is given by

$$\begin{cases} d\delta_t^\kappa = -a^\kappa \delta_t^\kappa dt + b^\kappa dB_t^2 \\ \delta_s^\kappa = \text{constant}, \end{cases} \quad (14)$$

where b^κ represents the volatility, a^κ is the speed of mean reversion, dB_t^2 is the differential of a Brownian motion and δ_s^κ is the initial value. In order for relation (9) to hold the same Brownian motion must be the uncertainty factor for the whole term structure of the stochastic convenience yield. It is also important to notice that the Brownian motion that drives the evolution of $\ln(\bar{F}(t))$ is independent of the Brownian motion representing the uncertainty in the process for δ_t^κ [10].

An analytic solution to equation (14) can be determined, see Appendix B and is given by

$$\delta_t^\kappa = \delta_s^\kappa e^{-a^\kappa(t-s)} + \int_s^t e^{-a^\kappa(t-u)} b^\kappa dB_u^2. \quad (15)$$

The second term in the above expression is a stochastic integral with a deterministic integrand and is therefore normally distributed with zero mean and variance $\int_s^t e^{-2a^\kappa(t-u)} (b^\kappa)^2 du$. Hence distribution for δ_t^κ is given by

$$\delta_t^\kappa \sim N \left(\delta_s^\kappa e^{-a^\kappa(t-s)}, \frac{(b^\kappa)^2}{2a^\kappa} (1 - e^{-2a^\kappa(t-s)}) \right). \quad (16)$$

[4].

According to [10] the model works for seasonal, non seasonal commodities and is possible to apply for futures with not equally spaced maturities. Due to that the model does not include the spot price it is possible to apply to commodities that are not storable such as electricity.

The dynamics that drive the evolution of futures prices for the seasonal cost-of-carry model can now be analysed. Starting by computing the logarithm of equation (7) which gives

$$\ln(F(t, T)) = \ln(\bar{F}(t)) + s(T) - (T - t)\delta(t, T - t).$$

Then let $\kappa = T - t$ and apply Ito's formula to the above equation and the following equation is obtained

$$d \ln(F(t, T)) = d \ln(\bar{F}(t)) - \kappa d\delta(t, \kappa) - \delta(t, \kappa) dt. \quad (17)$$

The solution to the above equation can be found see Appendix D. By properties of the stochastic integral the variance of futures prices according to the model is

$$\sigma_{futures}^2(t, \kappa) = b^{\kappa^2} \kappa^2 + \sigma^2. \quad (18)$$

From the above relation it can be noticed that the futures price according to (7) will have a variance that depends on only κ [10].

4.3 Properties of different models

Models presented in the previous section have different properties that make them applicable for different purposes. In this section positive and negative aspects of these models will be discussed. Lastly the method chosen to create the reference curve will be presented.

First models under the martingale based approach are presented. These models are appropriate to use for derivative pricing. However they are not applicable for risk measurement calculation since they model futures prices in the risk neutral world. Methods that are based on modelling under the risk neutral measure cannot be compared to market data. In this thesis it is proposed to validate the market forward curve by simulating a reference

curve. Therefore modelling approaches under the risk neutral measures are not applicable.

For models under the static arbitrage based approach futures prices can be modelled under both the risk neutral measure and the real world measure by changing measures for the state variable processes. This makes futures prices modelled under this approach possible to compare to market data [9].

The first model presented under the static arbitrage based approach was the two factors Gibson and Schwartz model. This model chooses to model the evolution of futures prices by using stochastic processes for the convenience yield and spot price. The main negative aspect of this model is that it is not applicable to seasonal commodities [10]. Another negative aspect of the model is that it includes state variables that are not directly observable [18].

Lastly the seasonal cost-of-carry model was presented. Positive aspects of this model are that it is applicable for seasonal commodities and that the spot price has been replaced by a more stable quantity represented by the average futures price. The seasonal cost-of-carry model is also possible to apply to a wider range of commodities than models using the classical cost-of-carry relation [10].

The method chosen to create the reference curve is to simulate futures prices using the seasonal cost-of-carry model and perform linear interpolation between the simulated values. The seasonal cost-of-carry model was chosen because

- The model can be used to simulate futures prices for futures with seasonal price patterns.
- Simulated values can be compared to market data.
- The first fundamental factor is the average futures price which is a more stable parameter than the spot price.

5 Application of seasonal cost of carry model

In this section it will be described how to apply the seasonal cost-of-carry model to historical price data. First parameter estimation from historical data is going to be described. After that methods for simulating new samples of the state variables together with maximum-likelihood estimation procedure will be presented. Lastly everything is put together to simulate futures prices and building the reference curve.

5.1 Estimation of parameters

Firstly a data set of historical forward prices is needed. The set of historical data is given by the following matrix

$$D = \begin{pmatrix} F(m, 1) & F(m, 2) & \cdots & F(m, 12) \\ F(m-1, 1) & F(m-1, 2) & \cdots & F(m-1, 12) \\ \vdots & \vdots & \cdots & \vdots \\ F(0, 1) & F(0, 2) & \cdots & F(0, 12) \end{pmatrix}, \quad (19)$$

where the first column represent futures prices for a contract with delivery in January for $m + 1$ trading days and the last column represent futures prices for $m + 1$ trading days for a contract with delivery in December.

By using data in matrix D and applying equation (9) a time series $\{\ln(\bar{F}(t))\}_{t=0}^m$ is constructed for the logarithm of average futures price.

In order to estimate the seasonal premia $s(T)$ one can start by computing the logarithm of equation (7) which gives

$$\ln(F(t, T)) = \ln(\bar{F}(t)) + s(T) - (T - t)\delta(t, T - t). \quad (20)$$

The seasonal premia is estimated as the mean value of the difference between the logarithm of the futures price at day t for a contract with maturity date T and the logarithm of the average futures for the same day. The formula for estimating the seasonal premia is given by

$$\hat{s}(T) = \frac{1}{m+1} \sum_{t=0}^m (\ln F(t, T) - \ln(\bar{F}(t))). \quad (21)$$

The aggregated convenience yield $\kappa\delta(t, \kappa)$ where $\kappa = T - t$ can be determined from equation (20) and is given by

$$\kappa\delta(t, \kappa) = \ln(F(t, T)) - \ln(\bar{F}(t)) - s(T). \quad (22)$$

Notice that the aggregated convenience gives the model residuals. Inserting $\hat{s}(T)$ gives the estimation equation for the aggregated convenience yield

$$\kappa \hat{\delta}(t, \kappa) = \ln(\bar{F}(t)) - \ln(F(t, T)) + \hat{s}(T). \quad (23)$$

From the above equation it follows that the stochastic convenience yield can be estimated by

$$\hat{\delta}(t, T - t) = \frac{1}{T - t} (\ln(\bar{F}(t)) - \ln(F(t, T)) + \hat{s}(T)). \quad (24)$$

From equation (24) the time series $\{\delta(t, T - t)\}_{t=0}^m$ is obtained. In the following calculations $\{\delta(t, T - t)\}_{t=0}^m$ will be denoted $\{\delta_t^\kappa\}_{t=0}^m$ where $\kappa = T - t$.

The observed time series given by $\{\ln(\bar{F}(t))\}_{t=0}^m$ and $\{\delta_t^\kappa\}_{t=0}^m$ can be used estimate parameters in the state variable dynamics. The sample points constructing the observed time series have equally spaced observation where the time between two observations is denoted Δt . The procedure for estimating parameters in state variable process will be presented in the following section together with a description of how new samples can be simulated. Lastly everything will be put together to simulate samples of futures prices using the seasonal cost-of-carry relation [10].

5.2 Simulating new samples

5.2.1 Simulation equations

Because the distribution of the logarithm of the average futures price is given by (13). The exact updating formula for simulating trajectories of the process is given by

$$X_t = X_{t-1} e^{-\alpha \Delta t} + \mu(1 - e^{-\alpha \Delta t}) + \sqrt{\frac{\sigma^2(1 - e^{-2\alpha \Delta t})}{2\alpha}} Z. \quad (25)$$

where μ , α , σ are constants, X_{t-1} is the starting guess, Δt is the time step and Z is a standard normal variable. The formula is iterative and simulates exact trajectories regardless of the size of the time step.

Since the distribution of the process representing the stochastic convenience yield is given by (16) new samples can be simulated by

$$\delta_t^\kappa = \delta_{t-1}^\kappa e^{-a^\kappa(\Delta t)} + \sqrt{\frac{(b^\kappa)^2}{2a^\kappa}(1 - e^{-2a^\kappa \Delta t})} W, \quad (26)$$

where α^κ , b^κ are constants, δ_{t-1}^κ is the start guess, Δt is the time step and W is a standard normal variable. This formula is also iterative and will simulate exact trajectories regardless of the time step. Notice that the simulation equations are autoregressive process of order one [14].

5.2.2 Interference for diffusion processes

In this sections the method for estimating parameters in equation (25) and (26) will be presented. In the article by [10] it is proposed to estimate parameters by exact maximum-likelihood method. This is a suitable method to use for these processes since the distribution can be found analytically [10].

From equation (26) it follows that the transitional density is given by

$$\delta_t^\kappa | \delta_{t-1}^\kappa \sim N \left(\delta_{t-1}^\kappa e^{-a^\kappa \Delta t}, \sqrt{\frac{(b^\kappa)^2}{2a^\kappa} (1 - e^{-2a^\kappa \Delta t})} \right).$$

For the discrete sample $\delta_0^\kappa, \dots, \delta_m$ the transitional density gives the following likelihood function

$$L(b^\kappa, a^\kappa) = \prod_{t=1}^m \frac{1}{\sqrt{2\pi \left(\frac{(b^\kappa)^2}{2a^\kappa} (1 - e^{-2a^\kappa \Delta t}) \right)}} \exp \left\{ -\frac{(\delta_t^\kappa - \delta_{t-1}^\kappa e^{-a^\kappa \Delta t})^2}{2 \left(\frac{(b^\kappa)^2}{2a^\kappa} (1 - e^{-2a^\kappa \Delta t}) \right)} \right\}.$$

Setting $(\sigma')^2 = \frac{(b^\kappa)^2}{2a^\kappa} (1 - e^{-2a^\kappa \Delta t})$ and taking the logarithm of the above equations gives the log-likelihood function

$$\ln(L(b^\kappa, a^\kappa)) = -\frac{m}{2} \ln(2\pi) - m \ln(\sigma') - \frac{1}{2(\sigma')^2} \sum_{t=1}^m (\delta_t^\kappa - \delta_{t-1}^\kappa e^{-a^\kappa \Delta t})^2 \quad (27)$$

[22].

Estimators for a^κ and b^κ are determined so that the log-likelihood function is maximized. This is done by finding for which a^κ and σ' the partial derivatives are zero. Hence the following set of equation need to be solved

$$\frac{\partial \ln(L(b^\kappa, a^\kappa))}{\partial a^\kappa} = 0$$

$$\frac{\partial \ln(L(b^\kappa, a^\kappa))}{\partial \sigma'} = 0$$

The above set of equation can be solved analytically and estimators for a^κ and σ' can be found. Due to the relation between b^κ and σ' the estimator of b^κ is also determined. Hence the maximum-likelihood estimators of the parameters are given by

$$a^\kappa = -\frac{1}{\Delta t} \ln \left(\frac{\sum_{t=1}^m \delta_t^\kappa \delta_{t-1}^\kappa}{\sum_{t=1}^m (\delta_{t-1}^\kappa)^2} \right) \quad (28)$$

and

$$b^\kappa = \sqrt{\frac{\frac{2a^\kappa}{m} \sum_{t=1}^m (\delta_t^\kappa - \delta_{t-1}^\kappa e^{-a^\kappa \Delta t})^2}{1 - e^{2a^\kappa \Delta t}}}. \quad (29)$$

[2].

Next, the steps for estimating parameters in equation (25) will be presented. From (25) it follows that the transitional density is given by

$$X_t | X_{t-1} \sim N \left(X_{t-1} e^{-\alpha \Delta t} + \mu(1 - e^{-\alpha \Delta t}), \sqrt{\frac{\sigma^2}{2\alpha}(1 - e^{-2\alpha \Delta t})} \right).$$

The transitional density gives the following likelihood function for observations X_0, \dots, X_m

$$L(\alpha, \mu, \sigma) = \prod_{t=1}^m \frac{1}{\sqrt{2\pi(\frac{\sigma^2}{2\alpha}(1 - e^{-2\alpha \Delta t}))}} \exp \left\{ -\frac{(X_t - X_{t-1} e^{-\alpha \Delta t} + \mu(1 - e^{-\alpha \Delta t}))^2}{2(\frac{\sigma^2}{2\alpha}(1 - e^{-2\alpha \Delta t}))} \right\}.$$

Setting $(\sigma'')^2 = \frac{\sigma^2}{2\alpha}(1 - e^{-2\alpha \Delta t})$ and taking the logarithm of the above equation gives the corresponding likelihood function

$$\begin{aligned} \ln(L(\alpha, \mu, \sigma)) &= -m \ln(\sqrt{2\pi}) - m \ln(\sigma'') - \\ &\quad \frac{1}{2(\sigma'')^2} \sum_{t=1}^m (X_t - X_{t-1} e^{-\alpha \Delta t} - \mu(1 - e^{-\alpha \Delta t}))^2. \end{aligned} \quad (30)$$

[22].

Now the aim is to determine estimators for parameters α , μ and σ so that the log-likelihood function maximized. The log-likelihood function is maximized if the following conditions are fulfilled

$$\frac{\partial \ln(L(\alpha, \mu, \sigma''))}{\partial \alpha} = 0 \quad (31)$$

$$\frac{\partial \ln(L(\alpha, \mu, \sigma''))}{\partial \mu} = 0 \quad (32)$$

$$\frac{\partial \ln(L(\mu, \alpha, \sigma''))}{\partial \sigma''} = 0 \quad (33)$$

From condition (32) to (33) estimators for α , μ and σ'' can be determined analytically. Due to the relation between σ'' and σ the estimator for σ can also be found. The maximum-likelihood estimators are given by

$$\alpha = -\frac{1}{\Delta t} \ln \left(\frac{m \sum_{t=1}^m X_{t-1} X_t - \sum_{t=1}^m X_t \sum_{t=1}^m X_{t-1}}{m \sum_{t=1}^m X_{t-1}^2 - (\sum_{t=1}^m X_{t-1})^2} \right) \quad (34)$$

$$\mu = \frac{\sum_{t=1}^m X_t - e^{-\alpha \Delta t} \sum_{t=1}^m X_{t-1}}{n(1 - e^{-\alpha \Delta t})} \quad (35)$$

$$\sigma = \sqrt{\frac{2\alpha(\sigma'')^2}{1 - e^{-2\alpha \Delta t}}}, \quad (36)$$

where

$$(\sigma'')^2 = \frac{1}{m} \sum_{t=1}^m \left(X_t - e^{-\alpha \Delta t} X_{t-1} - \mu(1 - e^{-\alpha \Delta t}) \right)^2$$

[2].

When parameters in (11) and (14) have been estimated new samples can be generated by using simulation equations (25) and (26).

5.2.3 Building references curves

The next step is to simulate futures prices. This is done by applying the seasonal cost-of-carry relation given by equation (7) together with simulated samples for the state variables and the estimated seasonal premia [10]. By performing linear interpolation between the simulated futures prices the reference curve is built. Since the seasonal cost-of-carry model models futures prices under the real world probability measures these curves can now be compared to corresponding market curves.

6 Results

In this section the seasonal cost-of-carry model is applied to commodity futures with seasonal price dependence. UK natural gas futures are chosen since they have a seasonal price pattern and equally spaced maturities up to one year. The result is presented in the following section.

6.1 UK natural gas futures

The historical data that will be used for estimations are prices for UK natural gas futures traded on ICE. The contract information is presented in Table 1.

Name	UK Natural Gas Futures
Maturities	Jan, Feb, Mar, Apr, May, Jun, Jul, Aug, Sep, Oct, Nov, Dec
Contract Size	1000 therms per day per delivery period
Price quotation	Price of contract per therm in sterling and pence
Smallest trading size	5000 therms per day

Table 1: Table shows contract information for UK natural gas futures traded on ICE [5].

From Table 1 it can be seen that UK natural gas futures have equally spaced maturities with contracts that mature every calendar month. It can also be seen that the contract size depend on delivery month. The different contract sizes are shown in Table 2.

Jan, Mar, May, Jul, Aug, Oct, Dec	31000 therms
Apr, Jun, Sep, Nov	30000 therms
Feb (365 days per year)	28000 therms
Feb (366 days per year)	29000 therms

Table 2: Table shows contract sizes for different maturity months for UK natural gas futures traded on ICE [5].

The seasonal cost-of-carry model will be used to generate reference curves for every trading day in December 2013. These curves will then be compared to the corresponding market curve. In order to simulate the model the following assumptions are made

- Every year is assumed to have 250 trading days.
- Every month is assumed to have 21 trading days.
- Natural gas futures have a delivery period during the month of maturity. Hence it will be assumed that every contract matures on the first every calendar month [19].
- The time to maturity is assumed to be constant for every available time to maturity in the data set. That is to say the contract with the closest maturity has $\kappa = \frac{1}{12}$ and the contract maturing in 11 months from the contract with the closest maturity has $\kappa = \frac{12}{12}$ [10].

The set of historical price data that is going to be used for parameter estimation are settlement prices for the time period 2011-01-01 to 2013-11-30 for futures that mature every calendar month during 2014. That is to say the historical data set used for parameter estimation is given by

$$F(t, T) \quad t \in \{0, \dots, 752\} \quad \text{for} \quad T \in \{1, \dots, 12\},$$

where $T = 1$ symbolises the calendar month January and $T = 12$ symbolises the month December. The total number of observation constructing the data set is 753.

Estimates based on the above described data are going to be used to simulate forward prices given by the following set

$$F(t, T) \quad t \in \{753, \dots, 774\} \quad \text{for} \quad T \in \{1, \dots, 12\}.$$

The reason for choosing contracts with maturities up to one year is because the state variable $\bar{F}(t)$ will then not have any seasonal properties which is a requirement for the chosen model.

To analyse the seasonal price pattern for UK natural gas futures the forward curve for a specific day is constructed. This is done by performing linear interpolation between market prices for contracts with maturities up to twelve months. The forward curve for 2013-01-01 is shown in Figure 3 where left end of the curve consist of the contract maturing the next month and the right end of the contract with the most distant maturity.

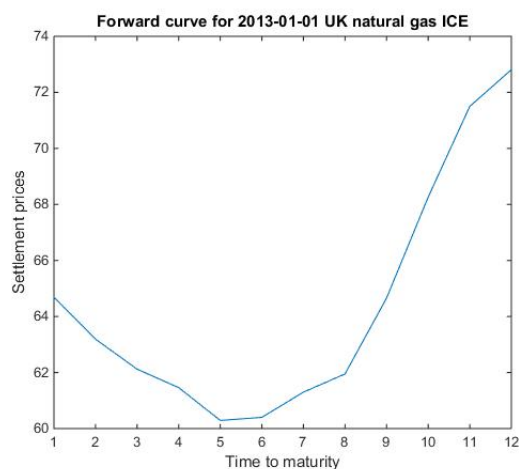


Figure 3: Forward curve for 2013-01-01 where the next contract to mature is February 2013.

From Figure 3 it can be seen that the price peaks for contracts maturing in the winter season. It can also be seen that futures prices drops for contracts with delivery in the summer months. The behaviour illustrated in Figure 3 is as expected since the demand for gas is higher in the winter because natural gas is mainly used for heating facilities. The aim is to generate reference curves by simulating futures prices with the seasonal cost-of-carry model. Hopefully the generated curves will reflect the seasonal behaviour shown in Figure 3 and not deviate significantly from the market curve.

First the modelling procedure for the average futures price is presented, and then the seasonal parameter followed by the stochastic convenience yield. Finally everything is put together by using the seasonal cost-of-carry relation generating reference curves.

6.1.1 The average futures price

Now the modelling procedure for $\bar{F}(t)$ is going to be presented. Starting by analysing the evolution of futures price for every $T = 1, \dots, 12$ that construct the historical data set. The time series of futures prices for maturity dates $T = 1, \dots, 12$ for the period 2011-01-01 to 2013-11-20 is shown in Figure 4.

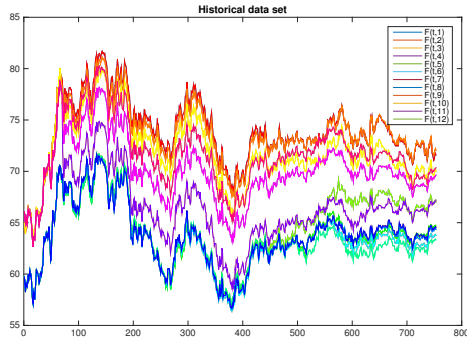


Figure 4: Time series for UK natural gas futures for every $T = 1, \dots, 12$ constructing the historical data set.

From Figure 4 it can be seen the futures prices seem to be more volatile in the beginning of the observation period and stabilising during the last 400 trading days.

Next, the logarithm of average futures price is calculated using the historical price data shown in Figure 4 and equation (9). The resulting time series together with the spectral density is shown in Figure 5.

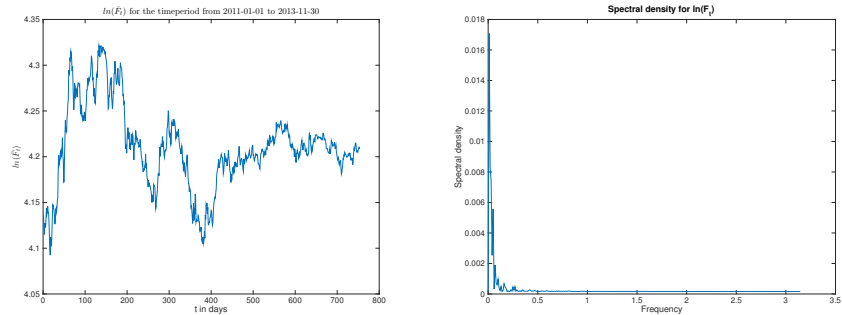


Figure 5: *Left:* Time series for logarithm of average futures price $\ln(\bar{F}(t))$ for the time period 2011-01-01 to 2013-11-30. *Right:* Spectral density for logarithm of average futures price.

From the left plot in Figure 5 it can be observed that time series seem to strive back to a long term mean. Hence the process appears to be mean reverting. However the speed of mean reversion seems to be quite slow in the beginning of the observation period. It can also be seen that the process seem to be more volatile in the beginning. From the right plot in Figure 5 it is verified that the seasonality has successfully been removed, since the spectral density peaks for frequencies close to zero [20]. This is as expected since the number of contracts used to calculate the logarithm of average

future price is 12.

In Figure 6 observed time series for $\ln(\bar{F}(t))$ is plotted together with $\ln(F(t, T))$ for $T = 1, \dots, 12$ for 2011-01-01 to 2013-11-30.

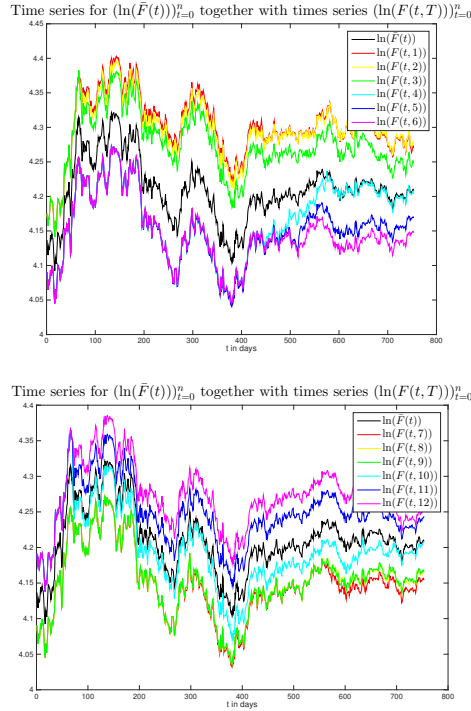


Figure 6: *Upper:* Time series for $\ln(\bar{F}(t))$ together with time series for logarithm of futures prices for maturity dates $T = 1, \dots, 6$ for $n=752$. *Lower:* Time series for $\ln(\bar{F}(t))$ together with time series for logarithm of futures prices for maturity dates $T = 6, \dots, 12$ for $n=752$.

In order to simulate forward price data, new trajectories for the process generating the logarithm of average futures price must be simulated. However first parameters in equation (11) must be estimated. This was done by performing maximum-likelihood estimation using observations shown in the left plot Figure 5. The estimated parameters are shown in Table 3.

μ	α	σ
4.2166	3.6722	0.1153

Table 3: Table shows estimates for μ , α and σ .

Estimates shown in Table 3 seem reasonable when comparing to the observed time series in Figure 5. Since it appears that the time series has a long term mean around 4.2, which is near the value obtained from the estimation. The time series also show that the speed of mean reversion seem to be quite slow which coincide with the estimated parameter. In the section *Evaluation of results* more detailed analysis of the estimation procedure will be presented.

The next step is to simulate 21 sample paths of $\ln(\bar{F}(t))$ for every trading day in December 2013. This was done by applying equation (25) together with estimates show in Table 3. The time step used was $\Delta t = \frac{1}{250}$ with the starting value given by the last observed value in the time series for $\ln(\bar{F}(t))$. Figure 7 shows the result when simulating one hundred trajectories for every trading day.

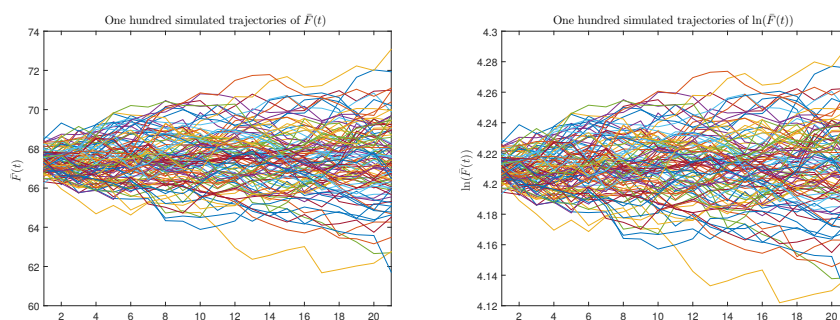


Figure 7: *Left:* One hundred simulated trajectories for $\ln(\bar{F}(t))$ for 21 days. *Right:* One hundred simulated trajectories for $\bar{F}(t)$ for 21 days.

6.1.2 Seasonal premia

The next parameter to estimate is the seasonal premia. This is done by using equation (21). The result for every calendar month is shown in Table 4.

Month	Seasonal premia in per cent
Jan	9.1601
Feb	8.7650
Mar	6.5831
Apr	-4.0886
May	-5.6631
Jun	-6.2542
Jul	-6.0660
Aug	-5.6815
Sep	-5.6362
Oct	-1.2644
Nov	3.8653
Dec	6.2807

Table 4: Table shows the estimated seasonal premia for UK natural gas futures traded on ICE.

The increase in futures prices for contracts with maturities in the winter months is verified by the result shown in Table 4. Since the seasonal premia is much larger for contracts with delivery in the winter in comparison to contracts with maturities in the spring, summer and early in the autumn. According to [10] the sum of the seasonal premia for all calendar months is zero. This is verified for the result presented in Table 4.

6.1.3 Convenience yield

After that the aggregated convenience yield is estimated. This is done by applying equation

$$\kappa \hat{\delta}(t, \kappa) = \ln(\bar{F}(t)) - \ln(F(t, T)) + \hat{s}(T),$$

where $T = 1, \dots, 12$. The resulting time series are shown in Figure 8 to Figure 13 for every $T = 1, \dots, 12$.

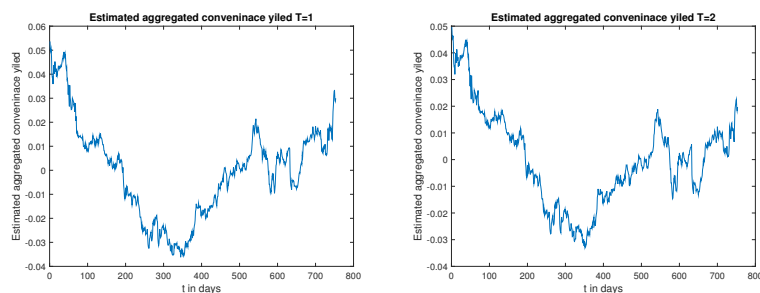


Figure 8: *Left:* Estimated time series for aggregated convenience yield for $T = 1$ for all trading days in the historical data set. *Right:* Estimated time series for aggregated convenience yield for $T = 2$ for all trading days in the historical data set.

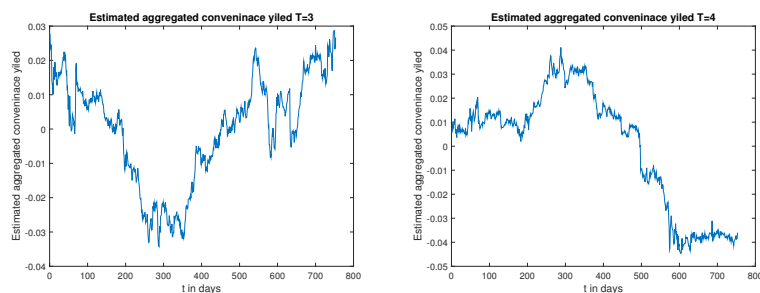


Figure 9: *Left:* Estimated time series for aggregated convenience yield for $T = 3$ for all trading days in the historical data set. *Right:* Estimated time series for aggregated convenience yield for $T = 4$ for all trading days in the historical data set.

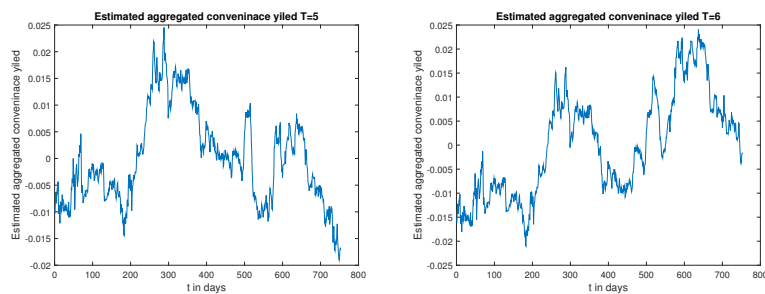


Figure 10: *Left:* Estimated time series for aggregated convenience yield for $T = 5$ for all trading days in the historical data set. *Right:* Estimated time series for aggregated convenience yield for $T = 6$ for all trading days in the historical data set.

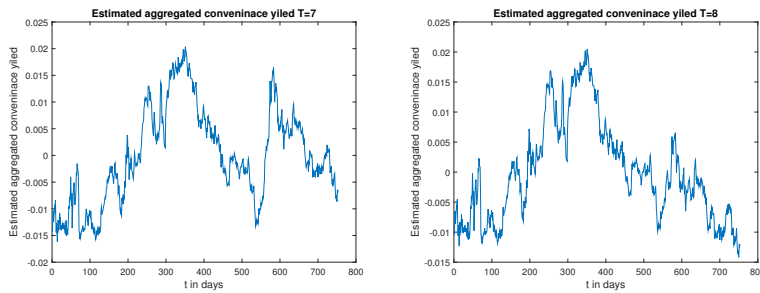


Figure 11: *Left*: Estimated time series for aggregated convenience yield for $T = 7$ for all trading days in the historical data set. *Right*: Estimated time series for aggregated convenience yield for $T = 8$ for all trading days in the historical data set.

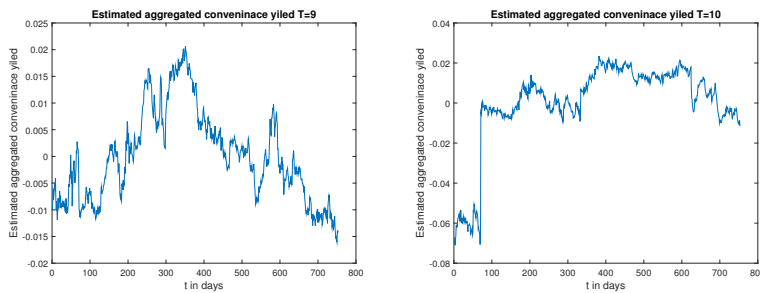


Figure 12: *Left*: Estimated time series for aggregated convenience yield for $T = 9$ for all trading days in the historical data set. *Right*: Estimated time series for aggregated convenience yield for $T = 10$ for all trading days in the historical data set.

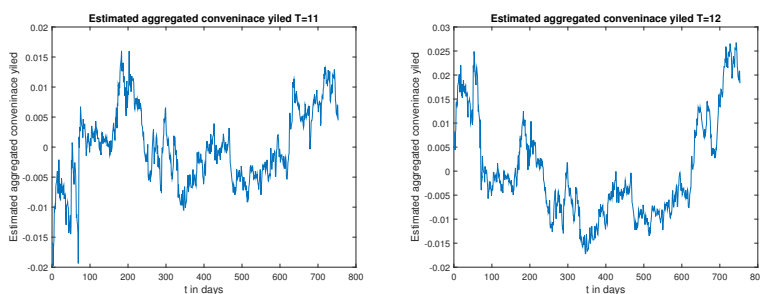


Figure 13: *Left*: Estimated time series for aggregated convenience yield for $T = 11$ for all trading days in the historical data set. *Right*: Estimated time series for aggregated convenience yield for $T = 12$ for all trading days in the historical data set.

According to [10] the estimated aggregated convenience is normally distributed for every T . This claim can be analysed graphically by investigating quantile quantile plots (qq-plots). Therefore qq-plots of standard normal quantiles against empirical quantiles of the aggregated convenience yield were computed. The result for $T = 1, \dots, 12$ is shown in Figure 14 to Figure 19.

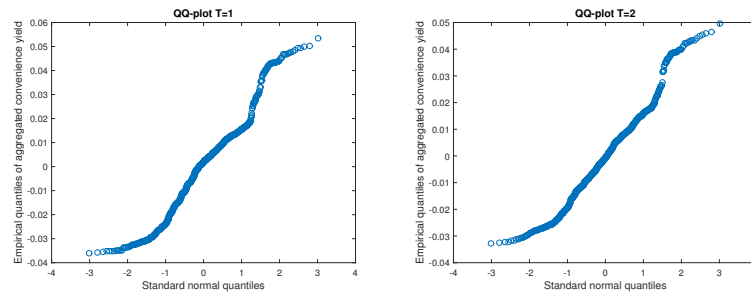


Figure 14: *Left:* QQ-plot for the model residuals for the contract with maturity date $T = 1$. *Right:* QQ-plot for the model residuals for the contract with maturity date $T = 2$.

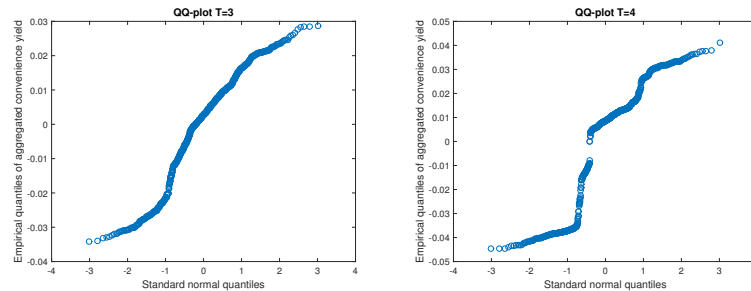


Figure 15: *Left:* QQ-plot for the model residuals for the contract with maturity date $T = 3$. *Right:* QQ-plot for the model residuals for the contract with maturity date $T = 4$.

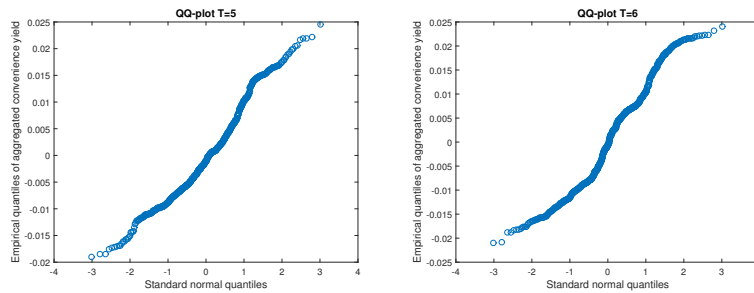


Figure 16: *Left:* QQ-plot for the model residuals for the contract with maturity date $T = 5$. *Right:* QQ-plot for the model residuals for the contract with maturity date $T = 6$.

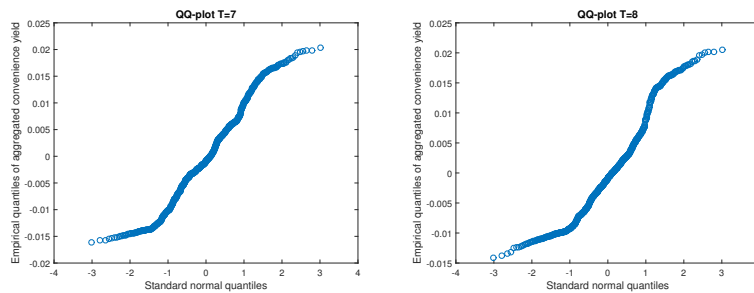


Figure 17: *Left:* QQ-plot for the model residuals for the contract with maturity date $T = 7$. *Right:* QQ-plot for the model residuals for the contract with maturity date $T = 8$.

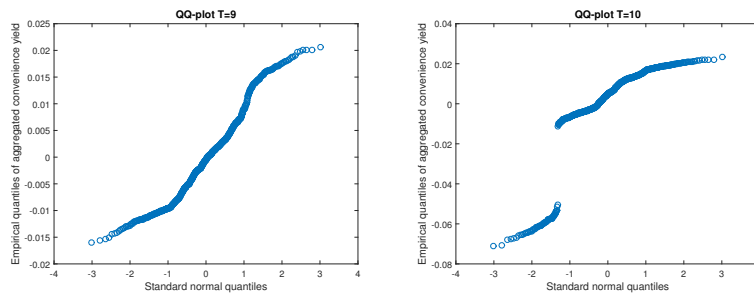


Figure 18: *Left:* QQ-plot for the model residuals for the contract with maturity date $T = 9$. *Right:* QQ-plot for the model residuals for the contract with maturity date $T = 10$.

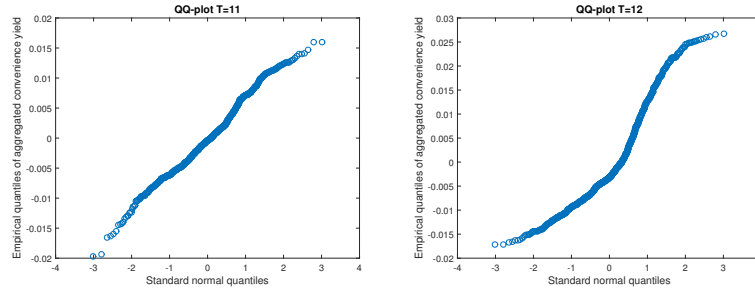


Figure 19: *Left:* QQ-plot for the model residuals for the contract with maturity date $T = 11$. *Right:* QQ-plot for the model residuals for the contract with maturity date $T = 12$.

Figure 14, 17, left plot in Figure 15, right plot in Figure 16 and left plot in Figure 18 shows S shaped qq-plots. This indicates that the left and right tail of the empirical distribution seem to be lighter than the tails of standard normal distribution.

The left plot in Figure 16 and Figure 19 seem linear. This indicates that the empirical distribution appear to be normally distributed. From the plots one can see that intersect is zero which corresponds to that the mean value is zero. However the slopes seem to be different from one, hence the empirical distribution has a standard deviation different from one. The slopes were calculated to be 0.0072 and 0.0059 respectively.

In the right plot in Figure 19 the left end of the qq-plot seems linear. Hence it appears that the left tail of the empirical distribution is normally distributed. However the right end of the plot curves down. This indicates that the right tail of the empirical distribution seem lighter than the normal distribution.

The right plots in Figure 15 and 18 are very different from linear. From Figure 6 it can be noticed that $F(t, 4)$ and $F(t, 10)$ go from deviating significantly from $\ln(\bar{F}(t))$ to not deviate much at all. Since equation (23) is used to estimate the time series for the aggregated convenience yield, these jumps of periods with little deviation from $\ln(\bar{F}(t))$ to periods with significant deviation probably explain the behaviour of the time series shown in the right plots in Figure 9 and 12. This is probably the reason for why the empirical distribution deviate significantly from the normal distribution shown in the right plots in Figure 15 and 18 respectively [7].

Summarising, the conclusion is drawn due to the result presented in Figure 14-19 that model residuals only for $\kappa = \frac{5}{12}, \frac{11}{12}$ seem to be normally distributed.

After that the stochastic convenience yield is estimated. This is done by

applying the following equation

$$\hat{\delta}(t, \kappa) = \frac{1}{\kappa} (\ln(\bar{F}(t)) - \ln(F(t, T)) + \hat{s}(T)).$$

It is chosen to normalize the time series for the aggregated convenience yield by dividing by months to maturity as an annualized quantity, that is to say $\kappa = \frac{1}{12}, \dots, \frac{12}{12}$ [10]. The resulting time series for the estimated stochastic convenience yield for every maturity date $T = 1, \dots, 12$ is shown Figure 20-25.

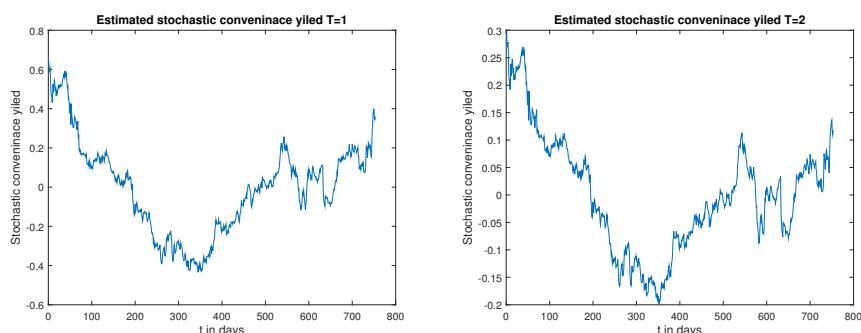


Figure 20: *Left:* Estimated stochastic convenience yield for contract with maturity date $T = 1$. *Right:* Estimated stochastic convenience yield for contract with maturity date $T = 2$.

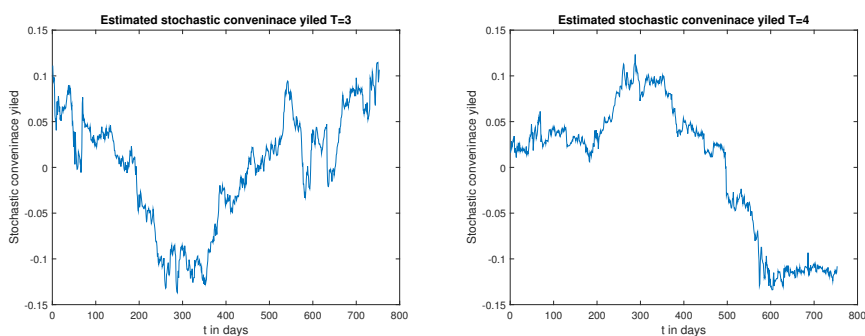


Figure 21: *Left:* Estimated stochastic convenience yield for contract with maturity date $T = 3$. *Right:* Estimated stochastic convenience yield for contract with maturity date $T = 4$.

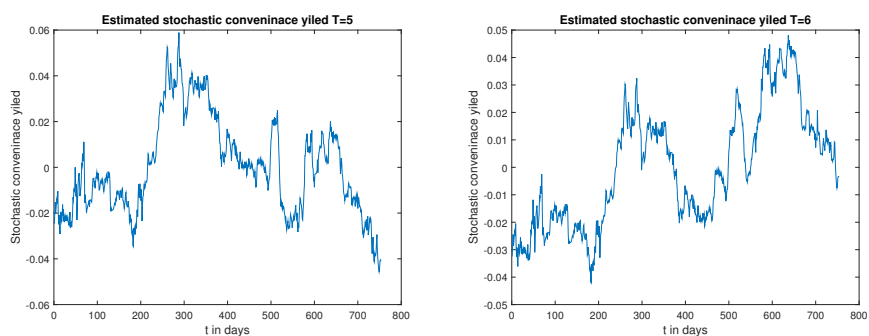


Figure 22: *Left:* Estimated stochastic convenience yield for contract with maturity date $T = 5$. *Right:* Estimated stochastic convenience yield for contract with maturity date $T = 6$.

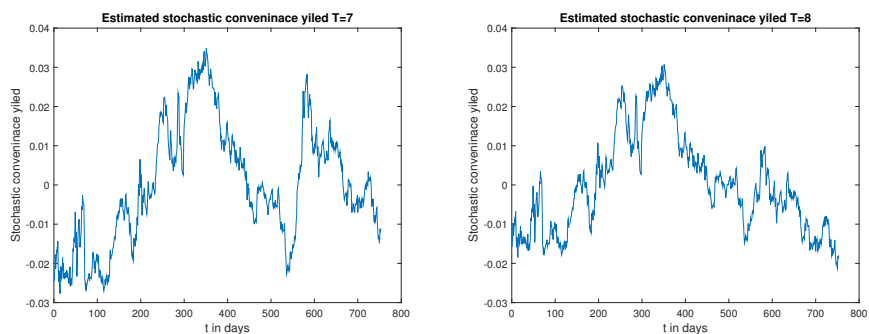


Figure 23: *Left:* Estimated stochastic convenience yield for contract with maturity date $T = 7$. *Right:* Estimated stochastic convenience yield for contract with maturity date $T = 8$.

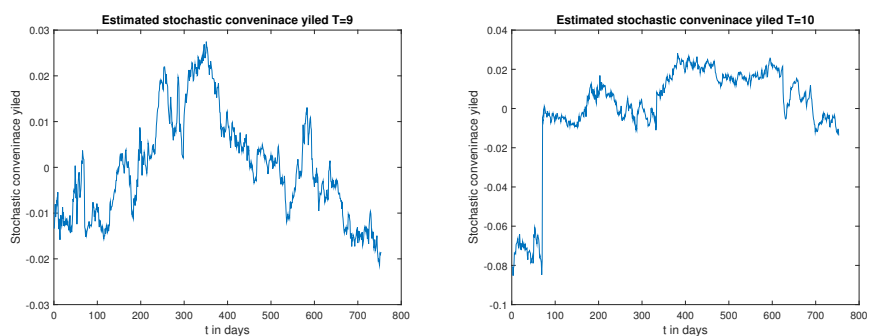


Figure 24: *Left:* Estimated stochastic convenience yield for contract with maturity date $T = 9$. *Right:* Estimated stochastic convenience yield for contract with maturity date $T = 10$.

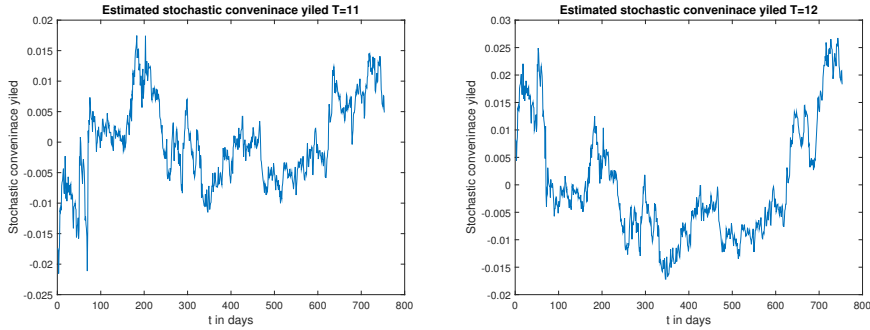


Figure 25: *Left:* Estimated stochastic convenience yield for contract with maturity date $T = 11$. *Right:* Estimated stochastic convenience yield for contract with maturity date $T = 12$.

In the section *Evaluation of results* the time series shown in Figure 20-25 are further analysed.

The next step is to estimate parameters in (14). This is done by using the time series $\{\delta_t^\kappa\}_{t=0}^{752}$ and maximum likelihood estimation. The result is shown in Table 5 as annual quantities.

κ	b^κ	a^κ
$\frac{1}{12}$	0.3355	1.8598
$\frac{2}{12}$	0.1627	2.3704
$\frac{3}{12}$	0.1147	1.7557
$\frac{4}{12}$	0.0776	0.2001
$\frac{5}{12}$	0.0523	2.7687
$\frac{6}{12}$	0.0441	2.5373
$\frac{7}{12}$	0.0354	3.0549
$\frac{8}{12}$	0.0304	2.9296
$\frac{9}{12}$	0.0274	2.7117
$\frac{10}{12}$	0.0532	3.8577
$\frac{11}{12}$	0.0289	10.0405
1	0.0263	2.7785

Table 5: Table shows estimates for b^κ and a^κ representing the volatility and speed of mean reversion for $\kappa = \frac{1}{12}, \dots, 1$.

The second column in Table 5 shows the estimated volatility for the convenience yield. It can be observed that the volatility goes to zero when κ goes to 1. Thus the modelling procedure seems to preserve Samuelssons Effect which says that contracts with nearer maturities are more volatile in comparison to more distant. This is because the futures price volatility according to the model is mainly determined by the convenience yield

volatility, see equation (18).

Parameters in Table 5 will now be compared to corresponding time series in Figure 20-25 since they were used as input in the maximum likelihood estimation.

Table 5 shows that for $\kappa = \frac{1}{12}, \frac{2}{12}, \frac{3}{12}$ the estimated volatilities are largest. This result seem reasonable when comparing to Figure 20-25. Because time series shown in Figure 20 and in the left plot in Figure 21 seem to have the largest spread of values in comparison to the rest of the plots. The estimated volatilities in Table 5 for $\kappa = \frac{4}{12}, \dots, \frac{12}{12}$ also seem reasonable since the spread of values shown in the right plot in Figure 21 to Figure 25 are quite small which corresponds to low estimates for the volatility. However it can be noticed that the volatility for $\kappa = \frac{10}{12}$ is larger than for $\kappa = \frac{9}{12}$. The reason for this is probably the jump the first one hundred trading days shown in the right plot in Figure 24.

Now the parameters for the speed of mean reversion shown in Table 5 are analysed. One can see that values in the third column in Table 5 do not deviate significantly from each other except for rows 4 and 11. The speed of mean reversion shown in Figure 20 to 25 except for the right plot in Figure 21 and the left plot in Figure 25 seem to be quite slow and near the same values. This corresponds to the result shown in Table 5. For row 4 in Table 5 it can be noticed that the speed of mean reversion is significantly lower than the other values shown in Table 5. However this coincide with the behaviour of the time series shown in the right plot in Figure 21 which seem to return to zero slowest among the time series shown in Figure 20-25. The speed of mean reversion for the left plot in Figure 25 is much larger than for the other time series shown in Figure 20-25 which coincide with the result in Table 5.

Now the values in Table 5 can be used to simulated new trajectories for the stochastic convenience yield. In order to simulated new samples equation (26) is used together with estimates given in Table 5, the time step $\Delta t = \frac{1}{250}$ and the starting value given by the last observed value in the time series shown in Figure 20-25.

6.1.4 Constructing the forward curve

Simulated sample paths for $\bar{F}(t)$ and $\delta(t, \kappa)$ can be used together with the estimated seasonal premia and (7) to simulate futures prices. By performing linear interpolation between the simulated futures prices reference curves are constructed. Since the simulation equations used to simulate samples for $\bar{F}(t)$ and $\delta(t, \kappa)$ involves a stochastic term the result from one simulation to another can deviate. Therefore it was chosen to simulate one hundred

trajectories for $\bar{F}(t)$ and $\delta(t, \kappa)$ for every day. These simulated values were then used together with estimated seasonal premia and equation (7) to create one 100 forward curves for every trading day in December 2013. The result is presented in the following section.

7 Evaluation of results

In the next section the created reference curves together with corresponding market curves are going to be presented and discussed. After that it will be analysed if historical data fulfil model assumptions and if state variable process could be reduced to random walks. Lastly the maximum likelihood estimation procedure will be investigated.

7.1 Evaluation of created reference curve

In order to investigate how close the created reference curve is to the market curve, one hundred reference curves were constructed for every trading day in December 2013. The result for the first, 11th and last trading day in December 2013 is shown in Figure 26 and Figure 27.

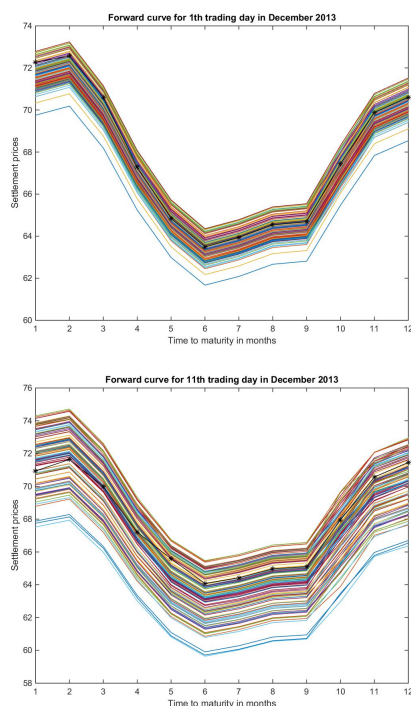


Figure 26: *Upper:* One hundred reference curves together with the corresponding market curve represented by the black line with stars. *Lower:* The figure shows one hundred reference curves together with the corresponding market curve represented by the black line with stars.

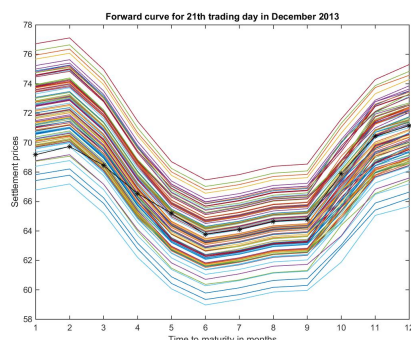


Figure 27: The figure shows one hundred reference curves together with the market forward curve represented by the black line with stars.

From Figure 26 and Figure 27 one can see that create reference curves captures the seasonal behaviour for UK natural gas futures in a correct way. Since futures prices for delivery in the winter are larger than for contract with delivery in the summer. It can also be seen that the spread among the reference curves increase when moving towards the end of the time period. For the presented results the market curve is captured in the spread among all possible reference curves, see Figure 26 and 27.

7.2 Does the model fit historical data?

In this part of the report it is analysed if historical data creates time series for the state variables that meet model assumptions. First the data set consisting of observations 2011-01-11 to 2013-11-30 is analysed. Then the observation period is shortened to 2012-07-01-2013-11-30 and the same analysis is repeated.

7.2.1 Original historical data set

According to the seasonal cost-of-carry model the logarithm of average future price and stochastic convenience yield for every κ follow stochastic process with dynamics given by (11) and (14) respectively. Therefore it will be analysed if time series generated from historical data fit model assumptions given in equation (26) and (25). The analysis will be performed by first evaluating if observed time series for state variables gives model residuals that are realisations of IID noise. If this is the case the assumption that the processes are autoregressive of order one with parameters specified in equation (25) and (26) seems to be satisfied. After that it is analysed if the residuals have the distribution according to equation (25) and (26). If these two criteria seem to be fulfilled, it reasonable to conclude that observed

time series for state variables satisfies the assumption about being discrete observations of Ornstein-Uhlenbeck process specified by (25) and (26) [20].

First the observed time series for $\ln(\bar{F}(t))$ is analysed. Model residuals are given by the following relation

$$R = X_t - X_{t-1}e^{-\alpha\Delta t} + \mu(1 - e^{-\alpha\Delta t}). \quad (37)$$

The residuals are calculated using the observed time series, parameters μ , α and σ determined from maximum likelihood estimation (see Table 3) together with equation (37). Realisation of model residuals together with the sample autocorrelation function (ACF) are shown in Figure 28.

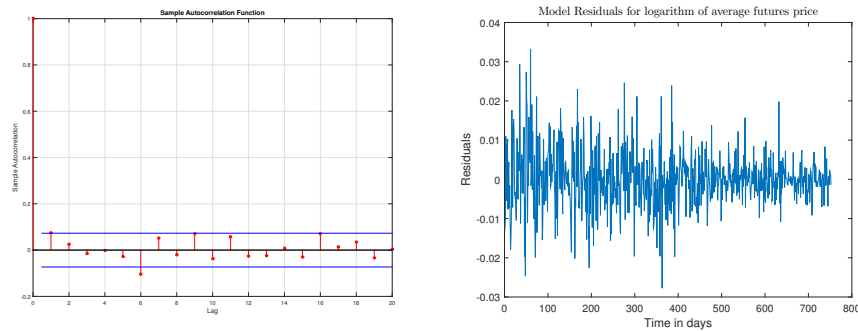


Figure 28: *Left:* ACF for model residuals for logarithm of average futures price, where the IID thresholds are given by the blue horizontal lines. *Right:* Time series representing model residuals for the logarithm of average futures price.

In the left plot in Figure 28 the total number of lags excluding lag zero are 20. Because the number of lags is 20 at most one lag is allowed to exceed the IID thresholds, for the sample to be considered as IID noise. Here the sample ACF exceeds the thresholds only at lag 6. Hence there is no reason for rejecting the hypothesis at level 0.05 that residuals are IID noise.

In order to control the graphical result a Ljung-Box Q-Test is computed in MATLAB by using the function `lbqtest()`. The test generated the p-value 0.0533. Hence the null hypothesis that sample ACF are not correlated was accepted at level 0.05. Therefore the conclusion is that there is not significant correlation between the residuals at level 0.05. Hence graphical result from analysing the sample ACF and the Ljung-Box Q-Test appear to agree. Because of the presented results the conclusion is that there is no reason for rejecting the null hypothesis that residuals are IID noise [20].

The next step was to analyse if model residuals seem to have the distribution according to equation (25). The analysis was performed by graphically

investigating qq-plots. First the residuals were normalized with the standard deviation $\sqrt{\frac{\sigma^2}{2\alpha} (1 - e^{-2\alpha\Delta t})}$. After that a qq-plot was computed of normalised model residuals against standard normal quantiles [21]. The result is shown in Figure 29 together with the corresponding histogram.

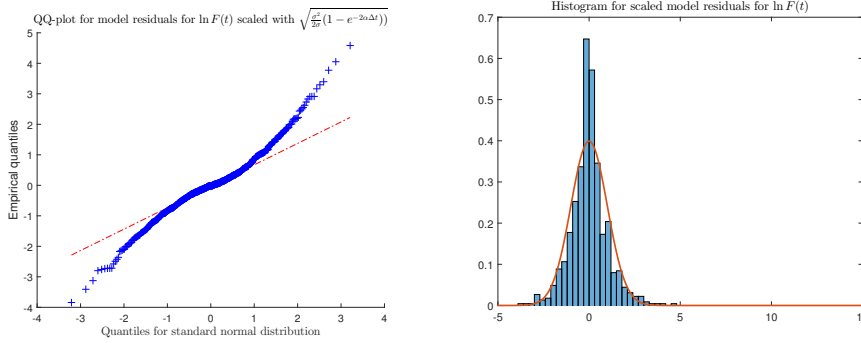


Figure 29: *Left:* QQ-plot for empirical quantiles given by model residuals normalised by standard deviation against quantiles of standard normal distribution. *Right:* Histogram for normalised model residuals together with standard normal density.

When the empirical distribution comes from the reference distribution the qq-plot is approximately linear with slope 1 and intercept 0 [7]. From Figure 29 one can see that the qq-plot does not seem linear. It appears instead that the tails of the empirical distribution are heavier than for the standard normal. This conclusion coincides with the histogram which shows that the density seems to deviate from the standard normal both in tails and center. Therefore the conclusion can be drawn that model residuals do not seem to have the distribution assumed by equation (25).

To verify the graphical analysis one sample Kolmogorov-Smirnov test was performed in MATLAB using the function `kstest()`. The test was performed at level 0.05 and the p-value generated was $1.1583 \cdot 10^{-4}$. Therefore the null hypothesis that data comes from a standard normal distribution was rejected. This result is consistent with the graphical analysis.

Finally the conclusion is drawn that historical data used to generate the observed time series for $\ln(\bar{F}(t))$ during 2011-01-01 to 2013-11-30 does not seem to meet assumption in equation (25).

The next step is to analyse if observed time series for the stochastic convenience yield meet the assumption given in equation (26). This is done the same way as for the logarithm of average futures price. For this case the model residuals can be represented by the following equation

$$R_\kappa = \delta_t^\kappa - \delta_{t-1}^\kappa e^{-\alpha^\kappa(\Delta t)}. \quad (38)$$

For every κ the model residuals are calculated by using the estimated time series from historical data by using equation (24), estimates for a^κ and b^κ given in Table 5 together with equation (38).

First it is analysed if model residuals seem to be realisations of IID noise. This analysis is performed by graphically investigating sample ACF. Results are presented together with corresponding realisations in Figure 30-31 and Figure 47-56, see Appendix E.

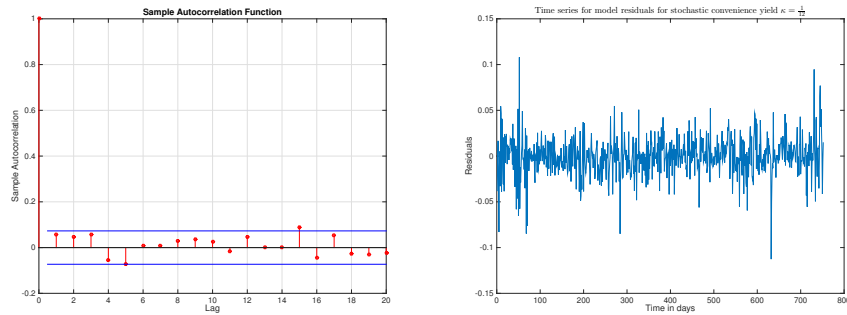


Figure 30: *Left:* ACF for model residuals for convenience yield time series for $\kappa = \frac{1}{12}$, where the IID thresholds are given by the blue horizontal lines. *Right:* Time series of model residuals for stochastic convenience yield.

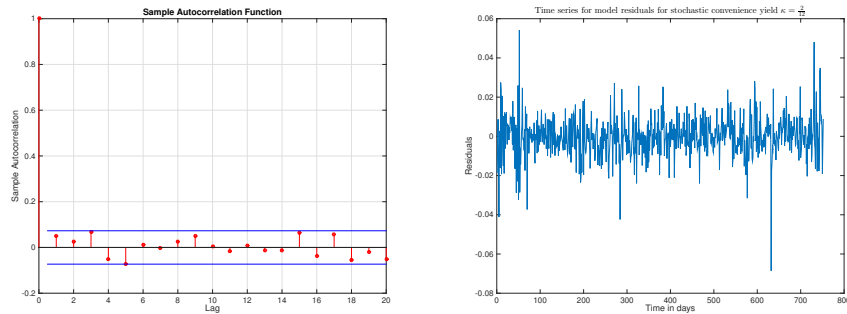


Figure 31: *Left:* ACF for model residuals for convenience yield time series for $\kappa = \frac{2}{12}$, where the IID thresholds are given by the blue horizontal lines. *Right:* Time series of model residuals for stochastic convenience yield.

In Figure 30-31 and Figure 47-56 except for Figure 48 at most one lag except lag zero exceeds the IID thresholds. Hence for every κ except $\kappa = \frac{4}{12}$ there is no reason for rejecting the null hypothesis that residuals are realisations of IID noise. Figure 48 shows that more than one lag except lag zero exceeds the IID thresholds. Therefore the null hypothesis is rejected and the residuals for $\kappa = \frac{4}{12}$ do not seem to be IID noise.

The graphical analysis is compared to results from Ljung-Box Q-Test. The test was computed in MATLAB using the function `lbqtest()`. Resulting p-values are presented in Table 6.

κ	p-value
$\kappa = \frac{1}{12}$	0.0939
$\kappa = \frac{2}{12}$	0.1576
$\kappa = \frac{3}{12}$	0.1167
$\kappa = \frac{4}{12}$	0.0283
$\kappa = \frac{5}{12}$	0.2996
$\kappa = \frac{6}{12}$	0.4706
$\kappa = \frac{7}{12}$	0.1978
$\kappa = \frac{8}{12}$	0.2454
$\kappa = \frac{9}{12}$	0.1715
$\kappa = \frac{10}{12}$	0.1731
$\kappa = \frac{11}{12}$	0.0839
$\kappa = \frac{12}{12}$	0.3215

Table 6: The table shows p-values for residuals for stochastic convenience yield when performing Ljung-Box Q-Test.

The result presented in Table 6 agrees with the graphical analysis of the sample ACF [20]. Therefore the conclusion is drawn that residuals for $\kappa = \frac{1}{12}, \frac{2}{12}, \frac{3}{12}, \frac{5}{12}, \frac{6}{12}, \frac{7}{12}, \frac{8}{12}, \frac{9}{12}, \frac{10}{12}, \frac{11}{12}, \frac{12}{12}$ seem to be realisations of IID noise.

Next, it was analysed if the residuals have the distribution according to equation (26). This was done with the same method as for the logarithm of average futures price. First the sample giving the model residuals was normalised by the standard deviation $\sqrt{\frac{(b^\kappa)^2}{2a^\kappa} (1 - e^{-2a^\kappa \Delta t})}$. After that qq-plots were computed where the empirical quantiles of the normalised residuals were potted against standard normal quantiles [21]. Results are shown in Figure 32 and 33 and Figure 57-65, see Appendix E together with histograms. Since residuals for $\kappa = \frac{4}{12}$ did not seem to be realisations of IID noise, the time series was excluded from further analysis.

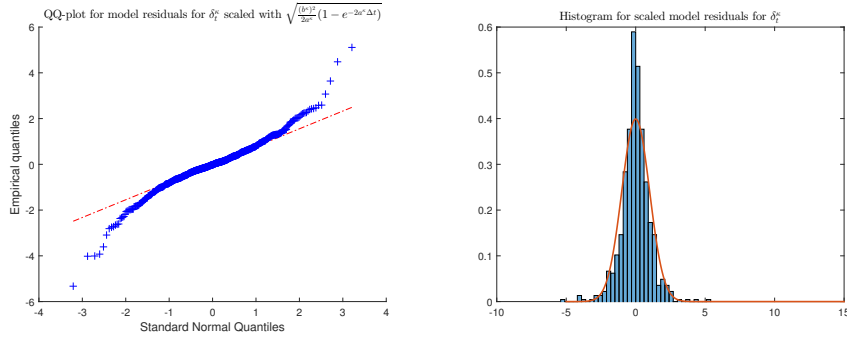


Figure 32: *Left:* QQ-plot for normalised model residuals against quantiles of standard normal distribution for $\kappa = \frac{1}{12}$. *Right:* Histogram for normalised model residuals together with density for standard normal distribution.

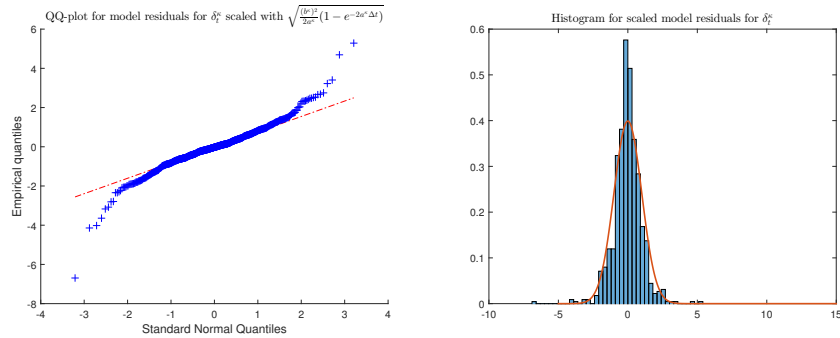


Figure 33: *Left:* QQ-plot for normalised model residuals against quantiles of standard normal distribution for $\kappa = \frac{2}{12}$. *Right:* Histogram for normalised model residuals together with density for standard normal distribution.

From Figure 32-33 and Figure 57-65 one can see that all qq-plots except for $\kappa = \frac{5}{12}, \frac{8}{12}$ does not seem to have slopes that are approximately equal to one. However in Figure 58 and 61 the plots seem to have a slope that is close to 1 except for some outliers. This result is confirmed by the histograms where it seems that the tails and center do not deviate significantly from the standard normal distribution for $\kappa = \frac{5}{12}, \frac{8}{12}$.

Because of the graphical analysis the conclusion is drawn that model residuals for $\kappa = \frac{5}{12}, \frac{8}{12}$ seem to agree with the specified distribution of the noise term in equation (26). To verify this result a one sample Kolmogorov-Smirnov test was performed in MATLAB. This was done by using the function `kstest()`. The result is presented in Table 7.

κ	p-value
$\kappa = \frac{1}{12}$	0.0083
$\kappa = \frac{2}{12}$	0.0049
$\kappa = \frac{3}{12}$	$9.7934 \cdot 10^{-4}$
$\kappa = \frac{5}{12}$	0.0861
$\kappa = \frac{6}{12}$	0.0239
$\kappa = \frac{7}{12}$	0.0137
$\kappa = \frac{8}{12}$	0.0527
$\kappa = \frac{9}{12}$	0.0346
$\kappa = \frac{10}{12}$	$1.7171 \cdot 10^{-18}$
$\kappa = \frac{11}{12}$	$5.1231 \cdot 10^{-4}$
$\kappa = \frac{12}{12}$	0.0021

Table 7: The table shows p-values for residuals for stochastic convenience yield when performing a one sample Kolmogorov-Smirnov test.

The result in Table 7 suggest that the hypothesis that the normalised residuals comes from a standard normal distribution at level 0.05 can be rejected for all κ except for $\kappa = \frac{5}{12}, \frac{8}{12}$. Hence results from the graphical analysis and the one sample Kolmogorov-Smirnov test are consistent. Therefore it seems plausible to conclude that observed model residuals for $\kappa = \frac{5}{12}, \frac{8}{12}$ seem to have the distribution assumed by the noise term in (26).

Finally the conclusion is drawn that historical data for the time period 2011-01-01 to 2013-11-30 appear to generate observed time series for the stochastic convenience yield that agrees with the assumption in (26) only for $\kappa = \frac{5}{12}, \frac{8}{12}$.

7.2.2 Different set of historical observations

Figure 4 shows that prices seem to be more volatile in the beginning of the observation period. According to [10] data used for estimation should be data for liquid contracts. Perhaps the volatility in the beginning of the observation period could be because contracts were not liquid. This could possibly be the reason for why model assumptions were not fulfilled by the majority of observed time series. Therefore the observation period was shorted to 2012-07-01-2013-11-30, see Figure 34. This observation period was chosen since prices seem to stabilise around the last 400 trading days in the original data set.

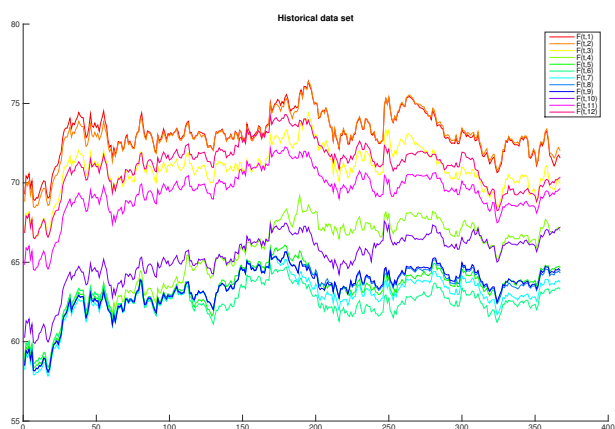


Figure 34: Time series for settlement prices for every $T = 1, \dots, 12$ for UK natural gas futures for the time period 2012-07-01 to 2013-11-30.

For data shown in Figure 34 the same procedure outlined in *Result* section was repeated. After that model residuals for the state variables were analysed using the same method as in the section *Original historical data set*. First the analysis is presented for the logarithm of average futures price and then for the stochastic convenience yield.

For the logarithm of average futures price, model residuals were calculated with equation (37) for observation period 2012-07-01 to 2013-11-30. The resulting time series together with the sample ACF is shown in Figure 35.

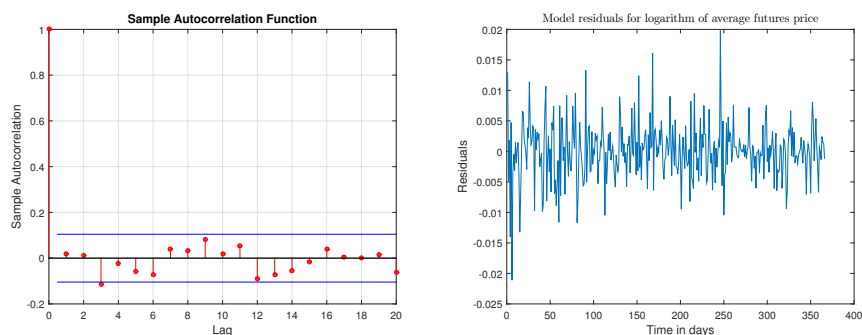


Figure 35: *Left*: ACF for model residuals for logarithm of average futures price, where the blue horizontal lines show the IID thresholds. *Right*: Time series of model residuals.

Figure 35 suggest that sample ACF does not exceed IID thresholds for any lag larger than zero. Hence it seems plausible to accept the null hypothesis that residuals are IID noise. This result was consistent with result from Ljung-Box Q-Test, since the p-value generated was 0.3574 [20].

After that it was analysed if the assumption about the distribution of the noise term in (25) seem to be fulfilled. This was done the same way as in section *Original historical data set*. The resulting qq-plot is shown in Figure 36 together with corresponding histogram.

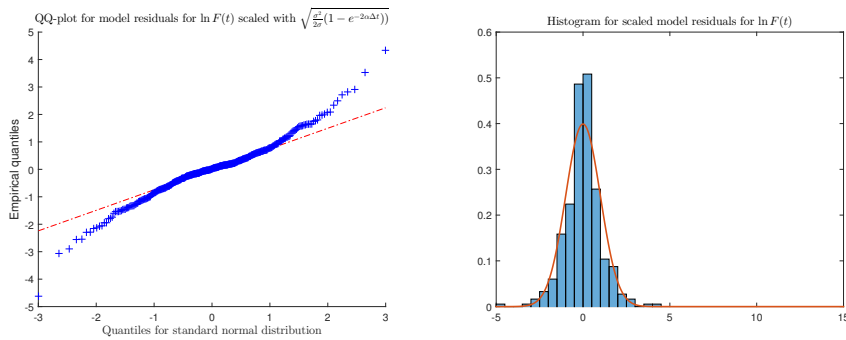


Figure 36: *Left:* QQ-plot for normalised residuals for logarithm of average futures price for observation period 2012-07-01 to 2013-11-30 against standard normal quantiles. *Right:* Histogram of normalised residuals together with standard normal density.

Figure 36 does not show a qq-plot that is approximately linear with slope one. It seems instead that the right and left tail are heavier than the standard normal distribution. This is confirmed by the histogram showing that the center and tails seem to deviate from the standard normal density [7]. The graphical analysis suggests that residuals do not meet the assumptions about the distribution of the noise term in equation (25). After that one sample Kolmogorov-Smirnov test was preformed to see if the result agrees with the conclusion drawn from the qq-plot and histogram. The test generated the p-value 0.041. Therefore the null hypothesis that the normalised residuals have standard normal distribution was rejected. Thus results from graphical analysis and one sample Kolmogorov-Smirnov appear to coincide.

Due to the presented results it seems reasonable to conclude that decreasing the observation period does not seem to improve the result. It still seems to be the case that the observed time series for logarithm of average futures does not meet assumptions in (25).

The same steps were repeated to analyse the observed time series for the stochastic convenience yield for the time period 2012-07-01 to 2013-11-30. Residuals were calculated from equation (38). Realisations together with

corresponding sample ACF is shown in Figure 37 and 38 and Figure 66-75, see Appendix F.

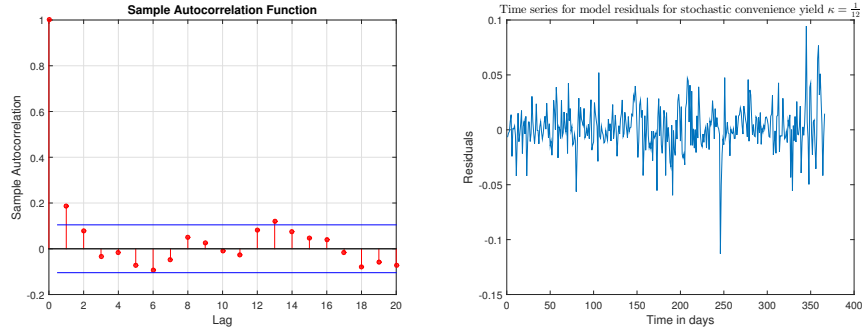


Figure 37: *Left:* ACF for model residuals for convenience yield time series for $\kappa = \frac{1}{12}$, where the horizontal blue lines represents the IID thresholds. *Right:* Time series of model residuals for convenience yield.

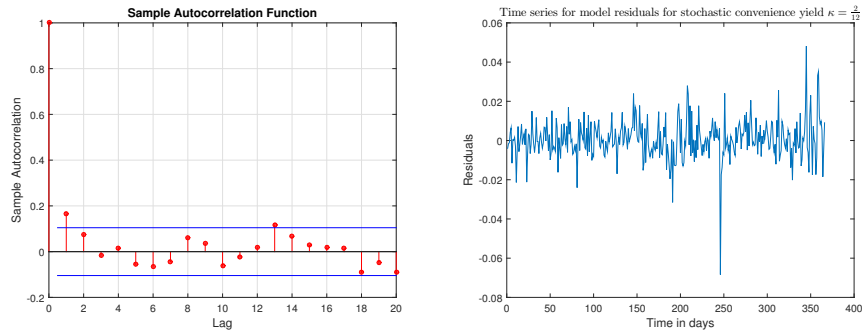


Figure 38: *Left:* ACF for model residuals for convenience yield time series for $\kappa = \frac{2}{12}$, where the horizontal blue lines represents the IID thresholds. *Right:* Time series of model residuals for convenience yield.

Figures 37, 38, 68 and Figure 73 suggest that more than one lag except lag zero exceeds the IID thresholds. Therefore the null hypothesis that residuals are IID noise is rejected for $\kappa = \frac{1}{12}, \frac{2}{12}, \frac{5}{12}, \frac{10}{12}$. In Figure 66-67, Figure 69-72 and Figure 74-75 approximately at most one lag except lag zero exceed the IID thresholds. Therefore the null hypothesis that residuals are IID noise is accepted for $\kappa = \frac{3}{12}, \frac{4}{12}, \frac{6}{12}, \frac{7}{12}, \frac{8}{12}, \frac{9}{12}, \frac{11}{12}, \frac{12}{12}$.

Results from analysing the sample ACF was compared to results from computing the Ljung-Box Q-Test [20]. Table 8 shows resulting p-values when computing Ljung-Box Q-Test.

κ	p-value
$\kappa = \frac{1}{12}$	0.0039
$\kappa = \frac{2}{12}$	0.0236
$\kappa = \frac{3}{12}$	0.1011
$\kappa = \frac{4}{12}$	0.2286
$\kappa = \frac{5}{12}$	0.0108
$\kappa = \frac{6}{12}$	0.3756
$\kappa = \frac{7}{12}$	0.2846
$\kappa = \frac{8}{12}$	0.4638
$\kappa = \frac{9}{12}$	0.4800
$\kappa = \frac{10}{12}$	0.2698
$\kappa = \frac{11}{12}$	0.3458
$\kappa = \frac{12}{12}$	0.4837

Table 8: The table shows p-values for residuals for stochastic convenience yield for the time period 2012-07-01 to 2013-11-30 when performing Ljung-Box Q-Test.

From Table 8 one can see that the result agrees with the conclusions drawn from analysing the sample ACF for all κ except for $\kappa = \frac{10}{12}$. When observing the ACF for residuals of $\kappa = \frac{10}{12}$, it can be seen that the majority of sample ACF are quite small. However two lags exceed the IID thresholds significantly. This could be the reason for why Ljung-Box Q-Test generated a large p-value. Since the sample ACF for two lags falls far outside the bonds it seems reasonable to reject the null hypothesis that residuals are IID noise for $\kappa = \frac{10}{12}$ and disregard the result from Ljung-Box Q-Test.

Next, the step was to analyse if the residuals fulfil the assumptions of the distribution of the noise term in equation (26). Because residuals for $\kappa = \frac{1}{12}, \frac{2}{12}, \frac{5}{12}, \frac{10}{12}$ did not seem to be realisation of white noise they were excluded from further analysis. The analysis was performed the same way as for the logarithm of average futures price. The result is presented in Figure 76-83 together with corresponding histograms, see Appendix F.

From Figure 76-83 it can be seen that for $\kappa = \frac{6}{12}, \frac{7}{12}, \frac{8}{12}, \frac{9}{12}, \frac{11}{12}, \frac{12}{12}$ the qq-plots seem to have a slope close to 1 if the outliers are disregarded. The corresponding histograms do not seem to deviate significantly from the standard normal density. However for $\kappa = \frac{3}{12}, \frac{4}{12}$ qq-plots seem to suggest that the empirical distribution has heavier tails than the standard normal distribution. This can also be seen from the corresponding histograms where the density deviates from the standard normal both in the tails and in the center. To confirm the graphical analysis one sample Kolmogorov-Smirnov test was performed. The result is presented in Table 9.

κ	p-value
$\kappa = \frac{3}{12}$	0.0060
$\kappa = \frac{4}{12}$	0.2148
$\kappa = \frac{6}{12}$	0.0625
$\kappa = \frac{7}{12}$	0.0975
$\kappa = \frac{8}{12}$	0.1534
$\kappa = \frac{9}{12}$	0.1693
$\kappa = \frac{11}{12}$	0.2886
$\kappa = \frac{12}{12}$	0.1598

Table 9: The table shows p-values for normalised residuals for stochastic convenience yield when performing a one sample Kolmogorov-Smirnov test for observations in the time period 2012-07-01 to 2013-11-30.

The result in Table 9 agrees with results from the graphical analysis for all κ except for $\kappa = \frac{4}{12}$. For $\kappa = \frac{4}{12}$ the qq-plot and histogram shows that the empirical distribution seem to deviates significantly from the standard normal. Hence the result from the one sample Kolmogorov-Smirnov is disregarded for this case.

Statistical test and graphical analysis suggest that for $\kappa = \frac{6}{12}, \frac{7}{12}, \frac{8}{12}, \frac{9}{12}, \frac{11}{12}, \frac{12}{12}$ the distribution of residuals seem to agree with the distribution of the noise given in (26). On the other hand for $\kappa = \frac{3}{12}, \frac{4}{12}$ the distribution of the noise does not appear to agree with the assumption in (26).

Lastly the conclusion is drawn due to the presented results that observed time series for stochastic convenience yield for $\kappa = \frac{1}{12}, \frac{2}{12}, \frac{3}{12}, \frac{4}{12}, \frac{5}{12}, \frac{10}{12}$ does not appear to meet assumptions in (26). However for $\kappa = \frac{6}{12}, \frac{7}{12}, \frac{8}{12}, \frac{9}{12}, \frac{11}{12}, \frac{12}{12}$ the assumptions in equation (26) seem to agree with historical data.

Summarising, shorting the observation period to 2012-07-01-2013-11-30 improved results slightly. For the observed time series for the logarithm of average futures the model assumptions were still not fulfilled. However for the stochastic convenience yield the result was somewhat improved, since for $\kappa = \frac{6}{12}, \frac{7}{12}, \frac{8}{12}, \frac{9}{12}, \frac{11}{12}, \frac{12}{12}$ assumptions specified in (26) seem to be met.

Finally the set of observations was decreased to one year that is to say 2012-11-30 to 2013-11-30. However the result was similar to the result found for the observation period 2012-07-01 to 2013-11-30.

7.3 Reduce processes to random walks?

In this section it is analysed if the stochastic process representing the average futures price and the stochastic convenience yield for $\kappa = \frac{1}{12}, \dots, \frac{12}{12}$

could be reduced to random walks. This was done by applying likelihood ratio test and analysing if the coefficient representing the speed of mean reversion could be set to zero. First the result for the process representing the logarithm of average futures price is presented and then for the stochastic convenience yield for every $\kappa = \frac{1}{12}, \dots, \frac{12}{12}$.

For the process representing $\ln(\bar{F}(t))$ the aim is to analyse if the observed time series $\{X_t\}_{t=0}^{752}$ for 2011-01-01 to 2013-11-30 could be represented by a random walk. Therefore the distribution for X_t under the null hypothesis is given by

$$X_t \sim (X_{t-1}, \tilde{\sigma}^2 \Delta t).$$

Hence the restricted model is

$$X_t = X_{t-1} + \sqrt{\tilde{\sigma}^2 \Delta t} Z,$$

where Z is a standard normal random variable.

The likelihood function for the restricted model is

$$L(\tilde{\sigma}) = \prod_{t=0}^m \frac{1}{\sqrt{2\pi\tilde{\sigma}^2\Delta t}} \exp\left\{-\frac{(X_t - X_{t-1})^2}{2\tilde{\sigma}^2\Delta t}\right\}, \quad (39)$$

and corresponding log-likelihood function is given by

$$\ln(L(\tilde{\sigma})) = -\frac{m \ln(2\pi)}{2} - \frac{m}{2}(\ln(\tilde{\sigma}^2 \Delta t)) - \frac{1}{2\tilde{\sigma}^2 \Delta t} \sum_{t=0}^m (X_{t-1} - X_t)^2. \quad (40)$$

In order to find the parameter $\tilde{\sigma}$ that maximizes the log-likelihood function the following equation must be solved

$$\frac{\partial \ln(L(\tilde{\sigma}))}{\partial \tilde{\sigma}} = 0.$$

The solution is given by

$$\tilde{\sigma}^2 = \frac{1}{m\Delta t} \left(\sum_{t=1}^m X_t - \sum_{t=1}^m X_t X_{t-1} + \sum_{t=1}^m X_{t-1} \right). \quad (41)$$

Inserting $\tilde{\sigma}$ calculated with (41) into the equation (40) gives the value of the log-likelihood function under the restricted model.

The model under the alternative hypothesis is given by equation (25). The log-likelihood function for the non-restricted model was calculated by inserting estimates for parameters μ , α and σ see Table 3 into equation (30).

Lastly two times log-likelihood ratio denoted $2 \ln(LR)$ was computed from the following relation

$$2 \ln(LR) = -2 \ln(L(\tilde{\sigma})) + 2 \ln(L(\alpha, \mu, \sigma))$$

The result when the historical data set is given by the observation period 2011-01-01 to 2013-11-30 together with the corresponding p-values is presented in Table 10.

$2 \ln(LR)$	p-value
6.3963	0.0408

Table 10: The table shows $2 \ln(LR)$ and p-value for the logarithm of average future price. The p-value was calculated as the probability $P(Y \geq 2 \ln(LR))$ where $Y \sim \chi_2^2$, since the model under the null hypothesis has one parameter and the model under the alternative hypothesis has three.

From Table 10 it can be seen that the p-value is 0.0408. Hence at level 0.05 the null hypothesis can be rejected. Therefore the conclusion can be drawn that the observed time series for $\ln(\bar{F}(t))$ is not possible to reduce to a random walk.

Next, likelihood ratio test was applied for the observed time series estimating the stochastic convenience yield. The goal was to analyse if data generating the observed time series, for the observation period 2011-01-01 to 2013-11-30 could be represented by random walks. Hence the distribution under the null hypothesis is

$$\delta_t^\kappa \sim N(\delta_{t-1}^\kappa, (\tilde{b}^\kappa)^2 \Delta t).$$

Consequently the restricted model is given by

$$\delta_t^\kappa = \delta_{t-1}^\kappa + \sqrt{\tilde{b}^2 \Delta t} W,$$

where W is a standard normal random variable. The likelihood function for the restricted model is given by

$$L(\tilde{b}^\kappa) = \prod_{t=0}^m \frac{1}{\sqrt{2\pi(\tilde{b}^\kappa)^2 \Delta t}} \exp - \frac{(\delta_t^\kappa - \delta_{t-1}^\kappa)^2}{2(\tilde{b}^\kappa)^2 \Delta t}.$$

Taking the logarithm of the above relation gives the log-likelihood function

$$\ln(L(\tilde{b}^\kappa)) = -\frac{m \ln(2\pi)}{2} - \frac{m}{2} (\ln((\tilde{b}^\kappa)^2 \Delta t)) - \frac{1}{2(\tilde{b}^\kappa)^2 \Delta t} \sum_{t=0}^m (\delta_{t-1}^\kappa - \delta_t^\kappa)^2.$$

In order to find the value of \tilde{b}^κ that maximizes the log-likelihood function the following equation must be solved

$$\frac{\partial \ln(L(\tilde{b}^\kappa))}{\partial \tilde{b}^\kappa} = 0.$$

The solution is given by

$$(\tilde{b}^\kappa)^2 = \frac{1}{m\Delta t} \left(\sum_{t=1}^m \delta_t^\kappa - \sum_{t=1}^m \delta_t^\kappa \delta_{t-1}^\kappa + \sum_{t=1}^m \delta_{t-1}^\kappa \right). \quad (42)$$

The next step is to calculate the log-likelihood function for the restricted model by using the maximum likelihood estimate calculated with equation (42) for every $\kappa = \frac{1}{12}, \dots, \frac{12}{12}$.

For this case the non-restricted model is given by equation (26). The corresponding log-likelihood function was calculated by using equation (27) and maximum likelihood estimates given in Table 5. Lastly two times log-likelihood ratio was calculated for every $\kappa = \frac{1}{12}, \dots, \frac{12}{12}$, with the following relation

$$2 \ln(LR) = -2 \ln(\tilde{b}^\kappa) + 2 \ln(L(b^\kappa, a^\kappa)).$$

The result is presented in Table 11.

κ	$2 \ln(LR)$	p-value
$\kappa = \frac{1}{12}$	5.1427	0.0233
$\kappa = \frac{2}{12}$	6.9004	0.00862
$\kappa = \frac{3}{12}$	2.7007	0.1003
$\kappa = \frac{4}{12}$	0.1091	0.7411
$\kappa = \frac{5}{12}$	3.6102	0.0572
$\kappa = \frac{6}{12}$	4.4821	0.0342
$\kappa = \frac{7}{12}$	5.1577	0.0231
$\kappa = \frac{8}{12}$	4.2585	0.0391
$\kappa = \frac{9}{12}$	3.7580	0.0526
$\kappa = \frac{10}{12}$	10.1266	0.001461
$\kappa = \frac{11}{12}$	16.6682	0.000044
$\kappa = \frac{12}{12}$	3.6188	0.0571

Table 11: Table shows $2 \ln(LR)$ and p-values for observed time series for the stochastic convenience yield. The p-values were calculated as the probability $P(Y \geq 2 \ln(LR))$ where $Y \sim \chi_1^2$. Since the models under the null hypothesis have one parameter and the model under the alternative hypothesis has two.

Table 11 shows that the p-value is less than 0.05 for $\kappa = \frac{1}{12}, \frac{2}{12}, \frac{6}{12}, \frac{7}{12}, \frac{8}{12}, \frac{10}{12}, \frac{11}{12}$. Therefore the null hypothesis is rejected at level 0.05. However for $\kappa = \frac{3}{12}, \frac{4}{12}, \frac{5}{12}, \frac{9}{12}, \frac{12}{12}$ the p-value is greater than 0.05 and the null hypothesis is accepted. Thus it appears possible to reduce the observed time series for $\kappa = \frac{3}{12}, \frac{4}{12}, \frac{5}{12}, \frac{9}{12}, \frac{12}{12}$ for the observation period 2011-01-01 to 2013-11-30 to random walk process.

The same procedure as described above was repeated for the observation period 2012-07-01 to 2013-11-30. It was found that the null hypothesis was only rejected for $\kappa = \frac{11}{12}$ and for the logarithm of average futures price. For the other processes the null hypothesis was accepted [23].

7.4 Analysis of maximum-likelihood estimation

In this part of the report the maximum-likelihood estimation (MLE) for estimating parameters in (11) and (14) will be analysed. First it is investigated if the estimation works by applying another estimation method. After that it is analysed how the estimates capture the behaviour in historical data. Lastly the accuracy is analysed.

7.4.1 OLS-estimation of parameters

In order to control that the estimation procedure works, parameters in equations (11) and (14) are estimated by applying another method. It was chosen to estimate parameters by Ordinary Least Squares (OLS) and compare the result to the maximum-likelihood estimation.

First equation (25) is rewritten by setting $\beta_0 = \mu(1 - e^{-\alpha\Delta t})$, $\beta_1 = e^{-\alpha\Delta t}$ and $\sigma'' = \sqrt{\frac{\sigma^2}{2\alpha}(1 - e^{-2\alpha\Delta t})}$. This gives

$$X_t = \beta_0 + X_{t-1}\beta_1 + \sigma''Z, \quad (43)$$

where Z is a standard normal random variable. Recall that the observed time series for $\ln(\bar{F}(t))$ is calculated with equation (9). Parameters in (43) can be estimated by applying OLS together with the set of observations X_0, \dots, X_n . Estimates of β_0 and β_1 are denoted $\hat{\beta}_0$ and $\hat{\beta}_1$ and calculated by solving the following equation

$$\hat{\beta} = (\mathbf{X}^T\mathbf{X})^{-1}\mathbf{X}^T\mathbf{Y},$$

where

$$\hat{\beta} = \begin{bmatrix} \hat{\beta}_0 \\ \hat{\beta}_1 \end{bmatrix}, \quad \mathbf{X} = \begin{bmatrix} X_0 & 1 \\ X_1 & 1 \\ X_2 & 1 \\ \vdots & \vdots \\ X_{n-1} & 1 \end{bmatrix} \quad \text{and} \quad \mathbf{Y} = \begin{bmatrix} Y_1 \\ Y_2 \\ Y_3 \\ \vdots \\ Y_n \end{bmatrix}.$$

The model residuals can then be determined from the following relation

$$\hat{\mathbf{e}} = \mathbf{Y} - \mathbf{X}\hat{\beta}.$$

By calculating the sample standard deviation from of the vector of residuals an estimate for σ'' is determined. After that the corresponding estimates for β_0 and β_1 where calculated using maximum-likelihood estimates given in Table 3. The result is presented in Table 12.

	β_0	β_1	σ''
MLE	0.0615	0.9854	0.0072
OLS	0.0615	0.9854	0.0072

Table 12: The table shows estimates for β_0 and β_1 when applying MLE and OLS.

Table 12 shows that the maximum-likelihood estimates and OLS-estimates do not deviate from each other. Hence the same parameters are obtained when applying two different estimation techniques. Therefore the conclusion is that the estimation procedure works since two estimation methods give consistent results.

After that the estimation procedure was analysed for parameters in the process representing the stochastic convenience yield. First equation (26) is rewritten by setting $\beta'_1 = e^{-a^\kappa \Delta t}$ and $\sigma' = \sqrt{\frac{(b^\kappa)^2}{2a^\kappa} (1 - e^{-2a^\kappa \Delta t})}$. This gives

$$\delta_t^\kappa = \beta'_1 \delta_{t-1}^\kappa + \sigma' W, \tag{44}$$

where W is a standard normal random variable. The observed time series are calculated using equation (24), which gives observations $\delta_0^\kappa, \delta_1^\kappa, \dots, \delta_n^\kappa$ where $n = 752$. The estimate of β'_1 is denoted $\hat{\beta}'_1$ and the OLS-estimate is calculated from the following relation

$$\hat{\beta}'_1 = (\mathbf{A}^T \mathbf{A})^{-1} \mathbf{A}^T \mathbf{B},$$

where

$$\mathbf{A} = \begin{bmatrix} \delta_0^\kappa \\ \delta_1^\kappa \\ \delta_2^\kappa \\ \vdots \\ \delta_{n-1}^\kappa \end{bmatrix} \quad \text{and} \quad \mathbf{B} = \begin{bmatrix} \delta_1^\kappa \\ \delta_2^\kappa \\ \delta_3^\kappa \\ \vdots \\ \delta_n^\kappa \end{bmatrix}.$$

Corresponding model residuals were determined from the following relation

$$\hat{\mathbf{e}}' = \mathbf{B} - \mathbf{A}\hat{\beta}'_1.$$

The parameter σ' is estimated from the sample standard deviation of the vector $\hat{\mathbf{e}}'$. Lastly the corresponding estimates for β'_1 and σ' were calculated with the maximum-likelihood estimates given in Table 5. The result is shown in Table 13.

	β'_1	σ'
MLE $\kappa = \frac{1}{12}$	0.9926	0.0211
OLS $\kappa = \frac{1}{12}$	0.9926	0.0211
MLE $\kappa = \frac{2}{12}$	0.9906	0.0102
OLS $\kappa = \frac{2}{12}$	0.9906	0.0102
MLE $\kappa = \frac{3}{12}$	0.9930	0.0072
OLS $\kappa = \frac{3}{12}$	0.9930	0.0072
MLE $\kappa = \frac{4}{12}$	0.9992	0.0049
OLS $\kappa = \frac{4}{12}$	0.9992	0.0049
MLE $\kappa = \frac{5}{12}$	0.9890	0.0033
OLS $\kappa = \frac{5}{12}$	0.9890	0.0033
MLE $\kappa = \frac{6}{12}$	0.9899	0.0028
OLS $\kappa = \frac{6}{12}$	0.9899	0.0028
MLE $\kappa = \frac{7}{12}$	0.9879	0.0022
OLS $\kappa = \frac{7}{12}$	0.9879	0.0022
MLE $\kappa = \frac{8}{12}$	0.9883	0.0019
OLS $\kappa = \frac{8}{12}$	0.9883	0.0019
MLE $\kappa = \frac{9}{12}$	0.9892	0.0017
OLS $\kappa = \frac{9}{12}$	0.9892	0.0017
MLE $\kappa = \frac{10}{12}$	0.9847	0.0033
OLS $\kappa = \frac{10}{12}$	0.9847	0.0033
MLE $\kappa = \frac{11}{12}$	0.9606	0.0018
OLS $\kappa = \frac{11}{12}$	0.9606	0.0018
MLE $\kappa = \frac{12}{12}$	0.9889	0.0017
OLS $\kappa = \frac{12}{12}$	0.9889	0.0017

Table 13: The table shows estimates of β'_1 and σ' with MLE and OLS.

From Table 13 it can be seen that MLE and OLS give consistent estimates.

Hence both estimation methods give the same result. Therefore the conclusion can be drawn that maximum likelihood estimation works for estimating parameters equation (26) for every κ [23].

7.4.2 MLE using rolling window of 200 days

In this section it is analysed how the maximum likelihood estimates capture the behaviour in historical data. Since the same method is used for parameter estimation for both state variable process it is choose to only analyse the logarithm of average futures price. The analysis was performed by computing maximum likelihood estimation of the parameters μ , σ and α with a rolling window of 200 trading days. Results are presented in Figure 39 and 40.

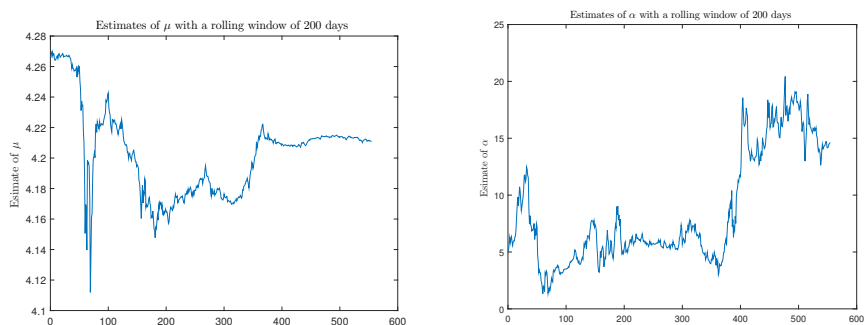


Figure 39: *Left:* Estimates of μ for a rolling window of 200 trading days. *Right:* Estimates of α for a rolling window of 200 trading days.

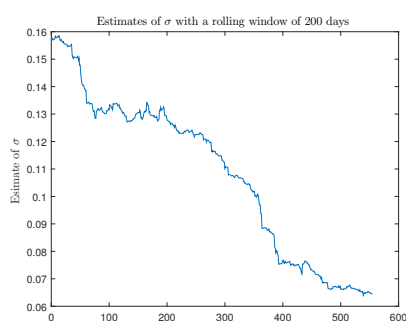


Figure 40: Estimates of σ for a rolling window of 200 trading days.

Estimates shown in left plot in Figure 39 seem to capture the behaviour in historical data. This is because the estimated parameters shown in the left plot in Figure 39 seem more volatile in the beginning of the observation

period which coincides with the behaviour shown in the left plot in Figure 5. The right plot in Figure 39 also seem to capture the behaviour in historical data since the speed of mean reversion is larger in the beginning of the observation period, which is confirmed by the left plot in Figure 5. The left plot in Figure 5 shows that the volatility seem to be larger in the beginning of the observation. This agrees with estimates for σ shown in Figure 40. From the results presented in Figure 39-40 it seems reasonable to conclude that maximum likelihood estimates seem to capture the behaviour in historical data in a correct way.

7.4.3 Accuracy for ML-estimators

In the next section the accuracy for maximum likelihood estimators for parameters in (11) and (14) will be analysed. Observed data is used as input when estimating parameters with methods such as maximum likelihood. Since historical data is assumed to be outcomes from stochastic processes, there is randomness in the sample. Due to the randomness, repeating an experiment to generate data gives different samples. This results in different estimates for the same parameter which leads to a *sampling distribution*. When using an estimator the aim is to obtain estimates that are close to the true parameter value. An estimator is said to be *unbiased* when the expected value of the estimator is equal to the true value. The bias of an estimator is given by the following relation

$$\text{Bias} = E(\hat{\gamma}) - \gamma$$

where $\hat{\gamma}$ is the estimator of the true parameter value γ . In many cases it is not possible to obtain estimators that are unbiased. Thus it is desirable that the bias is small. The mean squared error (MSE) gives the variance of the estimator around the true value and is defined by the following relation

$$\text{MSE} = E[(\hat{\gamma} - \gamma)^2].$$

When the MSE is low it indicates that estimates for any sample are likely to be close to the true value. Taking the squared root of the MSE gives the root mean squared error (RMSE). The standard error is defined as the standard deviation of the sampling distribution. A small standard error indicates that an estimator is precise since repeated experiments gives similar estimates [24].

In order to investigate the accuracy of the maximum likelihood estimators a simulation experiment was performed. This was done by computing a Monte Carlo experiment on the sample size used for parameter estimation. The simulation study was computed by using the maximum likelihood estimates determined from historical data given in Table 3 and Table 5 to simulate new

samples using equation (25) and (26). The sample size was chosen to 753 which is equal to the number of observations in the historical data set and the simulations were repeated 1000 times [22]. For every set of simulated data parameters in (11) and (14) were estimated by applying equation (34), (35), (36) and equation (28) and (29). This resulted in 1000 estimates for each parameter. After that the sample mean and sample standard deviation giving the standard error was calculated. Lastly the root mean squared error was estimated from the following relation

$$\widehat{\text{RMSE}} = \sqrt{\frac{1}{m} \sum_{i=1}^m (\hat{\gamma}_i - \gamma)^2},$$

where m is the number of replications, γ is the true parameter value and $\hat{\gamma}_i$ is the estimated value from simulation i where $i \in 1, \dots, m$ [25]. Results for parameters in (11) is presented in Table 14 and for parameters in (14) in Table 15-16.

	Sample mean	Standard error	RMSE
μ	4.2171	0.0193	0.0180
α	5.1259	2.1632	2.6690
σ	0.1154	0.0030	0.0030

Table 14: Table shows sample mean, standard error and RMSE for parameters μ , α and σ for 753 samples and 1000 replications.

a^κ	Sample mean	Standard error	RMSE
$\kappa = \frac{1}{12}$	2.3535	1.2128	1.5252
$\kappa = \frac{2}{12}$	2.9579	1.4939	2.2089
$\kappa = \frac{3}{12}$	2.2808	1.2601	1.6419
$\kappa = \frac{4}{12}$	0.5809	0.6871	0.1227
$\kappa = \frac{5}{12}$	3.2954	1.5366	2.7179
$\kappa = \frac{6}{12}$	3.2045	1.7300	2.4945
$\kappa = \frac{7}{12}$	3.6912	1.7845	3.0210
$\kappa = \frac{8}{12}$	3.5040	1.6531	2.9007
$\kappa = \frac{9}{12}$	3.2656	1.5752	2.6857
$\kappa = \frac{10}{12}$	4.5065	1.9539	3.8064
$\kappa = \frac{11}{12}$	10.7623	2.8955	10.0167
$\kappa = \frac{12}{12}$	3.3778	1.5856	2.7536

Table 15: The table shows sample mean, standard error and RMSE for parameters a^κ for $\kappa = \frac{1}{12}, \dots, \frac{12}{12}$ for 753 samples and 1000 replications.

b^κ	Sample mean	Standard error	RMSE
$\kappa = \frac{1}{12}$	0.3357	0.0086	0.0087
$\kappa = \frac{2}{12}$	0.1628	0.0042	0.0042
$\kappa = \frac{3}{12}$	0.1148	0.0030	0.0030
$\kappa = \frac{4}{12}$	0.0776	0.0020	0.0020
$\kappa = \frac{5}{12}$	0.0523	0.0013	0.0014
$\kappa = \frac{6}{12}$	0.0441	0.0011	0.0012
$\kappa = \frac{7}{12}$	0.0354	0.0009	0.0009
$\kappa = \frac{8}{12}$	0.0304	0.0008	0.0008
$\kappa = \frac{9}{12}$	0.0274	0.0007	0.0007
$\kappa = \frac{10}{12}$	0.0532	0.0014	0.0014
$\kappa = \frac{11}{12}$	0.0289	0.0008	0.0008
$\kappa = \frac{12}{12}$	0.0263	0.0007	0.0007

Table 16: The table shows sample mean, standard error and RMSE for parameters b^κ for $\kappa = \frac{1}{12}, \dots, \frac{12}{12}$ for 753 samples and 1000 replications.

Results presented in column 2 in Table 14-16 show that point estimates for long term mean and volatility parameter are on average close to the true values when comparing to Table 3 and Table 5. This is not the case for parameters representing the speed of mean reversion α and a^κ since point estimates are on average not close to the true value. This can be seen by comparing values in column 2 in Table 14 and Table 15 to Table 3 and 5.

Column 3 in Table 14-16 shows that estimators for μ , σ and b^κ have standard errors that are significantly smaller than for estimators of α and a^κ . Similar results are shown for RMSE, see column 4 in Table 14-16 where estimators of long term mean and volatility have smaller RMSE than for estimators of mean reversion parameters.

Summarising, results presented in Table 14-16 show that point estimates are on average close to the true value for estimators of σ and b^κ . The estimators also have the smallest RMSE and standard error among the analysed estimators. Therefore the conclusion is drawn that estimators for the volatility parameter appear to be the most accurate among the analysed estimators. Table 14-16 show that estimators for α and a^κ for $\kappa = \frac{1}{12}, \dots, \frac{12}{12}$ generated point estimates that were on average not close to the true parameter value. Results also suggest that these estimators had the largest standard errors and RMSE among the analysed estimators. This leads to the conclusion that estimators for parameters representing the speed of mean reversion seem to be the most inaccurate. This result is consistent with results found in literature see for example [22].

Next, the sample mean, standard error and RMSE was computed for different sample sizes. Since the same method for parameter estimation is used for both state variable processes it was chosen to analyse only the process representing the logarithm of average futures price. The result is presented in Figure 41-46.

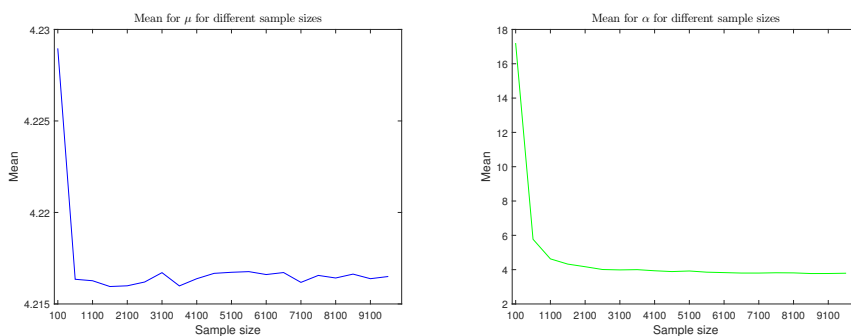


Figure 41: *Left:* Mean for estimates of μ when increasing the number of samples from 100 to 9600 with a step size of 500. The simulations were repeated 1000 times for every sample size. *Right:* Mean for estimates of α when increasing the number of samples from 100 to 9600 with a step size of 500. For every sample the simulation were repeated 1000 times.

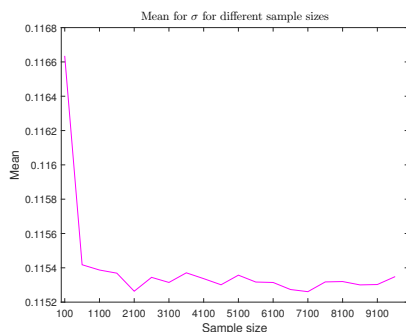


Figure 42: Mean for estimates of σ when increasing the number of samples from 100 to 9600 with a step size of 500. For every sample size the simulations were repeated 1000 times.

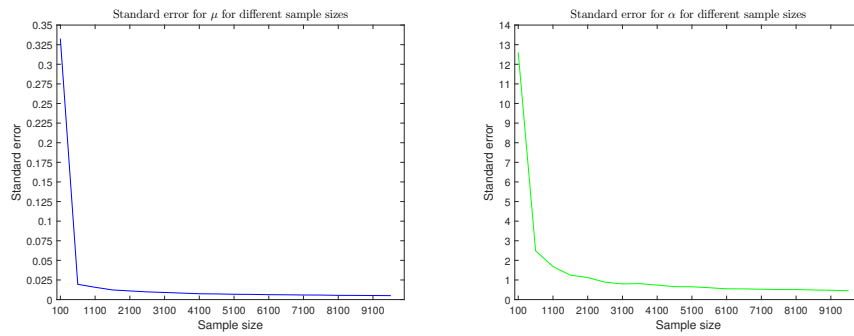


Figure 43: *Left:* Standard error for μ when increasing the number of samples from 100 to 9600 with a step size of 500. For every sample size the simulations were repeated 1000 times. *Right:* Standard error for α when increasing the number of samples from 100 to 9600 with a step size of 500. For every sample size the simulations were repeated 1000 times.

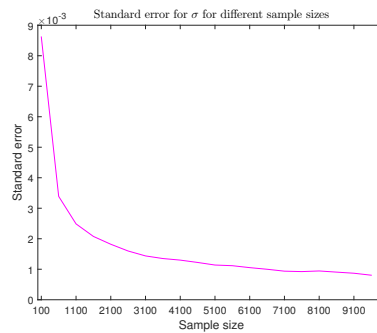


Figure 44: Standard error for σ when increasing the number of samples from 100 to 9600 with a step size of 500. For every sample size the simulations were repeated 1000 times.

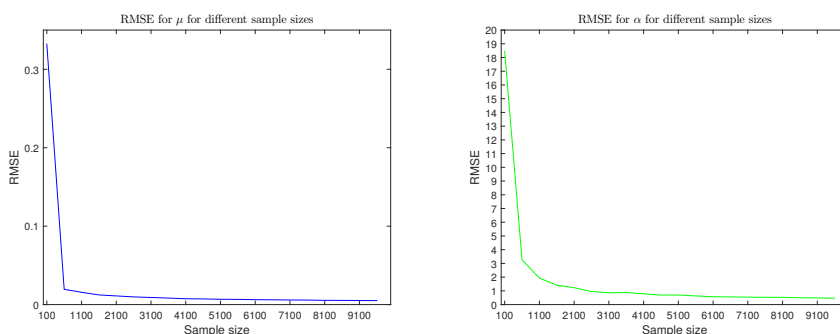


Figure 45: *Left:* RMSE for μ when increasing the number of samples from 100 to 9600 with a step size of 500. For every sample size the simulations were repeated 1000 times. *Right:* RMSE for α when increasing the number of samples from 100 to 9600 with a step size of 500. For every sample size the simulations were repeated 1000 times.

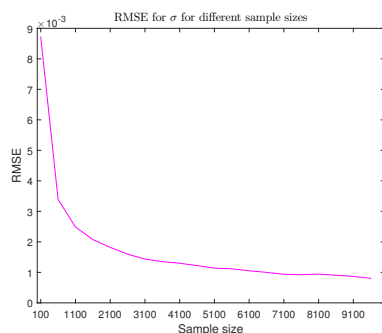


Figure 46: RMSE for σ when increasing the number of samples from 100 to 9600 with a step size of 500. For every sample size the simulations were repeated 1000 times.

From the left plot in Figure 41 and Figure 42 it can be seen that the sample mean was close to the true value for all sample sizes. This was not really the case for α , see right plot in Figure 41 where sample sizes greater than 1100 was needed to get a sample mean just over 4. However this is still not as close to the true value as for estimators of μ and σ .

Figure 43 and Figure 44 shown how the standard error depends on sample size for the three estimators. From the left plot in Figure 43 it can be seen that the standard error decrease significantly for sample sizes 600 which is needed to obtain standard errors of order 10^{-2} . In Figure 44 one can see that the standard error is of order 10^{-3} already for sample size 100. How the standard error depends on sample size for the estimator of α is shown in the right plot in Figure 43. The figure shows that in order to obtain standard errors that are of order 10^{-1} a sample sizes greater than 2100 is needed.

Lastly how the RMSE depends on sample size is discussed. For the estimator of α the right plot in Figure 45 shows that sample sizes greater than 2100 are needed to obtain RMSE of order 10^{-1} . This is not close to the estimator of σ that seem to have an RMSE of order 10^{-3} for all sample sizes analysed, see Figure 46. For the estimator of μ , see the left plot in Figure 45 showing that a sample size of 600 is needed to obtain RMSE of order 10^{-2} .

Due to the results in Figure 41-46 the conclusion is drawn that parameters representing the speed of mean reversion needs the largest number of samples among the estimators analysed in order to improve the accuracy. However the accuracy obtained for very large samples is still far from the accuracy for the estimator of σ .

8 Summery and conclusion

In this thesis the aim was to suggest a method to validate the market commodity forward curve. The method proposed was to create a reference curve using theoretical models. It was chosen to simulate futures prices with the seasonal cost-of-carry model and create the reference curve using linear interpolation between the simulated values. The seasonal cost-of-carry model was chosen because; it models futures prices under the real world probability measure, it is claimed to be applicable to commodities with seasonal patterns and uses a more stable quantity as state variable than the spot price.

The validation method was applied to UK natural gas futures for every trading day in December 2013. It was noticed that the simulated curves seemed to capture the seasonal behaviour of UK natural gas in a correct way. This is because futures prices for contracts maturing in the winter months were larger than for contracts maturing in the summer, see Figure 26 and 27. However the spread among the simulated curves increased when moving away from the last observed data point, compare Figure 27 to the upper plot in Figure 26.

In the seasonal cost-of-carry model the logarithm of the average futures price and stochastic convenience yield are assumed to follow Ornstein Uhlenbeck in discrete time given by equation (25) and (26). In section *Original data set* it was analysed if observed time series fulfil these assumptions.

First the logarithm of average futures prices was analysed for the observation period 2011-01-01 to 2013-11-30. The sample ACF for model residuals, see left plot in Figure 28 suggests that the residuals seem to be realisations of IID noise. Results were consistent with Ljung-Box Q-Test. However the distribution of the residuals did not seem to fulfil the assumption given in equation (25). The conclusion was drawn because the qq-plot in Figure 29 does not show a linear plot with slope equal to one. The graphical result was consistent with result generated from one sample Kolmogorov-Smirnov test. Therefore the conclusion was drawn that the observed time series for 2011-01-01 to 2013-11-30 did not meet assumptions in (25).

The same analysis was repeated for the stochastic convenience yield. Sample ACF shown in Figure 30-31 and Figure 47-56 in Appendix E suggests that for every κ except $\kappa = \frac{4}{12}$ the residuals seem to be realisations of IID noise. This result was consistent with Ljung-Box Q-test presented in Table 6. Graphical analyses of qq-plots and histograms, see Figure 32-33 and Figure 57-65 in Appendix E show that for $\kappa = \frac{5}{12}, \frac{8}{12}$ the residuals appear to satisfy the assumption of the distribution of the noise in (26). Results were consistent with one sample Kolmogorov-Smirnov test, see Table 7. Due to the presented

results it appears plausible to conclude that model assumptions for observed time series for stochastic convenience yield only satisfy assumptions in (26) for $\kappa = \frac{5}{12}, \frac{8}{12}$.

Since price data was volatile in the beginning of the observation period the data set was shorted to 2012-07-01-2013-11-30. An analysis was therefore performed to investigate if shortening the observation period could improve the result that the majority of observed time series did not satisfy model assumptions. This was done in section *Different set of historical observations* with the same method as for the original data set. Results suggests that the observed time series for $\ln(\bar{F}(t))$ still did not fulfil the assumption in (25). The conclusion was drawn by analysing Figure 35 and Figure 36. The results were consistent with results found when performing Ljung-Box Q-test and one sample Kolmogorov-Smirnov test.

For the stochastic convenience yield the results were slightly improved since for $\kappa = \frac{6}{12}, \frac{7}{12}, \frac{8}{12}, \frac{9}{12}, \frac{11}{12}, \frac{12}{12}$ the assumptions given in (26) seem to be fulfilled. The conclusion was drawn by investigating Figure 37-38, Figure 66-75 and Figure 76-83. The graphical analysis was consistent with statistical tests, see Table 8 and Table 9 except for $\kappa = \frac{4}{12}, \frac{10}{12}$.

In the section *Reduce processes to random walks?* an analysis was performed to investigate if there is a possibility to reduce observed time series for the state variables to random walks. This was done by applying likelihood ratio test with the null hypothesis of setting the speed of mean reversion equal to zero. Results are presented in Table 10 and Table 11 suggesting that for $\kappa = \frac{3}{12}, \frac{4}{12}, \frac{5}{12}, \frac{9}{12}, \frac{12}{12}$ the null hypothesis is accepted. Therefore it seemed possible to reduce these processes to random walks. Since observed time series for $\kappa = \frac{3}{12}, \frac{4}{12}, \frac{5}{12}, \frac{9}{12}, \frac{12}{12}$ could be reduced to random walks it is difficult to predict future values from these processes because the random walk is none stationary. Shorting the observation period 2012-07-01-2013-11-30 did not improve the results.

In the last section of the report the maximum likelihood method for estimating parameters in the stochastic process was analysed. First it was investigated if the parameter estimation procedure works. Estimating parameters with OLS gave consistent results with maximum likelihood estimates, see Table 12 and Table 13. Therefore the conclusion was drawn that the estimation procedure works. Then it was analysed if the maximum likelihood estimates captures the behaviour in historical data. From Figure 39 and 40 it could be concluded that the behaviour in historical data was correctly captured by the estimates.

Then the accuracy of the estimators was investigated. Results in Table 14-16 suggests that estimators of volatility parameters are the most accurate. This is because point estimates were on average close to the true values and

the estimators had smallest RMSE and standard errors among the analysed estimators. The presented results also show that estimators of mean reversion parameters have the poorest accuracy. This is because point estimates where on average not close to the true values and the estimators had the largest standard errors and RMSE.

Finally it was analysed how the accuracy of the estimators depend on sample size. Figure 41-46 show that estimator of mean reversion parameter needs large sample sizes to improve the accuracy. But even for large sample sizes the accuracy was still significantly less than for the estimator of the volatility.

The conclusion is drawn that the suggested model does not seem applicable for validating the market forward curve for UK natural gas futures. Firstly, due to that observed time series did not satisfy model assumptions. Perhaps the assumptions would be satisfied for all state variable process if the validation method was applied to another time period. However it is difficult to use a model for validation if it is not always the case that historical data meets model assumptions. The second reason is because it was found that for some observed time series it was possible to set the parameter representing the speed of mean reversion equal to zero. This is a negative aspect since these time series cannot be used for prediction.

References

- [1] Hull, J. *Fundamentals of Futures and Option Markets*. Pearson Education, 2014.
- [2] Brigo, D., Mercurio, F. *Interest Rate Models – Theory and Practice*. Springer, 2007.
- [3] Schofield, C. N. *Commodity Derivatives Markets and Applications*. Wiley, 2007.
- [4] Djehiche, B. *Stochastic Calculus An Introduction with Applications*. KTH, 2001.
- [5] <https://www.theice.com/products/910/UK-Natural-Gas-Futures>
- [6] Benth, E. F., Kholodnyi, A. V., Laurence, P. *Quantitative Energy Finance Modeling, Pricing, and Hedging in Energy and Commodity Markets*. Springer, 2014.
- [7] Hult, H., Lindskog, F., Hammarid, O., Rehn, J. C. *Risk and Portfolio Analysis*. Springer, 2012.
- [8] <https://www.theice.com/products/219/Brent-Crude-Futures>
- [9] Geman, H. *Risk Management in Commodity Markets: From Shipping to Agriculturals*. Wiley, 2008.
- [10] Borovkova, S., Geman, H. *Seasonal and stochastic effects in commodity forward curves*. Springer, 2006.
- [11] Geman, H. *Commodities and Commodity Derivatives Modeling and Pricing for Agriculturals, Metals and Energy*. Wiley, 2005.
- [12] Clewlow, L., Strickland, C. *Energy Derivatives: Pricing and Risk Management*. Lacima, 2000.
- [13] Björk, T. *Arbitrage Theory in Continuous Time*. Oxford University Press, 2009.
- [14] Gillespie, D. T., Seitaridou, E. *Simple Brownian Diffusion: An Introduction to the Standard Theoretical Models*, Oxford University Press, 2012.
- [15] Schwartz, E. *The stochastic behaviour of commodity prices: Implications for valuation and hedging*. Journal of Finance Vol 52 No. 3 pp 923-973, 1997
- [16] Blom, G., Egner, J., Englund, G., Grandell, J., Holst, L. *Sannolikhetsteori och statistikteori med tillämpningar*, Studentlitteratur, 2005.

- [17] Koski, T. *Lecture Notes: Probability and Random Processes at KTH*. KTH, 2014.
- [18] Gibson, R., Schwartz, E. *Stochastic convenience yield and pricing of oil contingent claims*. Journal of Finance Vol 45 No. 3 pp 959-976, 1990.
- [19] Fama, J., French, R. *Commodity Futures Prices: Some Evidence on Forecast Power, Premiums, and the Theory of Storage*. The Journal of Business Vol 60 No. 1 pp 55-73, 1987.
- [20] Brockwell, P. J., Davis R. A. *Introduction to Time Series and Forecasting*. Springer, 2010.
- [21] Cryer, J. D., Kung-Sik, C. *Time Series Analysis With Application in R*. Springer, 2008.
- [22] Andersen, T. G., Davis, R. A., Kreiss, J. P., Mikosch, Th.V. *Handbook of Financial Time Series*. Springer, 2009.
- [23] Lang, H. *Topics on Applied Mathematical Statistics*. KTH, 2012.
- [24] Coles, S. *An Introduction to Statistical Modeling of Extreme Values*. Springer, 2001.
- [25] Kennedy, P. *A Guide to Econometrics 6E*. Oxford, 2008.

Appendices

Appendix A Mathematical background

In this Appendix essential mathematical background needed in the report is presented, starting with probability theory and time series analysis. After that some stochastic calculus is presented and lastly maximum likelihood estimation.

A.1 Probability theory

In this section some concepts in probability theory will be presented. First the definition of sample space, empty space, sigma algebra and filtration are going to be discussed, following with the definition of probability measure, stochastic processes and the concept of martingales.

The *sample space* is denoted Ω and is defined as the set of all possible outcomes of a certain experiment. Outcomes of an experiment that are not possible to occur belong to the *empty set* symbolised by \emptyset .

The collection of subsets under the sample space is denoted \mathcal{F} and called a *sigma algebra* if the following properties are fulfilled:

- The empty \emptyset set belongs to \mathcal{F} .
- If an event X_i belong to \mathcal{F} , then also the complement event to X_i belongs to \mathcal{F} .
- If the events $X_1, X_2, X_3 \dots$ belong to \mathcal{F} , then the union of the events also belong to \mathcal{F} .

If there exists a set of increasing sigma algebra and if the following chain of sigma algebras can be constructed

$$\mathcal{F}_1 \subset \mathcal{F}_2 \subset \dots \subset \mathcal{F}_n,$$

where the sign \subset means that every set in \mathcal{F}_1 also belong to \mathcal{F}_2 , then the constructed chain is called a *filtration* [4].

The filtration will be denoted $\{\mathcal{F}_t\}_{t=1}^n$ and can be thought of as the information available up to time n [13].

Now the definition of a probability measure on (\tilde{P}, \mathcal{F}) is going to be presented. In order for \tilde{P} to be a probability measure the following properties must be fulfilled

- $\tilde{P}(\Omega) = 1$
- $\tilde{P}(\emptyset) = 0$
- $\tilde{P}(B) \geq 0$
- If for every event B_i for $i = 1, 2, 3, \dots$ that belong \mathcal{F} it holds that union of B_m and B_n for every $m \neq n$ is the empty set, then

$$\tilde{P}(\cup_{i=1}^{\infty} B_i) = \sum_{i=1}^{\infty} \tilde{P}(B_i).$$

The above properties are requirements that have to be fulfilled in order for a measure to be considered as a probability measure. In this report the real world probability measure will be all through the report be denoted P and the risk neutral measure will be denoted Q . The *probability space* is given by $(\tilde{P}, \Omega, \mathcal{F})$ and consist of the probability measure \tilde{P} , the sample space Ω and the sigma algebra \mathcal{F} of subsets of Ω [4].

Continuous stochastic processes can be viewed as models for how random events develop over time. A stochastic process is defined as the set of random variables given by

$$Y = \{Y_t\}_{t=1}^n,$$

where all Y_t are defined on the same probability space [17].

In order for a stochastic process Y to be a martingale with respect to the filtration $\{\mathcal{F}_t\}_{t=1}^n$ the following properties must be fulfilled

- Y must be measurable with respect to the sigma algebras \mathcal{F}_t that construct the filtration $\{\mathcal{F}_t\}_{t=1}^n$.
- For all t it must hold that $E[|Y_t|] < \infty$.
- $E[Y_t | \mathcal{F}_{t-1}] = Y_{t-1}$ *martingale property*

The martingale property can be interpreted as, that the best guess of the price tomorrow given the information today is the price today [13].

A.2 Time series analysis

Now some basic result in time series analysis will be presented. First the concepts of stationarity and the definition of autocovariance function and mean function, following with a presentation of IID noise and random walk. Lastly the autoregressive processes and its properties will be discussed.

The sequence $\{Z_t, t = 0, \pm 1, \pm 2, \dots\}$ is said to be a stationary time series if the statistical properties that drive the evolution of the process are independent of time. If outcomes from the sequence are given by Z_{t_1}, \dots, Z_{t_n}

and $Z_{t_1-h}, \dots, Z_{t_n-h}$ have the same joint distribution for all lags h and all time points t_1, \dots, t_n the series is said to be *strictly stationary* [21]. A time series is said to be *weakly stationary* if the following conditions are fulfilled

- The autocovariance function is independent of time for all lags.
- The mean function is independent of time.

In this report a time series that is weakly stationary will be referred to as a stationary time series.

If a stationary time series given is by the sequence $\{Z_t, t = 0, \pm 1, \pm 2, \dots\}$, the *autocovariance* function is defined as

$$\gamma_Z(h) = Cov(Z_{t+h}, Z_t),$$

where h is the lag.

The mean function is defined as

$$\mu_Z(t) = E[Z_t],$$

where $t = \pm 1, \pm 2, \dots$.

If the set of observations from $\{Z_t\}_{t=1}^n$ are given by z_1, \dots, z_n the sample autocovariance function can be calculated by the following relation

$$\hat{\gamma}(h) = \frac{1}{n} \sum_{t=1}^{n-|h|} (z_{t+|h|} - \bar{z})(z_t - \bar{z}), \quad -n < h < n,$$

where \bar{z} is the sample mean of the set of observations z_1, \dots, z_n . The sample autocorrelation function (ACF) is defined as

$$\hat{\rho}(h) = \frac{\hat{\gamma}(h)}{\hat{\gamma}(0)}$$

[20].

A.2.1 IID noise

A time series of random variables that are independent and identically distributed with zero mean and constant standard deviation is called *IID noise*. Since the IID noise is a sequence of independent random variables with mean zero and constant variance the autocovariance function for all lags h is given by

$$\begin{cases} \gamma(t, t) = \sigma^2 \\ \gamma(t+h, t) = 0 \quad \text{if } h \neq 0. \end{cases}$$

In order to check if data is a realisation of IID noise the sample ACF can be analysed. For an IID sequence it holds that for large sample sizes and lags greater than zero the sample ACF is normally distributed mean zero and variance $\frac{1}{n}$ where n is the sample size. Therefore a sample can be considered as IID noise if 95 percent of the sample ACF for lags larger than zero do not exceed the *IID threshold* given by $\pm \frac{1.96}{\sqrt{n}}$ [20].

A.2.2 Random walk

If a sequence $\{\epsilon_t, t = \pm 1, \pm 2, \dots\}$ consist of independent and identically distributed random variables with zero mean and constant standard deviation a new time series $\{Z_t, t = \pm 1, \pm 2, \dots\}$ can be constructed by performing the following steps

$$\begin{cases} Z_1 = \epsilon_1 \\ Z_2 = \epsilon_1 + \epsilon_2 \\ \vdots \\ Z_t = \epsilon_1 + \dots + \epsilon_t \end{cases}$$

which can be summerized as

$$Z_t = Z_{t-1} + \epsilon_t. \tag{45}$$

The time series given by equation (45) is called a random walk. Because the sequence $\epsilon_1, \epsilon_2, \dots$ has zero mean the time series given by (45) will also have zero mean for all t . For all lags $h > 0$ the autocovariance function can be calculated as

$$\begin{aligned} \gamma(t+h, t) &= Cov(Z_{t+h}, Z_t) \\ &= Cov(\epsilon_1 + \dots + \epsilon_t + \epsilon_{t+h}, \epsilon_1 + \dots + \epsilon_t) \\ &= t\sigma_\epsilon^2, \end{aligned}$$

where σ_ϵ is the standard deviation for every random variable in time series $\{\epsilon_t, t = \pm 1, \pm 2, \dots\}$. One can therefore notice that the random walk is not stationary since the autocovariance function is an increasing function of time [21].

A.2.3 Autoregressive process

If a random variable is a linear combination of the m most nearest past values together with random term given by IID noise the process is said to

be an autoregressive process of order m (AR(m)). If the series $\{Y_t\}_{t=1}^n$ is autoregressive process of order m then

$$Y_t = \beta_0 + \beta_1 Y_{t-1} + \beta_2 Y_{t-2} + \cdots + \beta_m Y_{t-m} + \epsilon_t,$$

where β_0, \dots, β_1 are coefficients. Letting the process be of order one gives

$$Y_t = \beta_0 + \beta_1 Y_{t-1} + \epsilon_t.$$

The above process is called an autoregressive process of order one and is stationary if $|\beta_1| < 1$. On the other hand if $|\beta_1| \geq 1$ the process is not stationary. For the case when $\beta_1 = 1$ and $\beta_0 = 0$ the process is reduced to a random walk, see equation (45) [21].

A.3 Stochastic calculus

In this section some stochastic calculus need in the report is presented. First the definition of Brownian motion, then some theory about stochastic differential equations. After that the definition of Ito's formula is presented. Lastly some examples of stochastic process are going to be outlined.

Brownian motion

On the real world probability space the Brownian motion is denoted B_t and defined as a continuous real valued stochastic process with the following properties

- At $t = 0$ the value of the process is zero.
- For every time point greater than zero it holds that B_t is measurable w.r.t \mathcal{F}_t .
- B_t is normally distributed with zero mean and variance t for every time point t greater than zero.
- The process has trajectories that are almost surely continuous [4].

The differential of the Brownian motion is written dB_t . Due to properties of the Brownian motion presented above, it will hold that dB_t normally distributed with mean zero and variance dt [11].

Stochastic differential equations

Deterministic differential equations can be used to describe dynamics of different phenomenon. The simplest differential equation is obtained when the dynamics can be described by first order derivatives. An example of

such a differential equation is given by

$$\begin{cases} y'(t) = a(t, y(t)) \\ y(0) = y_0. \end{cases}$$

In the above system the initial condition is a deterministic quantity. But in some cases the initial conditions is not deterministic but instead a function of some random event. For those cases the initial condition must instead be described as function of a noise term, where the distribution of the noise is known in advance. When the initial condition is stochastic the differential equation is called a *stochastic differential equation* (SDE) and the solution is given by a stochastic process. One can therefore describe the dynamics of a stochastic process by using stochastic differential equations. In many cases the random noise can be described by the differential of Brownian motions and for those cases a general form of the SDE is given by

$$\begin{cases} dY_t = a(t, Y_t)dt + b(t, Y_t)dB_t \\ Y_s = Z_s, \end{cases} \quad (46)$$

where the functions $a(t, Y_t)$ and $b(t, Y_t)$ are real valued deterministic functions representing the rate of change for dt and dB_t respectively. The dt term is called drift and dB_t term is called diffusion. A solution to the SDE (46) is obtained by integrating the left and right side of the above equation respectively. This gives

$$Y_t - Y_s = \int_s^t a(t, Y_u)du + \int_s^t b(t, Y_u)dB_u. \quad (47)$$

The second integral in equation (47) is a stochastic integral, these are called *Ito integrals* [4].

Ito's formula

For some SDE's there exists exact solutions, examples of such are the dynamics of the Geometric Brownian Motion (GBM) and Ornstein-Uhlenbeck process (mean reverting process). In order find a solution to a SDE Ito's formula can be used. If it is assumed that a function denoted g has continuous second order derivatives. Then for every t greater or equal to zero Ito's formula in differential form is given by

$$dg(B_t) = g'(B_t)dB_t + \frac{1}{2}g''(B_t)dt$$

[4].

Below some examples of SDE's for different stochastic process are going to be presented together with some properties for each process respectively.

Geometric Brownian motion

The stochastic process called Geometric Brownian motion (GBM) is often used for different financial applications. If a process Y_t is a GBM. Then it is a solution to the following SDE

$$\begin{cases} dY_t = \mu Y_t dt + \sigma Y_t dB_t \\ Y_s = Z_s, \end{cases}$$

where μ and σ positive constants [12]. The GBM is a process that can possibly take values between minus infinity and infinity. This property of a very large spread of possible values is not always applicable for financial applications. Hence in some cases another process called Ornstein–Uhlenbeck is more appropriate to use [11].

Ornstein–Uhlenbeck (mean reversion)

An Ornstein–Uhlenbeck (mean reverting) process is a solution to the following SDE

$$\begin{cases} dY_t = \alpha(\mu - Y_t)dt + \sigma dB_t \\ Y_s = Z_s, \end{cases} \quad (48)$$

where α is called the speed of mean reversion, μ is the long term mean, dB_t is the differential of the Brownian motion and Y_s is the initial condition. The mean reverting process has the property of always striving back to its long term mean given by μ with speed given by α [12]. In contrary to GBM the mean reverting process cannot take values between minus infinity and infinity. It is instead a process that fluctuates around its mean value. The mean reverting property can be analysed by considering the expected value of equation (48)

$$E[dY_t] = E[\alpha(\mu - Y_t)dt + \sigma dB_t] = E[\alpha(\mu - Y_t)dt] = \alpha(\mu - Y_t)dt. \quad (49)$$

In the above calculations it was used that the differential of a Brownian motion has zero mean and that Y_t is observed at time t . From equation (49) it can be concluded that if $\mu > Y_t$, the expected value will be positive and the process will increase to approach the long term mean. On the other hand if $\mu < Y_t$ the expected value is negative and the process will decrease to reach the long term mean.

For commodities it has been observed that the spot price tend to revert back to a long term mean representing the marginal production cost. Hence the mean reverting process is often used to model price dynamics for commodities [11].

A *strong solution* to equation (48) is given by (see Appendix B for computations)

$$Y_t = Y_s e^{-\alpha(t-s)} + \mu(1 - e^{-\alpha(t-s)}) + \int_s^t \sigma e^{-\alpha(t-u)} dB_u.$$

In the above relation it can be noticed that the third term is a stochastic integral with a deterministic integrand. Therefore due to properties of the stochastic integral the distribution is

$$\int_s^t \sigma e^{-\alpha(s-u)} dB_u \sim N\left(0, \frac{\sigma^2}{2\alpha} (1 - e^{-2\alpha(t-s)})\right).$$

Hence given the observation Y_s the distribution of the process is

$$Y_t \sim N\left(Y_s e^{-\alpha(t-s)} + \mu(1 - e^{-\alpha(t-s)}), \frac{\sigma^2}{2\alpha} (1 - e^{-2\alpha(t-s)})\right). \quad (50)$$

[4].

Because the future value Y_t depends only on the past through the current observation given by Y_s , the mean reverting process is a *Markov process*. Thus the process has no memory of the past because it only needs the current observation in order to decide the next future value [14].

A.4 Maximum likelihood estimation

Parameters in the SDE giving the dynamics of a process can be determined by a method called maximum likelihood estimation. When estimating parameters with maximum likelihood the goal is to find parameters so that the likelihood of obtaining a set of observations is maximized [12]. The interpretation of the method is intuitive for the case when observations have a discrete distribution. Then the likelihood function is a product of the probabilities for every observation in the set. When random variables have a continuous distribution the likelihood function is given by the joint density function for the random variables constructing the set. The likelihood function for a set of random variables with a continuous distribution is given by

$$L(\Theta) = f_{Y_0, \dots, Y_n}(\Theta),$$

where Y_0, \dots, Y_n are observations. If observations are independent and identically distributed the likelihood function can be simplified to

$$L(\Theta) = \prod_{i=0}^n f_{Y_i}(\Theta).$$

Where Θ is the set of unknown parameters. Taking the logarithm of the above relation gives the *log-likelihood function*

$$\ln L(\Theta) = \sum_{i=0}^n \ln f_{Y_i}(\Theta).$$

The aim of the maximum likelihood estimation is to find the set of parameters Θ so that the likelihood function is maximized. Often the log-likelihood function is considered instead since calculations are simplified when considering a sum instead of products. Because the logarithm is a strictly increasing function the same parameters are found when maximizing the log-likelihood function instead of the likelihood function [16]. It is also important to notice that likelihood estimates for large number of observations are consistent, efficient and that the distribution of the estimators are asymptotically normal [12].

A.4.1 Independent normally distributed set of observations

Application of maximum likelihood estimation will now be shown on a set of observations $\{Y_t\}_{t=1}^M$ that are independent and normally distributed with mean γ and standard deviation β . The density function for one observation Y_t is given by

$$f_{Y_t}(\Theta) = \frac{1}{\sqrt{2\pi\beta^2}} \exp -\frac{(Y_t - \gamma)^2}{2\beta^2},$$

where $\Theta = \{\gamma, \beta\}$. When observations are independent and normally distributed the likelihood of observing the entire set is given by

$$L(\gamma, \beta) = \prod_{i=1}^M \frac{1}{\sqrt{2\pi\beta^2}} \exp -\frac{(Y_i - \gamma)^2}{2\beta^2}.$$

The aim is now to find parameters γ and β so that the likelihood of observing Y_1, \dots, Y_M is maximized. For this case the log-likelihood function is given by

$$\ln(L(\gamma, \beta)) = \sum_{i=0}^M -\ln(\sqrt{2\pi\beta^2}) - \frac{(Y_i - \gamma)^2}{2\beta^2}.$$

Parameters β and γ can be determined by computing the gradient of the log-likelihood function with respect to β and γ and setting it equal to zero and solving each equation respectively [12].

A.4.2 Interference for parameters in mean reverting process

Maximum likelihood estimation can be used to determine parameters in equation (48) given a set of historical observations. However observations from a mean reverting process are not independent due to the Markov property of the process. One can start by letting discrete observations from the mean reverting process with dynamics given by (48) for equally spaced time differences be denoted Y_0, \dots, Y_N . The time difference between observation is written Δt .

The exact updating formula for the discrete representation of the mean reverting process with dynamics given by equation (48) is

$$Y_t = Y_{t-1}e^{-\alpha\Delta t} + \mu(1 - e^{-\alpha\Delta t}) + \left(\frac{\sigma^2}{\alpha^2} (1 - e^{-\alpha^2\Delta t})\right) \epsilon, \quad (51)$$

where ϵ is a standard normal variable. The density function for observation Y_t follow from the updating formula (51) and is given by

$$f_{Y_t|Y_{t-1}}(\alpha, \mu, \sigma) = \frac{1}{\sqrt{2\pi \left(\frac{\sigma^2}{\alpha^2} (1 - e^{-\alpha^2\Delta t})\right)}} \exp - \frac{(Y_t - Y_{t-1}e^{-\alpha\Delta t} - \mu(1 - e^{-\alpha\Delta t}))^2}{2 \left(\frac{\sigma^2}{\alpha^2} (1 - e^{-\alpha^2\Delta t})\right)}.$$

The likelihood function for observing the entire set is given by

$$L(\alpha, \mu, \sigma) = f_{Y_1|Y_0, \dots, Y_n|Y_{n-1}}(\alpha, \mu, \sigma).$$

Which is equivalent to

$$L(\alpha, \mu, \sigma) = \prod_{t=1}^N f_{Y_t|Y_{t-1}}(\alpha, \mu, \sigma).$$

Hence the likelihood function is given by

$$L(\alpha, \mu, \sigma) = \prod_{t=1}^N \frac{1}{\sqrt{2\pi \left(\frac{\sigma^2}{\alpha^2} (1 - e^{-\alpha^2\Delta t})\right)}} \exp - \frac{(Y_t - Y_{t-1}e^{-\alpha\Delta t} - \mu(1 - e^{-\alpha\Delta t}))^2}{2 \left(\frac{\sigma^2}{\alpha^2} (1 - e^{-\alpha^2\Delta t})\right)}.$$

Setting $\beta^2 = \frac{\sigma^2}{\alpha^2} (1 - e^{-\alpha^2\Delta t})$ and computing the logarithm gives the log-likelihood function

$$\ln(L) = -\frac{N}{2} \ln(2\pi) - \frac{N}{2} \ln(\beta^2) - \frac{1}{2\beta^2} \sum_{t=1}^N (Y_t - Y_{t-1}e^{-\alpha\Delta t} - \mu(1 - e^{-\alpha\Delta t}))^2$$

Parameters maximizing the log-likelihood are found by solving the following set of equations

$$\frac{\partial \ln(L)}{\partial \beta} = 0 \tag{52}$$

$$\frac{\partial \ln(L)}{\partial \alpha} = 0 \tag{53}$$

$$\frac{\partial \ln(L)}{\partial \mu} = 0. \tag{54}$$

From equation (52)-(54) estimators for parameters α , μ and σ can be determined. Since the mean reverting process has a density that can be expressed analytically it is one of few processes for which exact maximum likelihood estimation can be performed [22]. It can be noticed that the model representing the exact updating formula given by (51) is an autoregressive process of order one. If the speed of mean reversion is zero the process given by (51) will be reduced to a random walk.

Appendix B Analytic solution

In this Appendix steps for calculating analytic solutions for equation (48), (11) and (14) will be presented.

An exact solution to equation (48) can be found by computing the ansatz $X_t = e^{\alpha t} Y_t$ and apply Ito's formula to $X_t = e^{\alpha t} Y_t$, this gives

$$dX_t = \alpha e^{\alpha t} Y_t dt + e^{\alpha t} dY_t.$$

Hence the following expression is obtained

$$dX_t = \alpha \mu e^{\alpha t} dt + e^{\alpha t} \sigma dB_t.$$

Integrating the left and right hand side from s to t while assuming that $s < t$ gives

$$X_t - X_s = \mu(e^{\alpha t} - e^{\alpha s}) + \int_s^t e^{\alpha u} \sigma dB_u.$$

The initial condition for the process is Y_s . This implies that $X_s = Y_s e^{\alpha s}$ which gives

$$X_t = Y_s e^{\alpha s} + \mu(e^{\alpha t} - e^{\alpha s}) + \int_s^t e^{\alpha u} \sigma dB_u.$$

Now the solution is transformed back to a solution for Y_t

$$Y_t = Y_s e^{-\alpha(t-s)} + \mu(1 - e^{-\alpha(t-s)}) + \int_s^t e^{-\alpha(t-u)} \sigma dB_u. \quad (55)$$

The third term in (55) is a stochastic integral with a deterministic integrand and is therefore normally distributed with mean 0 and variance $\int_s^t e^{-2\alpha(t-u)} \sigma^2 du$. Hence the distribution for Y_t is given by

$$Y_t \sim N \left(Y_s e^{-\alpha(t-s)} + \mu(1 - e^{-\alpha(t-s)}), \int_s^t e^{-2\alpha(t-u)} \sigma^2 du \right) \quad (56)$$

An analytic solution to equation (11) can be found by performing the same steps as described above for (48). The analytic solution for (11) is

$$X_t = X_s e^{-\alpha(t-s)} + \mu(1 - e^{-\alpha(t-s)}) + \int_s^t e^{-\alpha(t-u)} \sigma dB_u^1.$$

An exact solution to (14) is also obtained by computing the same steps as for equation (48). The solution is given by the following equation

$$\delta_t^k = \delta_s^\kappa e^{-a^\kappa(t-s)} + \int_s^t e^{-a^\kappa(t-u)} b^\kappa dB_u^2.$$

[4].

Appendix C Model constraints

In this Appendix constraints that are need to be fulfilled in order for equation (9) to hold are going to be analysed. One can start by computing the logarithm of equation (7). This gives

$$\ln(F(t, T)) = \ln(\bar{F}(t)) + s(T) - \delta(t, T - t)(T - t).$$

Which is equivalent to

$$\ln(\bar{F}(t)) = \ln(F(t, T)) - s(T) + \delta(t, T - t)(T - t).$$

Inserting relation (9) gives

$$\ln(\bar{F}(t)) = \ln(F(t, T)) - s(T) + \delta(t, T - t)(T - t) = \frac{1}{n} \left(\sum_{T=1}^n \ln(F(t, T)) \right).$$

This is equivalent to

$$\begin{aligned} \ln(\bar{F}(t)) &= \frac{1}{n} \left(\sum_{T=1}^n \ln(\bar{F}(t)) + (s(T) - \delta(t, T - t)(T - t)) \right) = \\ &= \ln(\bar{F}(t)) - \frac{1}{n} \left(\sum_{T=1}^n s(T) \right) + \frac{1}{n} \left(\sum_{T=1}^n \delta(t, T - t)(T - t) \right). \end{aligned}$$

The second term in the above relation is zero since the model claims that the sum of seasonal components for all calender months is zero. Therefore the following relation is obtained

$$\ln(\bar{F}(t)) = \ln(\bar{F}(t)) - \frac{1}{n} \left(\sum_{T=1}^n \delta(t, T-t)(T-t) \right).$$

Hence it can be concluded that the sum of aggregated convenience yield must be zero in order for equation (9) to hold [10].

Appendix D Futures price dynamics

In order to analyse the dynamics of futures prices for the seasonal cost-of-carry model the following calculations must be performed.

Inserting the dynamics of the state variables given by (11) and (14) in (17) and setting $\delta(t, \kappa) = \delta_t^\kappa$ gives

$$d \ln(F(t, T)) = \alpha \mu dt - \alpha X_t dt + \sigma dB_t^1 - \kappa(-a^\kappa \delta_t dt + b^\kappa dB_t^2) - \delta_t^\kappa dt.$$

Integrating the above equation while assuming that $0 < t$ together with the initial condition $\ln(F(0, T)) = \ln(\bar{F}(0)) + s(T) - \delta_0^\kappa$ gives

$$\begin{aligned} \ln(F(t, T)) - \ln(F(0, T)) = & \\ & \int_0^t (\alpha \mu - \alpha X_u + \kappa a^\kappa \delta_u^\kappa - \delta_u^\kappa) du \\ & - \kappa \int_0^t b^\kappa dB_u^2 + \int_0^t \sigma dB_u^1. \end{aligned}$$

The second and third term in the above equation are stochastic integrals with deterministic integrands. Since the Brownian motions B_t^1 and B_t^2 are independent, the logarithm of the futures price will be normally distributed and equivalently the futures price is log-normally distributed [10].

Appendix E Figures original set of observations

In this Appendix figures are presented used for analysis in the section *Original historical data set*. First figures giving the sample ACF and realisation of model residuals given by relation (38) are presented in Figure 47-56. Following with qq-plots of empirical quantiles of normalised model residuals against standard normal quantiles together with histograms in Figure 57-65.

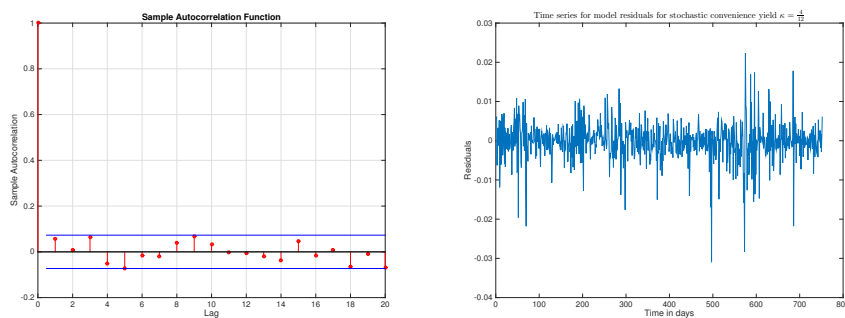


Figure 47: *Left:* ACF for model residuals for convenience yield time series for $\kappa = \frac{3}{12}$, where the IID thresholds are given by the blue horizontal lines. *Right:* Time series of model residuals for convenience yield.

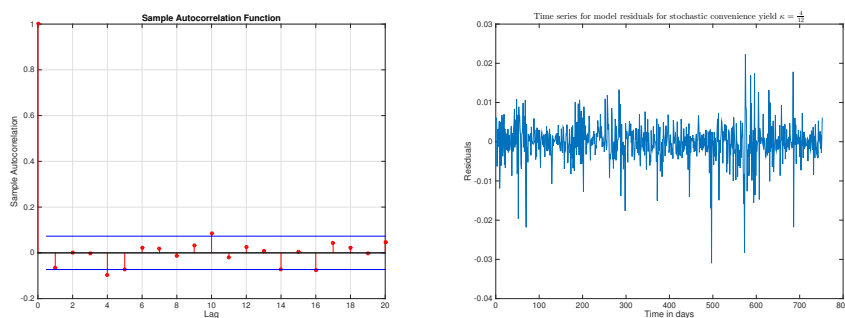


Figure 48: *Left:* ACF for model residuals for convenience yield time series for $\kappa = \frac{4}{12}$, where the IID thresholds are given by the blue horizontal lines. *Right:* Time series of model residuals for convenience yield.

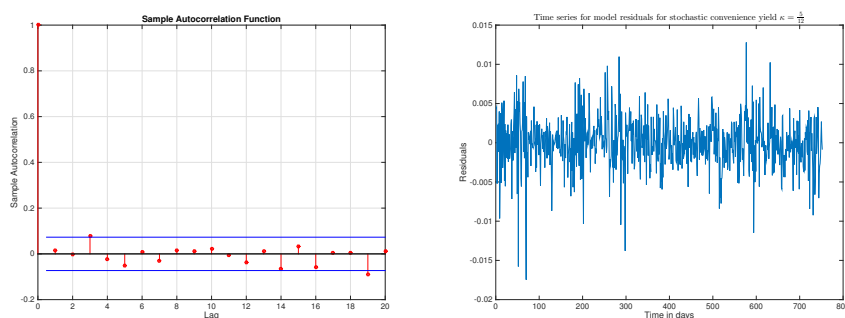


Figure 49: *Left:* ACF for model residuals for convenience yield time series for $\kappa = \frac{5}{12}$, where the IID thresholds are given by the blue horizontal lines. *Right:* Time series of model residuals for convenience yield.

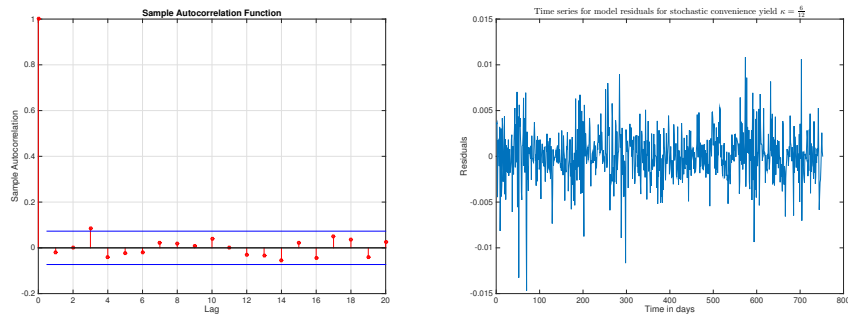


Figure 50: *Left:* ACF for model residuals for convenience yield time series for $\kappa = \frac{6}{12}$, where the IID thresholds are given by the blue horizontal lines. *Right:* Time series of model residuals for convenience yield.

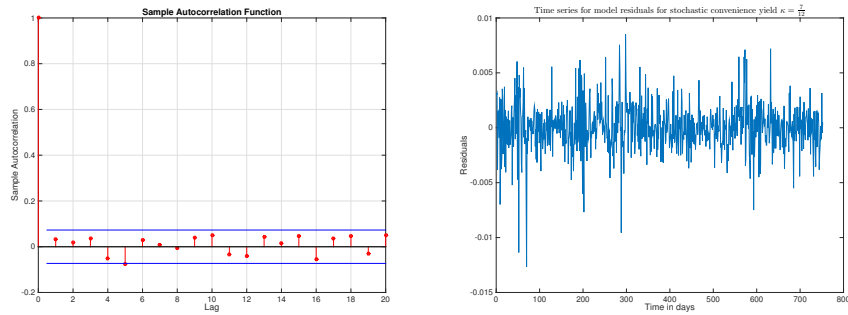


Figure 51: *Left:* ACF for model residuals for convenience yield time series for $\kappa = \frac{7}{12}$, where the IID thresholds are given by the blue horizontal lines. *Right:* Time series of model residuals for convenience yield.

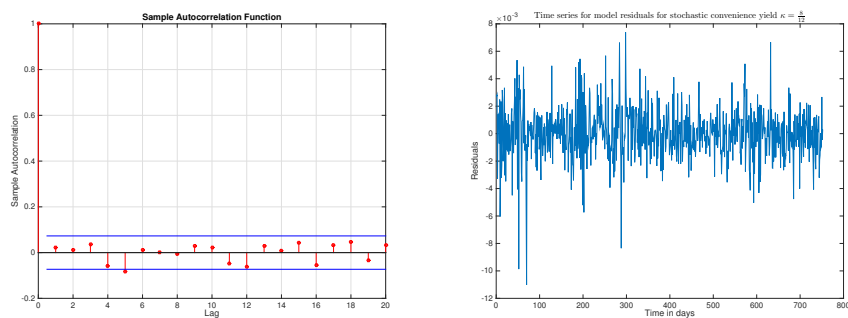


Figure 52: *Left:* ACF for model residuals for convenience yield time series for $\kappa = \frac{8}{12}$, where the IID thresholds are given by the blue horizontal lines. *Right:* Time series of model residuals for convenience yield.

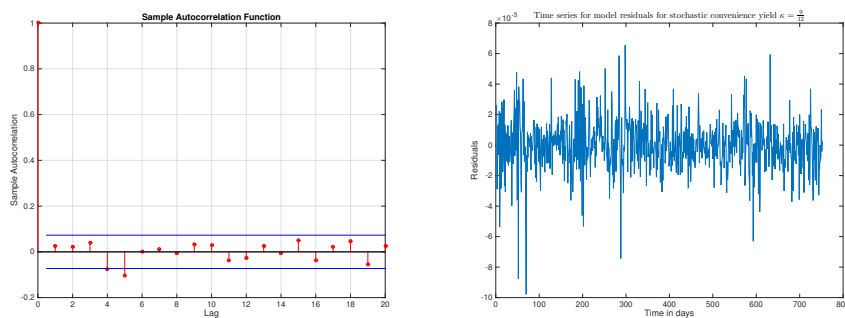


Figure 53: *Left:* ACF for model residuals for convenience yield time series for $\kappa = \frac{9}{12}$, where the IID thresholds are given by the blue horizontal lines. *Right:* Time series of model residuals for convenience yield.

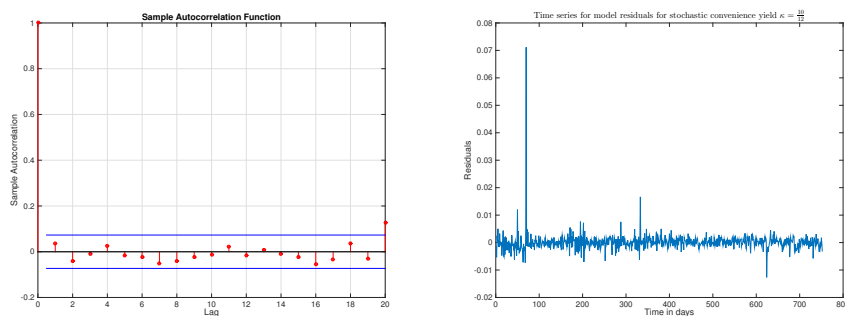


Figure 54: *Left:* ACF for model residuals for convenience yield time series for $\kappa = \frac{10}{12}$, where the IID thresholds are given by the blue horizontal lines. *Right:* Time series of model residuals for convenience yield.

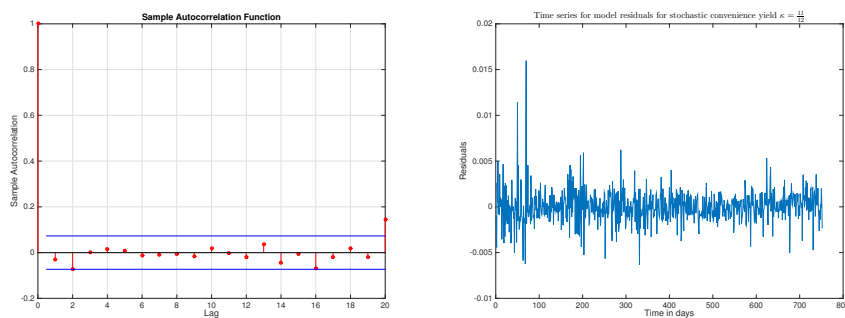


Figure 55: *Left:* ACF for model residuals for convenience yield time series for $\kappa = \frac{11}{12}$, where the IID thresholds are given by the blue horizontal lines. *Right:* Time series of model residuals for convenience yield.

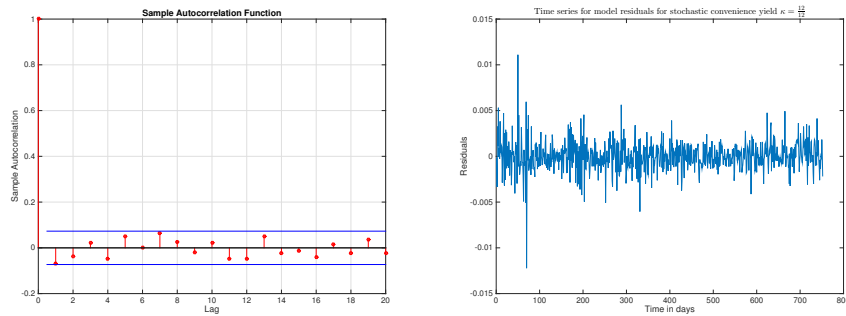


Figure 56: *Left*: ACF for model residuals for convenience yield time series for $\kappa = \frac{12}{12}$, where the IID thresholds are given by the blue horizontal lines. *Right*: Time series of model residuals for convenience yield.

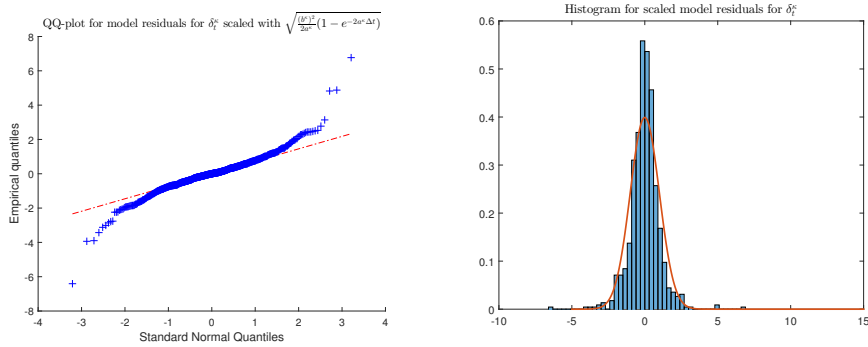


Figure 57: *Left*: QQ-plot for normalised model residuals against quantiles of standard normal distribution for $\kappa = \frac{3}{12}$. *Right*: Histogram of normalised residuals together with density of standard normal distribution.

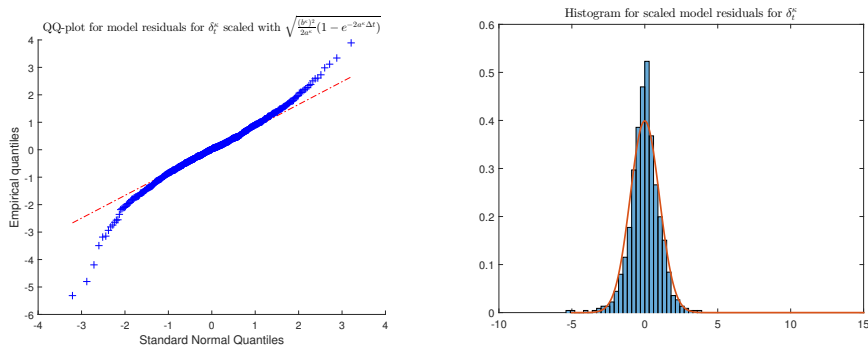


Figure 58: *Left*: QQ-plot for normalised model residuals against quantiles of standard normal distribution for $\kappa = \frac{5}{12}$. *Right*: Histogram of normalised residuals together with density of standard normal distribution.

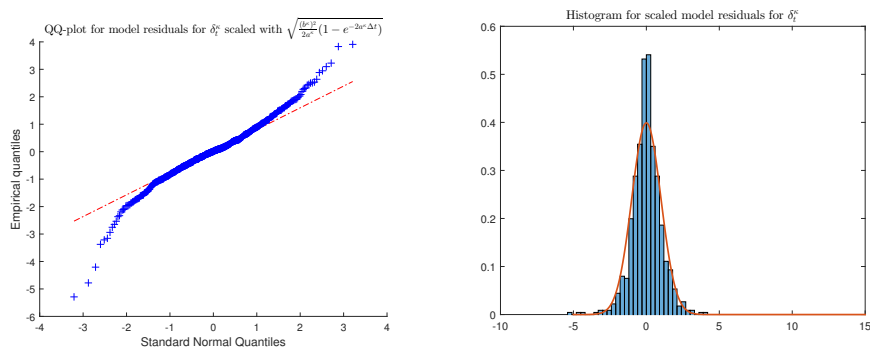


Figure 59: *Left:* QQ-plot for normalised model residuals against quantiles of standard normal distribution for $\kappa = \frac{6}{12}$. *Right:* Histogram of normalised residuals together with density of standard normal distribution.

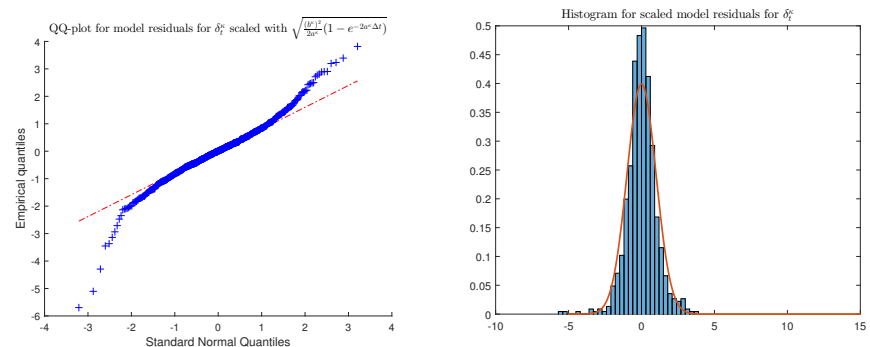


Figure 60: *Left:* QQ-plot for normalised model residuals against quantiles of standard normal distribution for $\kappa = \frac{7}{12}$. *Right:* Histogram of normalised residuals together with density of standard normal distribution.

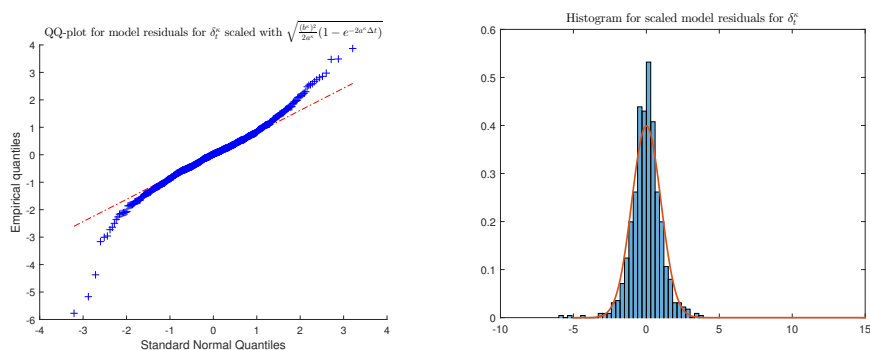


Figure 61: *Left:* QQ-plot for normalised model residuals against quantiles of standard normal distribution for $\kappa = \frac{8}{12}$. *Right:* Histogram of normalised residuals together with density of standard normal distribution.

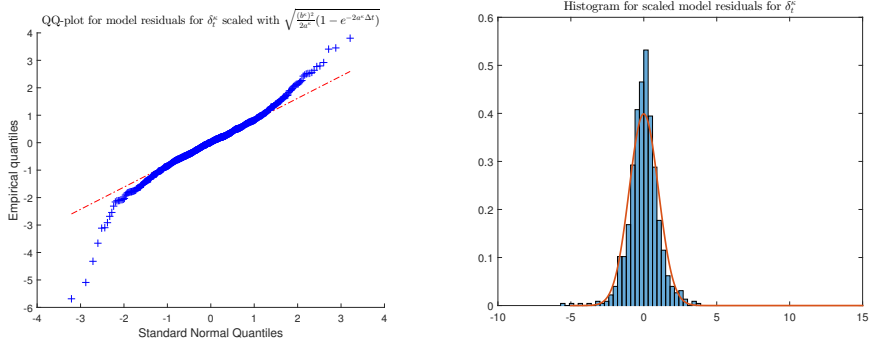


Figure 62: *Left:* QQ-plot for normalised model residuals against quantiles of standard normal distribution for $\kappa = \frac{9}{12}$. *Right:* Histogram of normalised residuals together with density of standard normal distribution.

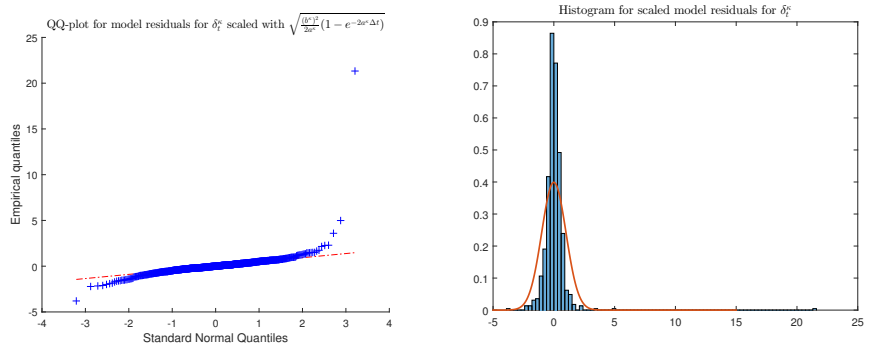


Figure 63: *Left:* QQ-plot for normalised model residuals against quantiles of standard normal distribution for $\kappa = \frac{10}{12}$. *Right:* Histogram of normalised residuals together with density of standard normal distribution.

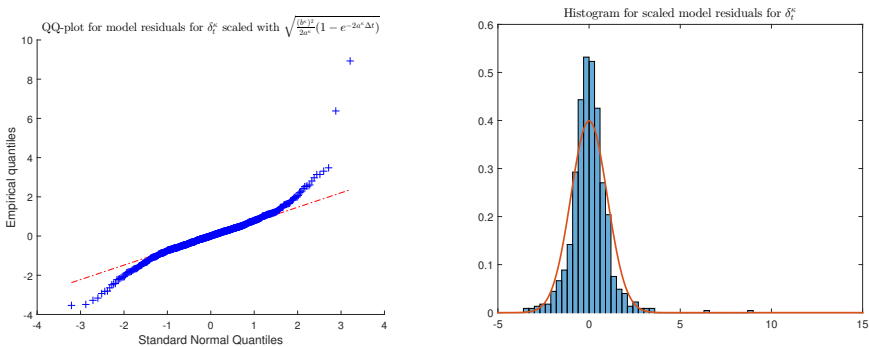


Figure 64: *Left:* QQ-plot for normalised model residuals against quantiles of standard normal distribution for $\kappa = \frac{11}{12}$. *Right:* Histogram for normalised residuals together with density for standard normal distribution.

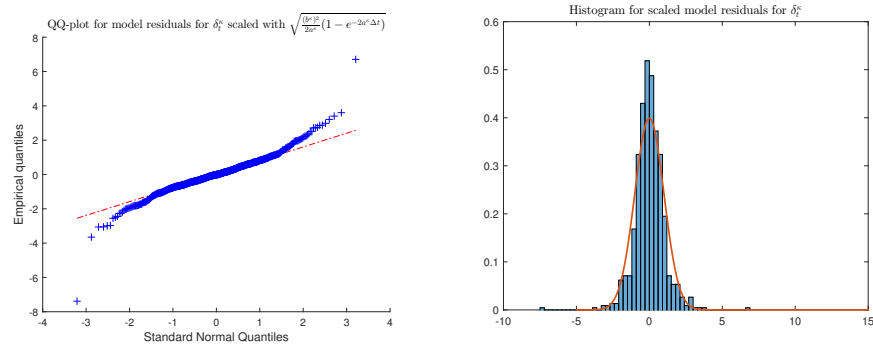


Figure 65: *Left:* QQ-plot for normalised model residuals against quantiles of standard normal distribution for $\kappa = \frac{12}{12}$. *Right:* Histogram for normalised residuals together with density for standard normal distribution.

Appendix F Figures different set of observations

In this section figures are presented used in the analysis in section *Different set of historical observations*. First sample ACF plots and time series for model residuals calculated with (38) for the time period 2012-07-01 to 2013-11-30 are presented, see Figure 66-75. After that qq-plots are presented where the empirical quantiles are given by normalised residuals plotted against standard normal quantiles together with histograms, see Figure 76-83.

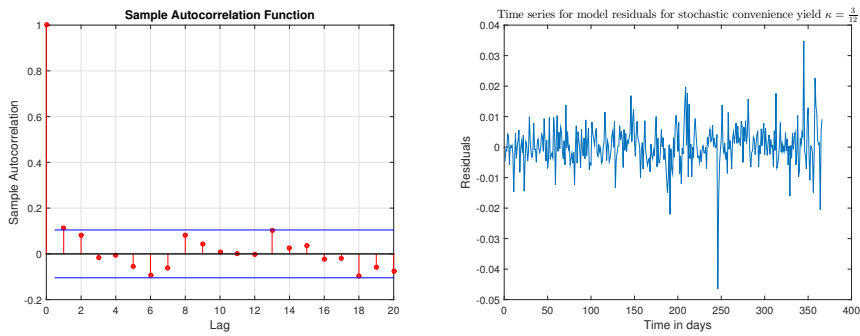


Figure 66: *Left:* ACF for model residuals for convenience yield time series for $\kappa = \frac{3}{12}$, where the blue horizontal lines represent the IID threshold. *Right:* Time series of model residuals for convenience yield.

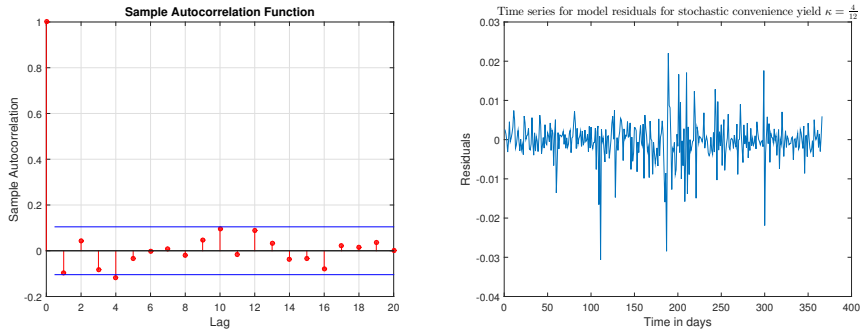


Figure 67: *Left:* ACF for model residuals for convenience yield time series for $\kappa = \frac{4}{12}$, where the blue horizontal lines represent the IID threshold. *Right:* Time series of model residuals for convenience yield.

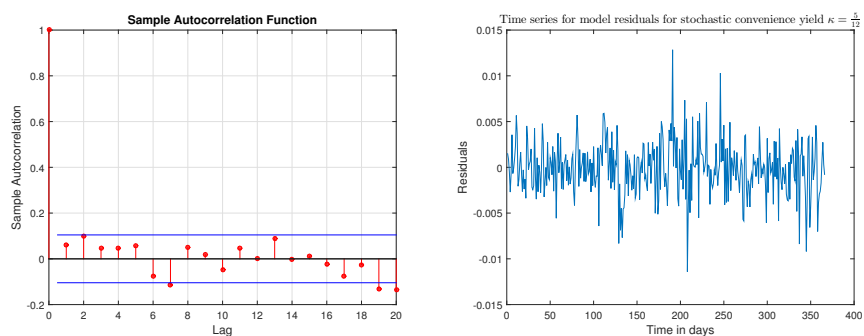


Figure 68: *Left:* ACF for model residuals for convenience yield time series for $\kappa = \frac{5}{12}$, where the blue horizontal lines represent the IID threshold. *Right:* Time series of model residuals for convenience yield.

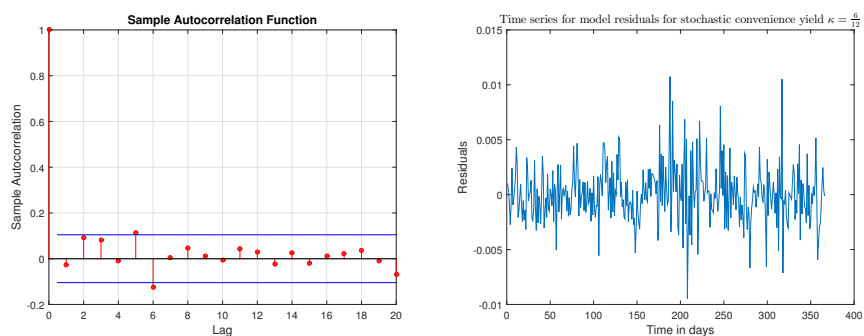


Figure 69: *Left:* ACF for model residuals for convenience yield time series for $\kappa = \frac{6}{12}$, where the blue horizontal lines represent the IID threshold. *Right:* Time series of model residuals for convenience yield.

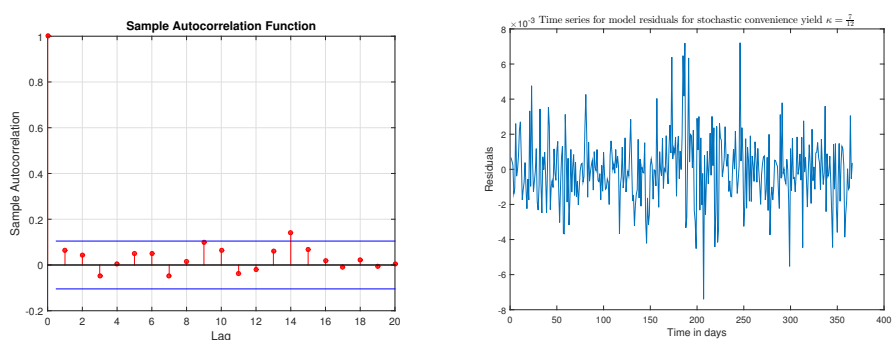


Figure 70: *Left:* ACF for model residuals for convenience yield time series for $\kappa = \frac{7}{12}$, where the blue horizontal lines represent the IID threshold. *Right:* Time series of model residuals for convenience yield.

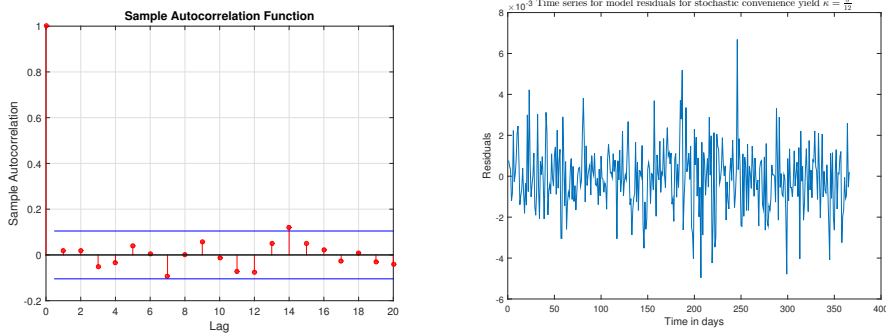


Figure 71: *Left:* ACF for model residuals for convenience yield time series for $\kappa = \frac{8}{12}$, where the blue horizontal lines represent the IID threshold. *Right:* Time series of model residuals for convenience yield.

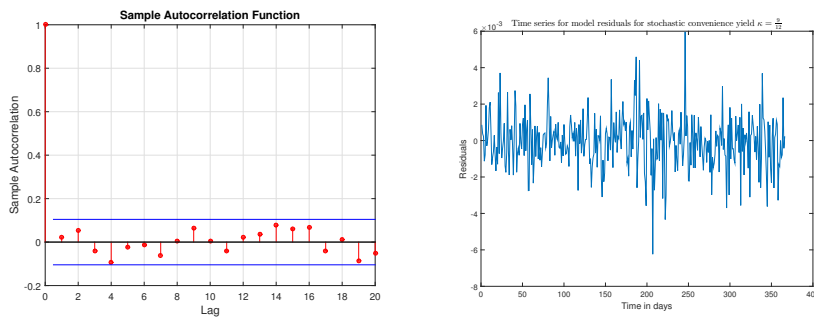


Figure 72: *Left:* ACF for model residuals for convenience yield time series for $\kappa = \frac{9}{12}$, where the blue horizontal lines represent the IID threshold. *Right:* Time series of model residuals for convenience yield.

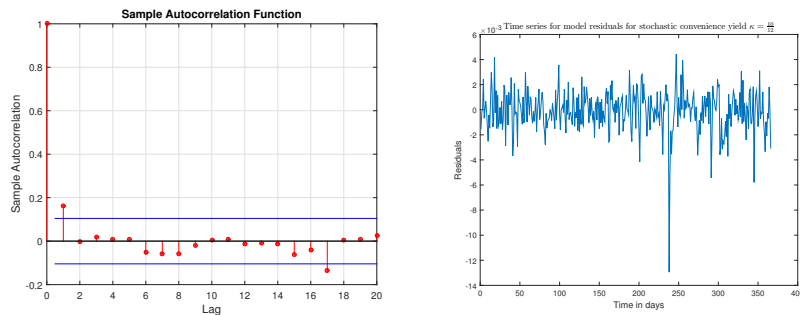


Figure 73: *Left:* ACF for model residuals for convenience yield time series for $\kappa = \frac{10}{12}$, where the blue horizontal lines represent the IID threshold. *Right:* Time series of model residuals for convenience yield.

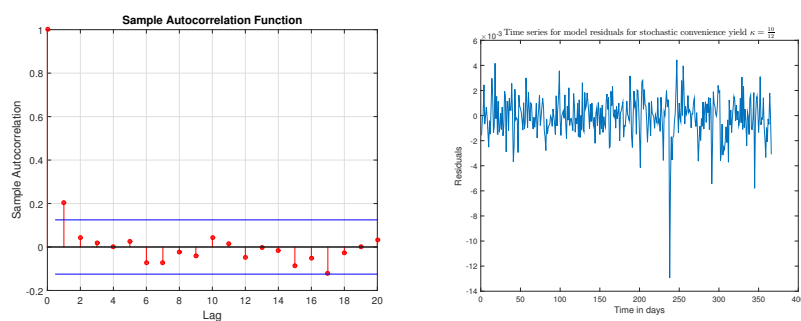


Figure 74: *Left:* ACF for model residuals for convenience yield time series for $\kappa = \frac{11}{12}$, where the blue horizontal lines represent the IID threshold. *Right:* Time series of model residuals for convenience yield.

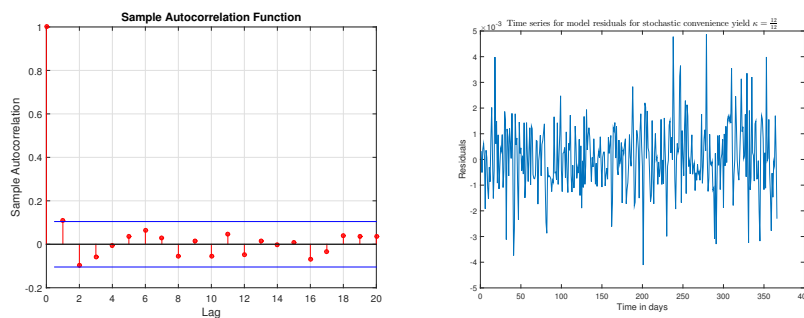


Figure 75: *Left:* ACF for model residuals for convenience yield time series for $\kappa = \frac{12}{12}$, where the blue horizontal lines represent the IID threshold. *Right:* Time series of model residuals for convenience yield.

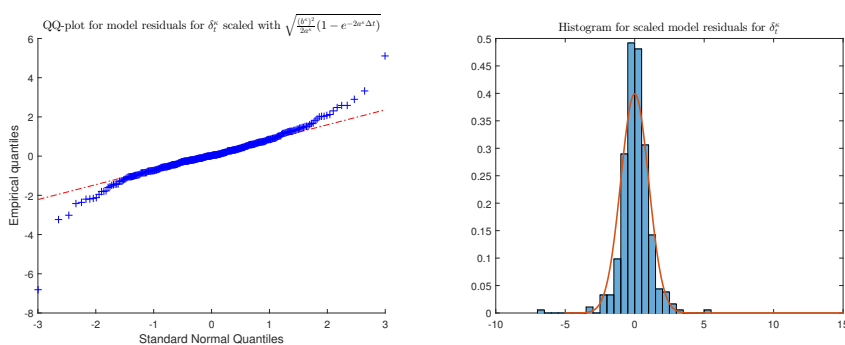


Figure 76: *Left:* QQ-plot for normalised model residuals for stochastic convenience yield for $\kappa = \frac{3}{12}$ against standard normal quantiles. *Right:* Histogram of normalised residuals together with density of standard normal distribution.

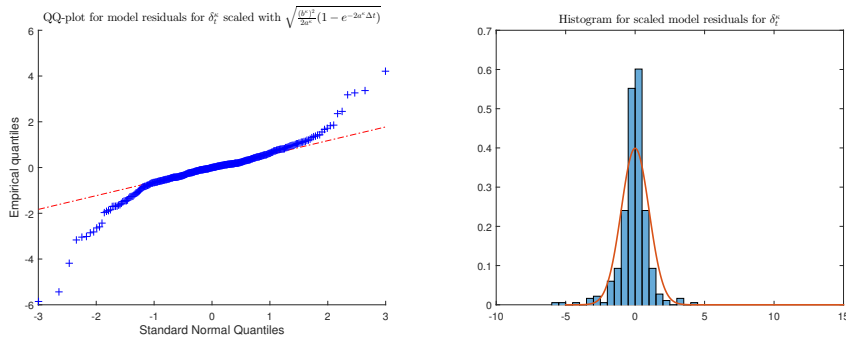


Figure 77: *Left:* QQ-plot for normalised model residuals for stochastic convenience yield for $\kappa = \frac{4}{12}$ against standard normal quantiles. *Right:* Histogram of normalised residuals together with density of standard normal distribution.

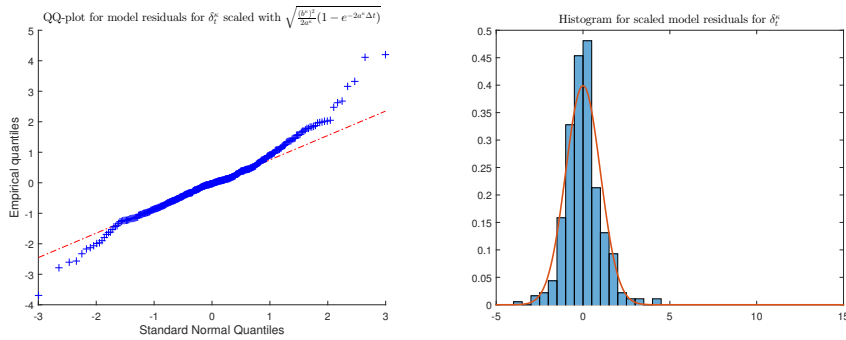


Figure 78: *Left:* QQ-plot for normalised model residuals for stochastic convenience yield for $\kappa = \frac{6}{12}$ against standard normal quantiles. *Right:* Histogram of normalised residuals together with density of standard normal distribution.

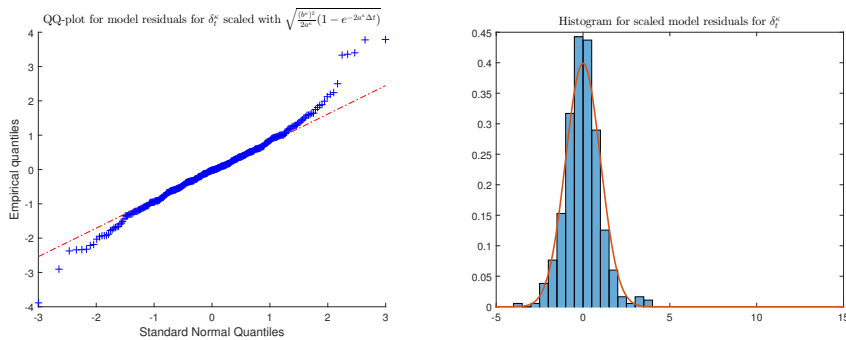


Figure 79: *Left:* QQ-plot for normalised model residuals for stochastic convenience yield for $\kappa = \frac{7}{12}$ against standard normal quantiles. *Right:* Histogram of normalised model residuals together with standard normal density.

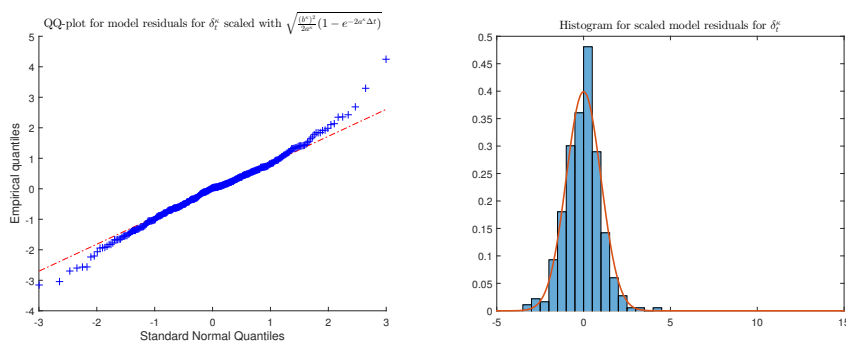


Figure 80: *Left:* QQ-plot for normalised model residuals for stochastic convenience yield for $\kappa = \frac{8}{12}$ against standard normal quantiles. *Right:* Histogram of normalised model residuals together with density of standard normal distribution.

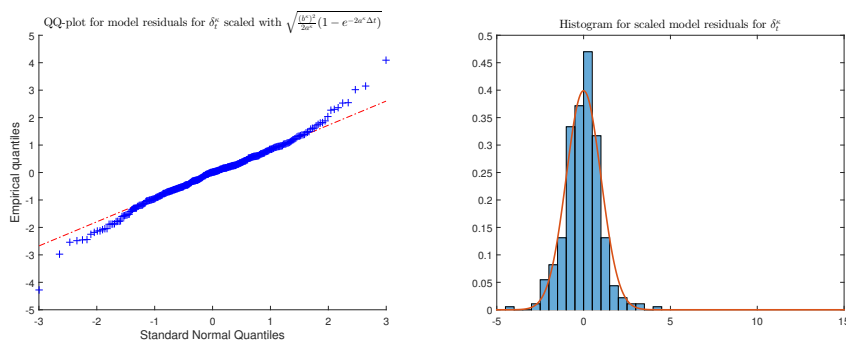


Figure 81: *Left:* QQ-plot for normalised model residuals for stochastic convenience yield for $\kappa = \frac{9}{12}$ against standard normal quantiles. *Right:* Histogram of normalised model residuals together with standard normal density.

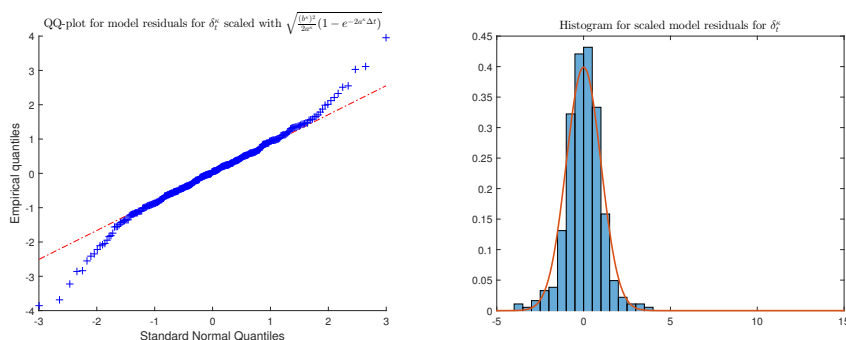


Figure 82: *Left:* QQ-plot for normalised model residuals for stochastic convenience yield for $\kappa = \frac{11}{12}$ against standard normal quantiles. *Right:* Histogram of normalised model residuals together with density of standard normal distribution.

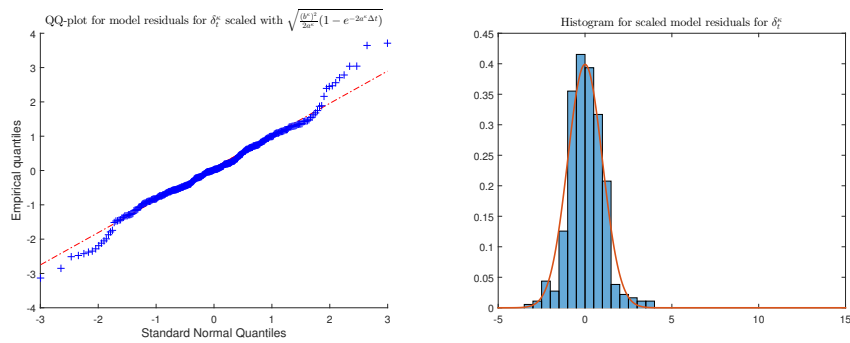


Figure 83: *Left:* QQ-plot for normalised model residuals for stochastic convenience yield for $\kappa = \frac{12}{12}$ against standard normal quantiles. *Right:* Histogram of normalised model residuals together with standard normal density.